DIVE ANGLE SENSITIVITY ANALYSIS FOR FLIGHT TEST
SAFETY AND EFFICIENCY

THESIS

Matthew Schneider, 2nd Lieutenant, USAF

AFIT/GAE/ENY/10-M20

DEPARTMENT OF THE AIR FORCE
AIR UNIVERSITY

AIR FORCE INSTITUTE OF TECHNOLOGY

Wright-Patterson Air Force Base, Ohio

AFIT/GAE/ENY/10-M20

DIVE ANGLE SENSITIVITY ANALYSIS FOR FLIGHT TEST SAFETY AND EFFICIENCY

THESIS

Presented to the Faculty

Department of Aeronautics and Astronautics

Graduate School of Engineering and Management

Air Force Institute of Technology

Air University

Air Education and Training Command

in Partial Fulfillment of the Requirements for the

Degree of Master of Science in Aeronautical Engineering

Matthew Schneider, BS

2nd Lieutenant, USAF

March 2010

Dive Angle Sensitivity Analysis for Flight Test Safety and Efficiency

Matthew Schneider, AFIT, BS

2nd Lieutenant, USAF

Approved: Date:

—————————————————   ——————
Lt. Col. Richard Huffman (Chairman)

—————————————————   ——————
Lt. Col. Christopher Shearer (Member)

—————————————————   ——————
Lt. Col. Frederick Harmon (Member)

AFIT/GAE/ENY/10-M20

Abstract

Flutter envelope expansion is one of the most critical types of developmental flight tests. The regions that present the most dangerous flight profiles are those test points in the negative P_S realm of the flight envelope. These points develop into high-speed dives and require an accurate predictive model to prevent possible testing accidents. As a flight test is conducted, several conditions such as aircraft weight and ambient air temperature can change, causing a drastic shift in the excess power profiles resulting in significant alteration in the test conditions. Using a dive planning model, a number of parameters were analyzed to determine the sensitivity to variations in data. This sensitivity analysis provided detailed information regarding the parameters that are most effected by minor variations in test conditions. The goal of this study was to improve the safety of flight test programs and increase test efficiency by improved test planning and execution.

Acknowledgements

I would like to thank first and foremost my advisor, Lt. Col. Richard Huffman. He has provided much insight into the flight test world and his patient support through some slow times and a few unique situations ultimately proved to be the drive and motivation needed for a successful completion. I would also like to thank my parents and sister for their unending support. They have always provided me with the motivation and encouragement to succeed and have never doubted me in any way. Special thanks also go out to Lt. Col. Evan Dertien and the 40th Flight Test Squadron at Eglin Air Force Base, Florida. Their support and assistance throughout the experiment is what led to a successful completion. Lastly, I would like to thank my friends, particularly those from the Incarnation Young Adults group that have made my experiences in Dayton unforgettable. It was through this group that I was able to always step away from a stressful situation and know that I had close friends who were always willing to help me through my most difficult times. These same friends are the ones that were there during my surgery and knew that in the end I would still succeed. Thank you Tom, Nina, and Beth. And special thanks to my close friend Erin, who was always there when I needed her most.

Matthew Schneider, 2nd Lt., AFIT

Table of Contents

List of Figures

List of Symbols

Symbol		Definition
$\dfrac{d(\bullet)}{dt}$	$\equiv$	Time derivative of included variable
$\dfrac{\partial(\bullet)}{\partial V}$	$\triangleq$	Partial derivative with respect to velocity of included variable
α	$=$	Angle of attack
Δt_{Band}	$=$	Time spent in test window
Δh_{Band}	$=$	Altitude tolerance
ε	$=$	Angle between thrust axis and zero-lift axis
$\eta_{\circ}$	$=$	Overall powerplant efficiency
γ	$=$	Flight path angle or dive angle
D	$=$	Drag
dt	$=$	Time step
dW_f	$=$	Differentiable fuel weight
E	$=$	Aircraft total energy
E_h	$=$	Energy height
$\dfrac{E}{W}$	$=$	Specific energy
g	$=$	Gravitational force
g_c	$=$	Gravitational change associated with position and altitude over the Earth
h	$=$	Altitude
H_c	$=$	Heat content of fuel
$h_{geopotential}$	$=$	Geopotential altitude

Symbol		Definition
h_t	=	Tape altitude
K.E.	=	Aircraft kinetic energy
L	=	Lift
m	=	Mass
M	=	Mach number
P.E.	=	Aircraft potential energy
P_S	=	Specific excess power
$P_{S_{Book}}$	=	Book values for specific excess power
$P_{S_{Test}}$	=	Test values for specific excess power
T	=	Thrust
T.E.	=	Aircraft total energy
T_a	=	Temperature of ambient air
V	=	Velocity
V_T	=	Transverse velocity
W	=	Aircraft gross weight
W_{Book}	=	Aircraft recorded book weight
$W_{S.L.}$	=	Aircraft gross weight at sea level
W_{Test}	=	Aircraft gross weight at test point

DIVE ANGLE SENSITIVITY ANALYSIS FOR FLIGHT TEST

SAFETY AND EFFICIENCY

I. Introduction

1.1 History of Flight Test

Since as early as 1890, flight testing has been an integral part to the design and successful production of aircraft. Whether these aircraft are powered or unpowered, designers have been scrupulous in following flight testing regiments to improve their designs and determine the operational limits of their aircraft. Some of the early pioneers for flight testing were Wilbur and Orville Wright, Otto Lilienthal, Octave Chanute, and Samuel Pierpont Langley. Over nearly a twenty year span, these three gentlemen conducted flight tests on a number to different styles of early aircraft. The primary goal behind their flight test techniques was to determine the controllability of air vehicles, from unpowered gliders to full scale powered aircraft. However, the true realization that these gentlemen acquired was not the information gathered from their flight tests, but the importance of flight testing in and of itself [10].

Langley, with the help of his assistant, Charles Manley, conducted their first human-controlled powered flight test in 1903 near Tidewater, Virginia. Having failed several times and crashing his prototypes into an ice cold Potomac River, Langley became discouraged. It was this set back that provided the Wright brothers the opportunity to make their first successful powered flight on December 17, 1903 prior to any others. Hence, this allowed the Wright brothers to be recorded as the first to

successfully conduct controlled-powered flight. This historical perspective provides important insight. Even the Wright brothers noted that the only way to build a successful airplane was through experiments using wind tunnels and actual flight test experiments [10].

Flight testing has become a critical portion of the design and successful marketing of aircraft. Since the 1930s and continuing through today, jet engines have drastically changed the performance capabilities of aircraft. It was in 1937 in England that Sir Frank Whittle was able to develop the jet engine. Because of this development, and in comparison to today's aircraft (particularly military fighter aircraft), the flight envelope has more than doubled in size. From aircraft such as the P-51 Mustang that were limited to subsonic flight only (primarily due to restrictions of the propeller driven engines), to now having an F-16 Fighting Falcon with the capability of exceeding Mach 2.0, all aspects and capabilities of an aircraft must be tested before the air vehicle can be deployed into service [1].

1.2 Importance of Flight Testing

So the next question of significant importance is, "Why are we conducting flight testing?" The Aerospace Research Pilot School [5], later called the U.S. Air Force Test Pilot School, is the Air Force's official training program for the training of experimental test pilots, flight test navigators, and flight test engineers. The purpose of this school is to prepare pilots, navigators, and engineers so that they can conduct and supervise flight tests for the purpose of research and experimentation. This specialized school, enrolling

only the most qualified applicants, defines three primary reasons for the purpose of flight testing:

- *To determine the actual characteristics of the machine (as contrasted to the computed or predicted characteristics)*

- *To provide developmental information*

- *To obtain research information*

Although these reasons cover the primary fundamentals behind flight test, they do not quite make a strong enough statement in regards to modern flight vehicles.

As aircraft have continued to develop over the past century, they have become more than just framing and simple controls. Modern aircraft are often now referred to as a "system of systems". They must be able to interact and be integrated with ground, space, and other air based systems. It is because of this integration of systems that makes flight testing so crucial. An aircraft that is placed into a combat role without a proper verification of the functionality of its individual systems, as well as its communication abilities with other assets could cause serious problems. Ensuring the system's functionality and its ability to seamlessly communicate with all the necessary resources is one of the fundamental reasons behind a rigorous flight test program. It is for this same reason that flight testing is a crucial component towards the development and successful operation of air vehicles.

However, flight testing is still a critical part of the development of aircraft. Aircraft have transformed the world, allowing people to move themselves and goods farther and faster. As the world economy continues to expand, the need to keep the pace

of transportation becomes a vital component. This need for transportation is only driven by the general population's feeling of safety behind using such systems. The safer that a customer feels about the quality of an aircraft or any system, the more likely they are to use it. It is because of this reason that aircraft are able to undergo these rigorous and costly flight test programs, because the international market will support them. Companies and governments are always looking for ways to save costs in development of aircraft systems. In order to save money in the testing phase, flight test programs must become more efficient and safer to reduce the probability of loss of life and equipment as well as valuable time, and one of the primary ways to accomplish these goals is through forms of predictive modeling.

1.3 Need for Predictive Modeling

Predictive modeling has had an even greater impact than originally anticipated. It has had such an impact that it is often considered even more important than the actual flight testing in regards to predicting the performance of an aircraft prior to risking personnel and costly aircraft systems. It is also critical in the mitigation of risk during flight test programs. Because of these high costs associated with flight tests, costs in both time and budgetary expenses, it is essential that predictive modeling be used to provide the flight test community with an accurate forecast of what the air vehicle's performance will be prior to beginning an actual flight test program [23].

From this point, it can be determined that predictive modeling is fundamental to a well-developed air vehicle. This process of developing accurate models may be frequently iterative and is often limited by the uncertainty that is contained within certain

parameters. However, these models have an extension beyond just development. Although it will not be discussed in this document, mathematical and predictive models can also be used to improve design, develop training simulators, reconstruct aircraft accidents, and observe the effects of design modifications [21].

The modeling and flight testing of aircraft must not be taken lightly though. It is crucial that a well developed plan be executed with precision and the results must not be rushed. In Norton's paper he discusses how a fast-paced flight test program led to many crucial setbacks that eventually led to higher than predicted costs and non-optimal testing techniques [11]. The importance of incorporating models and ensuring their accuracy is critical to keeping costs at a minimum and mitigating the risk for each test scenario. With the staggering costs associated with flight testing, it is crucial to make the investment in the earliest stages of design possible to eliminate the excessive cost overrun that can grow exponentially as development continues.

Predictive modeling, a crucial part of the systems engineering life cycle, or the developmental program for the creation of an air vehicle system, can have drastic effects on cost overrun and cost incurred for a system without proper planning. Figure 1.1, taken from a NASA Comptroller's Office, 1980, shows how systems engineering is a critical part of the development process. This process, which often incorporates the necessary developmental flight test plans and modeling, illustrates an exponential increase in the cost overrun. Without an adequate systems engineering analysis and developmental test plan in place, the cost of these flight test programs continues to grow exponentially [4].
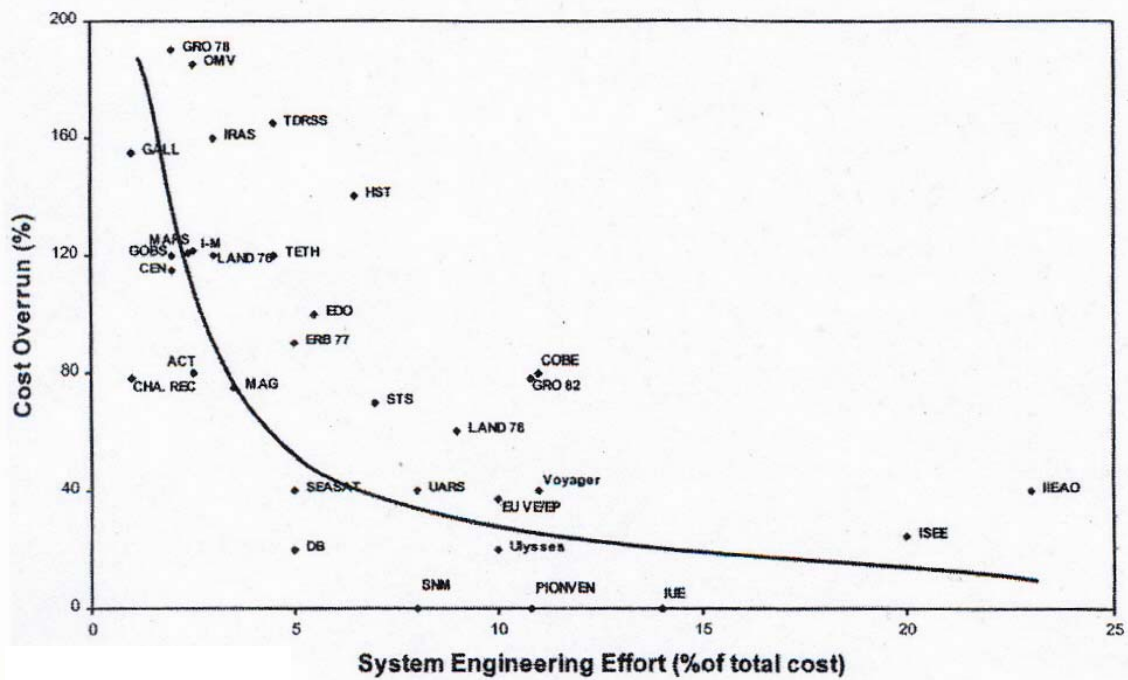
Figure 1.1: Exponential Change in Cost versus Life Cycle (taken from [4])

However, this predictive modeling, associated with the systems engineering effort, is not just crucial to cost savings in both time and finances, but it is critical in determining aircraft performance as well.

1.4 Connections to Aircraft Performance

Predictive modeling and aircraft performance are directly related, particularly in the discussion of high-speed military fighter aircraft because the primary focus is around envelope expansion and determining the operational limits for a specific aircraft. The primary relation to military aircraft is associated with the increase in flutter problems around the flutter bucket near the transonic region of the flight envelope as will be

6

discussed later. An engineer that understands the parameters of aircraft design that can primarily affect performance can incorporate these parameters with a greater emphasis in the model allowing the simulator or predictive model to provide a much more realistic feel or result. All this information can be incorporated to provide the engineers and pilots with an idea of where the particular air vehicle will be advantageous and provide the most effective support all without even building a prototype [17].

For this paper, the most relevant area of flight testing revolves around the maximum performance envelope. The primary performance characteristics of concern are the "absolute performance characteristics". Saarlas [17] defines these characteristics as:

- *Maximum speed*
- *Stalling speed*
- *Best climbing speed*
- *Best glide angle*
- *Rate of climb*
- *Ceiling*
- *Maximum range and speed for maximum range*
- *Maximum endurance and speed for maximum endurance*
- *Take-off distance*
- *Landing distance*

The focus of this paper will be on maximum speed, best climbing speed, and rate of climb. The reason behind this is associated with the definition of negative excess power. Although it will be discussed in more detail later, negative excess power is the region of the flight envelope beyond the steady-level flight maximum speed [17].

Many of the speeds and altitudes (defining a particular test point for a given flight test) are extremely hazardous for both aircraft and pilots since negative excess power requires steep angled dive angles, and in some cases test points and timely maneuvers at

low altitudes. Most of the test points of interest in this maximum performance region must be achieved using high-speed and steep angle dives. The reason behind using this unobtainable region of the flight envelope is for the determination of flutter envelope expansion. The details of this information will be discussed in Chapter II, but it is important to understand that this type of flight testing is particularly "hazardous" and thus drives the importance behind analytical and predictive modeling of the air vehicle prior to actual manned flight tests [22]. "Hazardous" flight testing, as defined by Strganac [22] is any flight testing involving high risk scenarios where minor errors, such as approaching a flutter region too quickly, can cause a catastrophic event.

However, the information gained from these flight tests is not strictly used for flutter envelope determination, but can be used to determine operational envelopes as well as providing a pilot with a region of advantage over a given adversaries aircraft. Using predictive modeling to determine these test points allows the safest possible flight test program. Having a flutter test point in theory, does not necessarily define the actual test point, particularly when the configuration of external stores is modified. The actual flight flutter envelope is therefore determined by evaluating the accuracy of the theoretical flutter test envelope through the evaluation of data collected from several of these test points.

1.5 Objectives of Simulations and Analysis

Because of the inherent danger associated with diving an aircraft at high-speed toward the ground, particularly at low altitude conditions, these dives must be carefully planned. Mathematical models, such as those previously discussed, must be used to

predict proper dive angles and starting altitudes to ensure a safe flight test. Currently, the models that have been developed to predict these dive angles, starting altitudes, and recovery altitudes are subject to several levels of uncertainty. These uncertainties are theoretically linked to several interrelated variables that are embedded throughout the predictive model currently in use and the equations that drive it.

The objective of this sensitivity analysis will be to provide a sensitivity analysis on the variability of these parameters driving the model. Determining the variables that are susceptible to even minor variations can help with the improvement of prognostic models and also indicate to test pilots and flight test engineers which tests are higher risk and should be postponed until more accurate predictions can be made. This paper will discuss a detailed background behind high-speed dive planning, its origin, then review the results of a sensitivity analysis, and lay out those results in a form that can be used by the flight test community.

By looking at research accomplished as early as the 1950s relating performance to energy and power, the background theory behind high-speed dive planning can be developed. Once this background and the necessary equations for the development of a predictive model have been discussed, the origin of the model used for this sensitivity analysis will be discussed in greater detail. Finally, the results from the sensitivity analysis will be examined. This paper will present the parameters that are particularly susceptible to variations and indicate the variables that have minimal impact on the results of the model. Finally, the results will be organized into a format that the flight test community can utilize to help ensure the safety and efficiency of flight test programs, including both military and commercial uses.

II. Background and Theory

Despite that negative excess power flight testing was never vocalized in the manner that this thesis will discuss, research began on similar topics as early as the 1950s. Edward S. Rutowski, along with others such as Arthur E. Bryson Jr., set out to solve a different problem and ended up eventually stumbling across the excess power discussion. The motivation behind their original work was associated with solving the optimal performance problem. From there it developed into an entire discussion and field of study on optimal control and optimal aircraft performance.

2.1 Original Performance Calculations

The original research, aimed at determining the optimal rate of climb and optimal time to climb was started two-fold by competing parties. Edward Rutowski worked for Douglas Aircraft Company out of Long Beach, California. Douglas Aircraft, later becoming McDonnell Douglas and currently under Boeing Aircraft's Commercial Airplanes division, sponsored Rutowski's research in order to determine a simple solution to the general aircraft performance problem. Arthur E. Bryson, Jr., worked for Raytheon and conducted research through Stanford University, published many papers and texts on energy-state approximation and optimization, looking to solve the same problem as Rutowski.

2.1.1 Rutowski's Research

Rutowski presented his research at the Institute of Aeronautical Sciences (IAS – a predecessor to the AIAA – American Institute of Aeronautics and Astronautics) Annual

meeting in July of 1953. Rutowski focused on the concept that with the development of faster aircraft and more prevalently the jet aircraft engine, the simple performance calculations for time to climb and rate of climb no longer proved to be the optimal solution. With the expansion of the flight envelope to include supersonic and transonic flight, optimum no longer implied fastest or shortest lateral distance, but rather focused on minimum time and minimum fuel [16].

Rutowski suggested that by observing the energy approach to the problem and considering an aircraft's potential and kinetic energy, a better analysis on the performance capabilities of an aircraft could be determined. By using this approach, he determined that he could solve a more generalized problem than just reaching a given altitude. This problem, originally solved using simple mathematics, provided a completely different and opposing outlook to the problem and created revolutionary solutions. The reason that the original simplistic approach was primarily taken was associated with the fact that aircraft typically did not cross into the realm of supersonic and transonic flight. As technology improved and aircraft gained the capability to operate at supersonic flight conditions, this conventional approach to performance no longer became the norm for determining climb rates and time to climb for developmental aircraft.

By understanding that aircraft velocity can be expressed in terms of kinetic energy and altitude can be expressed in terms of potential energy, the concept of the total energy approach was derived. This total energy equation for an aircraft is shown in Equation 2.1,

$$E = Wh + \frac{WV^2}{2g} = W\left(h + \frac{V^2}{2g}\right) = \left(\frac{E}{W}\right)W \qquad (2.1)$$

where E, defined as the total energy of an aircraft, can be broken into potential and

kinetic energy. The potential energy is a product of the aircraft weight, W, and the

altitude above sea level, h. The second term, the kinetic energy is the product of weight

and the square of velocity, V, divided by a factor of two times the gravitational force, g.

The combination of the kinetic and potential energy divided by the weight provides the

specific energy, or energy per unit mass of the aircraft, E/W. When multiplied through

again by the weight, the total energy of the aircraft, E, at its specific weight is

determined.

The next step was to take this information and obtain the energy balance

relationship to develop the specific energy equation of an aircraft, or its time rate of

change of energy.

$$\frac{d\left(E/W\right)}{dt} = \frac{\eta_\circ H_c}{W}\frac{dW_f}{dt} - \frac{DV}{W} \qquad (2.2)$$

By taking the time derivative of the specific energy, $d(\cdot)/dt$, Equation 2.1 now takes on a

new form shown above in Equation 2.2. The heat content of the fuel, H_c, is multiplied

by the aircraft's power plant efficiency, $\eta_\circ$, to provide the useful work of propulsion per

pound of fuel. Dividing by the weight and then multiplying the value by dW_f/dt, the rate

at which the engine is consuming fuel, this term develops into the thrust generated by the

aircraft. The drag of the aircraft, D, multiplied by the velocity and divided by the weight

is the energy required by the aircraft. These terms can then be simplified into Equation 2.3.

$$\frac{d\left(E/W\right)}{dt} = \left(V/W\right)\left(T - D\right) \tag{2.3}$$

Here, by separating out the velocity component and the weight, present in both terms, the time rate of change of specific energy, or specific power is defined by the difference of thrust and drag all multiplied by velocity per unit weight.

Using an assumption that the weight of the total aircraft over the course of time is fairly constant (for the purpose of this mathematical development, by which Rutowski takes care to note the consumption of fuel has a considerable effect on the rate at which an aircraft's weight will change), Equation 2.4, the standard approximation for specific energy, can be written. Since weight is assumed to be constant, it can be taken outside the derivative term of the specific energy and then multiplied from both sides to reveal Equation 2.4.

$$\frac{dE}{dt} = \left(T - D\right)V \tag{2.4}$$

It should be noted however, that this simplification becomes ever more crucial and increasingly important as the speed and altitude capability of an aircraft increase. The fact that the assumption of a constant weight is made for simplification purposes is greatly flawed. Potential energy in particular is directly related to the weight of an aircraft at a particular altitude. Neglecting this term becomes even more relevant as the aircraft performance envelope is expanded. Higher altitudes and faster airspeeds make it

increasingly vital to include the energy change due to the weight change of an aircraft [16].

Despite the relevance to the problem currently being evaluated, the original performance problem of discussion was determining the optimum climb profile in terms of both minimum time to climb and minimum fuel required to climb to a given altitude. Looking back at this concept and approach, Equation 2.1 and 2.4 are combined to obtain Equation 2.5.

$$\frac{dh}{dt} = \left[\frac{V}{W}(T-D) \right] - \frac{V}{g}\frac{dV}{dt} \tag{2.5}$$

Identified as a "fundamental" performance equation, Rutowksi's research was taken one step further and he considered the definition behind this rate of change of specific energy. Looking at the change in altitude over time, dh/dt, the solution is a combination of the time derivative of specific energy, Equation 2.3, subtracted from the velocity over the gravitational force multiplied by the acceleration of the aircraft, dV/dt.

By understanding that the rate of change of specific energy is related to the excess power per pound of fuel, this information can then be interpreted as the solution to "longitudinal acceleration at constant altitude" [16]. In early subsonic aircraft, this assumption provided little to zero variation in rate of climb at constant speed. However, as can be seen in Figure 2.1, there is a significant correction factor needed as Mach number increases. In this figure, the correction factor discussed is the appreciable error generated from increasing Mach number values even in the case of steady climb and a changing speed. When plotted against the Mach number, several lines can be drawn.

14

The figure below shows a line of constant indicated airspeed, V_i, for the case where the altitude is under 35,000 feet and a line of constant climb Mach when the altitude is held constant at 20,000 feet. For example, when a climb at a constant Mach of 2.0 is conducted, the correction factor to account for the variation in speed is greater than 2.0. This correction factor is then applied to the kinetic energy term based on the climbing speed of the aircraft, or the rate at which the aircraft is increasing its kinetic and potential energy.
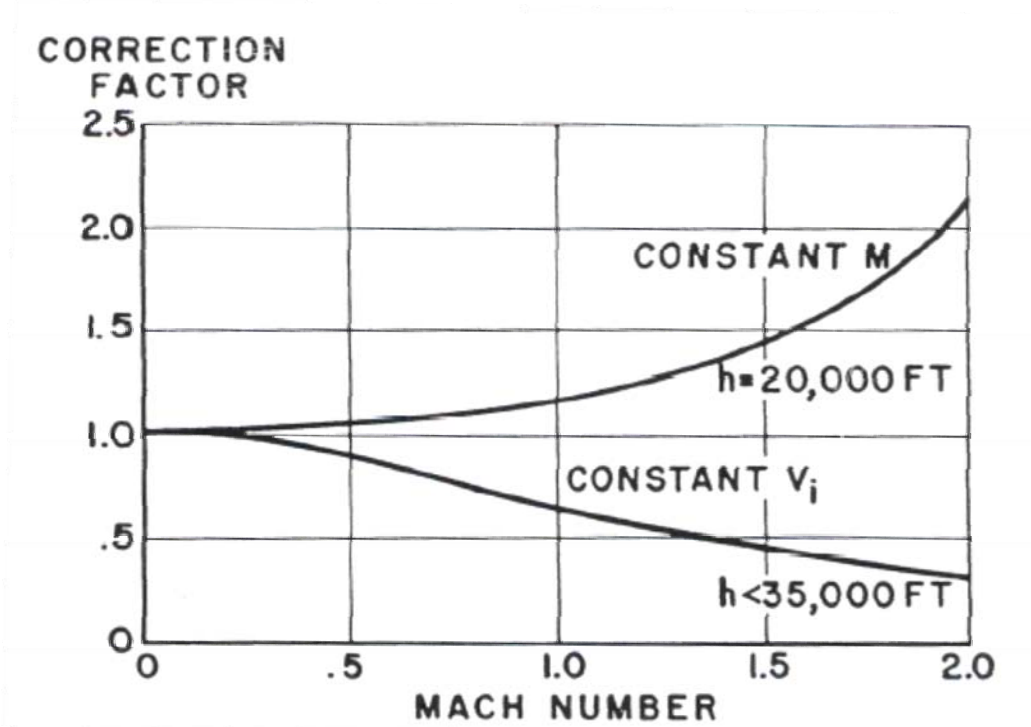
Figure 2.1: Kinetic Energy Correction to Rate of Climb at Constant Speed (from [16])
Reprinted with permission of the American Institute of Aeronautics and Astronautics

This figure is important to note because it drove the research behind determining better solutions for the high-speed flight test condition. The original assumptions behind subsonic flight could no longer be simply applied and more considerations were needed.

15

Because of this large variation and large correction factor that must be applied at high speed flight test conditions, the full equation for climb performance must be used and is shown in Equation 2.6.

$$\frac{dh}{dt} = \frac{V}{W}(T-D)\left[\frac{1}{1+\left(\frac{V}{g}\right)\left(\frac{dV}{dh}\right)}\right]$$ (2.6)

Equation 2.6, still solving for the rate of climb, or the change in altitude, now incorporates the full development of the Mach effects. The specific excess power, or time derivative of specific energy, $\frac{V}{W}(T-D)$, is now multiplied by correction factor. This correction factor is taken from the acceleration term from Equation 2.5. Taking the $\frac{dV}{dt}$ term and rewriting it to be a rate of velocity change per unit altitude, $\frac{dV}{dh}$, multiplied by the velocity per the gravitational pull of the Earth, $\frac{V}{g}$, yields the final result.

Now that the mathematics for the correction factor are incorporated to the rate of climb calculations, the next step was determining that the general performance problem for high speed aircraft could also no longer be discussed as just an open function of four variables. Rather, there was a realization that it was critical to include not only rate of climb, but also the time to climb in the same calculations. From this conclusion, Rutowski returned to his original equation for specific energy and started solving the equation for constant values and plotted them against altitude and velocity. Figure 2.2 illustrates the energy curves that he was able to generate [16].

In Figure 2.2, the altitude is shown in thousands of feet above sea level and the horizontal axis is the speed of the aircraft. The use of indicated airspeed is used merely to provide consistency to the source that was primarily available at the time. Since aircraft were primarily subsonic, the need for a calibrated airspeed plot was not yet necessary. The constant value of specific energy was then plotted and is shown as the solid parabolic lines indicated at 50,000, 100,000, and 150,000 feet. These are the lines of constant specific energy. Note how at zero velocity, the energy is entirely potential and is merely the altitude that the aircraft is above the Earth. The long dashed lines indicate the lines of constant Mach number. These are important to consider since the figure is plotted as altitude against constant airspeed and the correction factor previously discussed was associated primarily with increasing Mach effects.
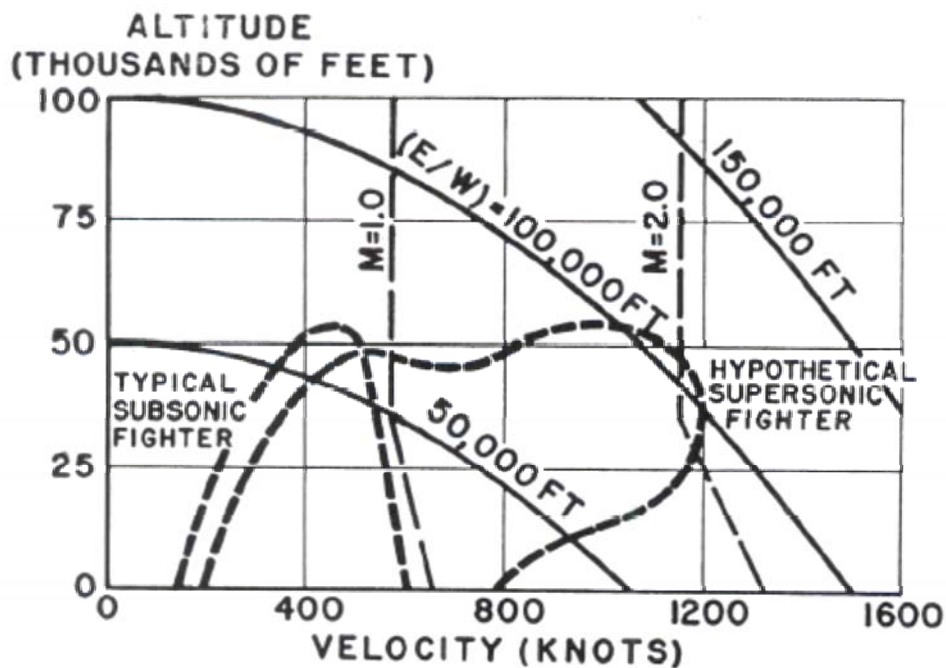
Figure 2.2: Typical Fighter Speed-Altitude Envelopes Superimposed on Contours of Constant Specific Energy (taken from [16])

17

The dashed lines indicate two different types of aircraft. The subsonic fighter is indicated by the inverse parabolic shape with a smaller enclosed area and a hypersonic fighter is the oblong shaped envelope. The purpose of this figure is to show that through this energy approach discussion, the performance envelope of a supersonic aircraft far exceeds that of a subsonic fighter. Although there are minor advantages such as the capability of a subsonic fighter to travel higher at lower speeds and slower at lower altitudes, the supersonic fighter has a greater operational envelope in which to fly.

Using this research as a basis and the development on contours of constant specific energy, a vast amount of information spawned from this chart. Lines of constant energy became a standard in determining performance levels and the maneuverability of one aircraft over another. This information will be discussed in more detail later.

From all of this data, a conclusion was derived that the climb problem was no longer simply the time or rate to get from one altitude to another, but rather from a specific altitude and speed to another. This can be rewritten as the achievement of a final energy level based on an initial energy level. From this determination, the research then proceeds to state that the exact amount of kinetic energy and potential energy are not necessarily important throughout the climb, but only realistically come into play at the final condition. It is much more important that the balance or the total energy provide an optimal path from which to climb from one altitude and airspeed to another. This determination was made by looking at Figure 2.3, or Fig. 3 from Rutowski's paper.

Figure 2.3, again plotting altitude versus velocity, indicates the improvement of the energy approach to optimal climb over the conventional approach that was previously used. The solid lines running from left to bottom indicate lines of constant specific

energy as discussed before. Here they are shown in 15,000 foot increments. The

inverted parabolas indicate lines of constant excess power per pound of weight, as is

shown by the equation $\dfrac{d\left(E/W\right)}{dt}$. The curve reaching the highest would indicate a curve

of zero excess power, or a point at which the aircraft could not accelerate beyond that

condition at steady-level flight based on the difference between the engine's thrust and

the drag from the aircraft. Four specific excess power curves are shown. The two dashed

lines indicate the optimal path to reach a given altitude and airspeed based on the two

different methods mentioned.
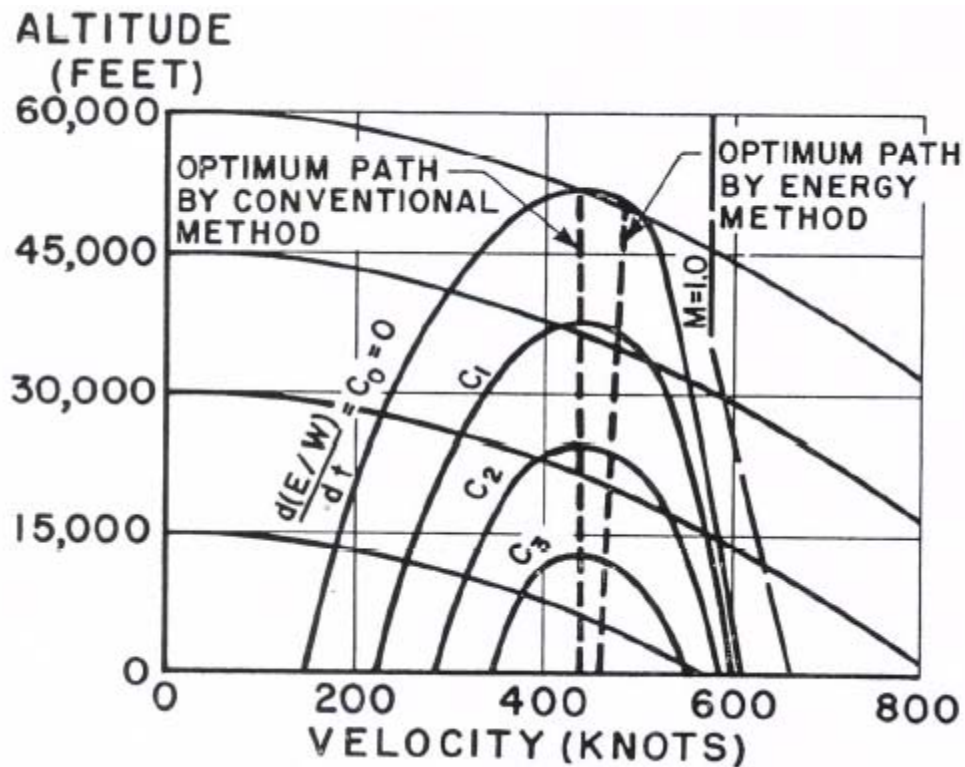
Figure 2.3: Comparison of Minimum Time to Climb Paths for Typical Subsonic Fighter
(taken from [16])

By observing this figure, it can be shown that the difference in the subsonic region of flight plays little variation on the final result using conventional performance calculations or the developed energy calculations. However, when research began looking at the predicament of changing an aircraft's energy state from one level to another, particularly for the supersonic case, this problem showed vast improvements over the previous methods of calculations.

Equation 2.7 was then developed to determine the time that it would take to theoretically change energy levels, using specific energy as the independent variable to solve this specific problem of optimal time to climb.

$$t = \int_{(E/W)_1}^{(E/W)_2} \frac{1}{\dfrac{d\left(E/W\right)}{dt}} d\left(\frac{E}{W}\right) \qquad (2.7)$$

Time, defined as t, was taken as the integral from the first energy state to the second. Taking the time rate of change of specific energy, $\dfrac{d\left(E/W\right)}{dt}$, and integrating its inverse in terms of the specific energy, the optimal time to climb can be determined. This integration became fundamental in determining optimal time to climb from the energy perspective.

Using this equation, it was realized that the problem of optimal climb could be simplified as minimizing the above integral using the method of calculus of variations. The method of calculus of variations looks for the condition where the equation for specific energy is constant at every point. Holding the E/W term as a constant and taking the partial derivative with respect to the velocity must provide a solution that is

zero at all points in time. From here, the optimal condition or path of minimum time was one that satisfies the derived equation, Equation 2.8, at every point along the path.

$$\frac{\partial}{\partial V}\left[\frac{(T-D)V}{W}\right]_{E/_W=const.} = 0 \qquad (2.8)$$

Although the solution cannot be solved generally through analytical methods, the path of minimum time or optimal climb is one that can satisfy the above equation at every condition. The conventional method was one that used Equation 2.9. By holding the altitude, h, as a constant, the optimal time to climb was determined based on the minimum time to change altitude and not the minimum time to change energy states.

$$\frac{\partial}{\partial V}\left[\frac{(T-D)V}{W}\right]_{h=const.} = 0 \qquad (2.9)$$

The difference then between Equation 2.8 and 2.9 is shown on Figure 2.3 above. Equation 2.8 uses a method where the speed is chosen where it is tangent to the lines of constant specific energy. This is considered the energy method. Equation 2.9 corresponds to lines of excess power are tangent to lines of constant altitude or the conventional method. This fundamental difference illustrated by these two equations was the purpose behind Rutowski's research: separating the two methods of calculation.

However, as was previously mentioned, there is little improvement in the energy method versus the conventional method for optimal climb in regards to subsonic flight. It changes when the discussion switches to a supersonic fighter. Equation 2.9 becomes useless when the desired speed approaches the maximum. This is due to the correction factors that were illustrated in Figure 2.1. The specific energy method does not run into this problem since it is normalized with respect to the maximum excess power per pound

of aircraft. The optimal climb path can be shown easily for a larger range of speeds and

altitudes and by plotting the energy variation. This can also show acceleration

capabilities through a dive as part of the optimal climb path. Figure 2.4 shows what later

became known as the Rutowski Climb Schedule or the optimal time to climb solution

using the energy method.
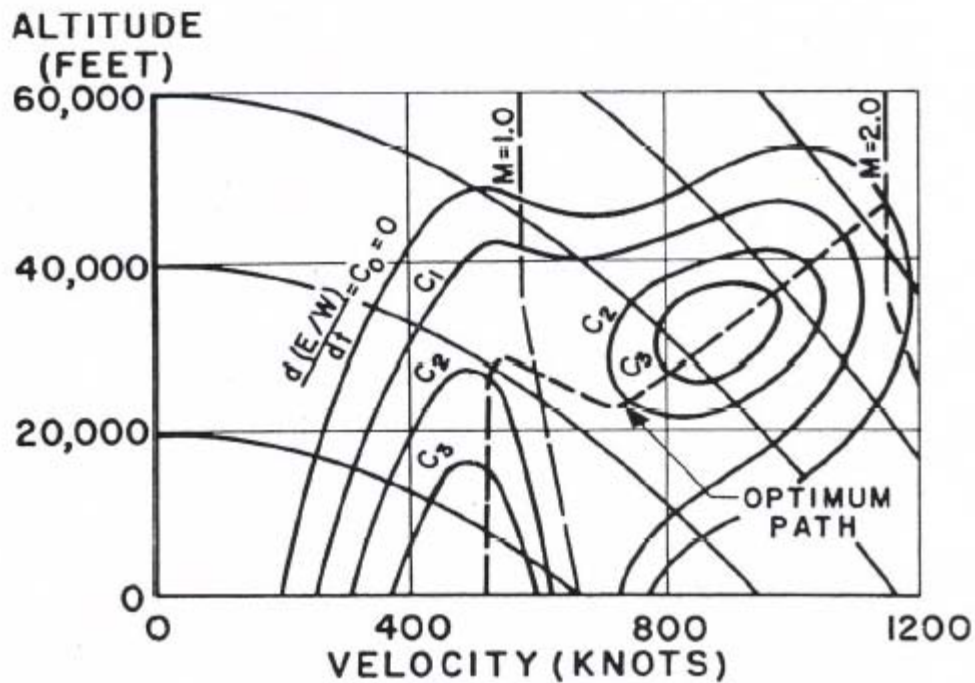
Figure 2.4: Minimum Time Path by Energy Method for Hypothetical Supersonic Fighter
(taken from [16])

Reprinted with permission of the American Institute of Aeronautics and Astronautics

Plotting altitude versus velocity, the downward curving lines are indicating curves

of constant specific energy in 20,000 foot intervals. The specific excess power curves are

also plotted, as they were for Figure 2.3, but the envelope is now expanded to indicate the

performance of a supersonic aircraft. The Rutowski Climb Schedule is this optimal path

indicated by the dashed line. Note that this dashed line, the Rutowski Climb Schedule,

runs through the same path as the subsonic condition, and the optimal path includes a

supersonic acceleration through points perpendicular to the specific excess power curves.

However, when approaching the transonic region of the flight envelope, the

aircraft actually performs a dive through this region and then continues on its supersonic

acceleration. The time spent in this transonic region of high drag is now minimized,

producing the alternate benefit of reducing fuel costs while attempting to reach high

velocities and altitudes. Note that the Rutowski Climb Schedule corresponds to speeds

where the excess power contours align tangent to lines of constant energy.

This research indicating the improvements to the optimal climb path can be

summarized in Figure 2.5. Here, the time to transition from one specific energy level to

another is shown as the area under the curve for each method.
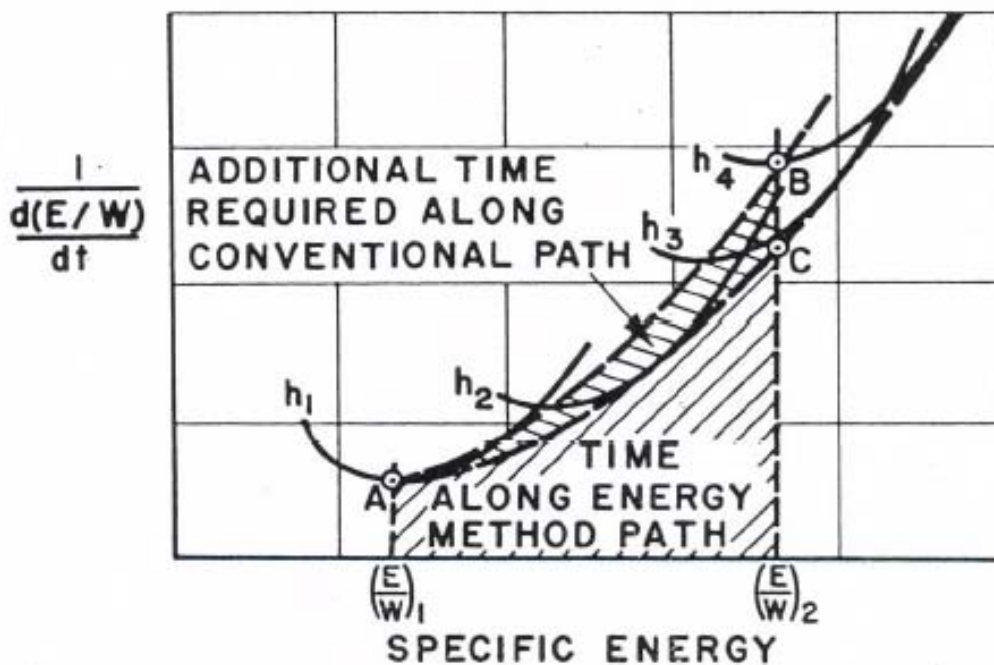
Figure 2.5: Comparison of Time to Climb Integrals as Represented by Areas (taken from [16])

Plotting the inverse of the rate of change of specific energy to the specific energy of the aircraft, the previous plot was generated. The goal of the figure is to show the improvement of the energy method in comparison to the conventional method for supersonic aircraft. The previous discussion indicated almost no improvement for subsonic aircraft but this figure illustrates the decrease in fuel and time spent in the energy state transition.

The goal is for the aircraft to travel from the first specific energy level to the second shown on the horizontal axis. Both methods start at condition A. The conventional method to reach the final energy state is shown as point B and the energy method is shown as point C. Looking at the area under each curve (the heavier dashed line indicating the energy method calculation) shows that there is an additional time required to reach the same altitude and airspeed using the conventional approach. The altitude curves, shown as h_1 through h_4 indicate lines of increasing altitude. In summary, the energy method using the Rutowski Climb Schedule shows marked improvement in time required to climb and increase altitude, in general showing improved performance capability.

Rutowski's paper continued on to discuss using the energy balance approach as it applies to the range equations, but that information is beyond the scope of this paper. In summary, this energy approach research led the way for many others, such as Bryson, to look at other optimal condition problems in more detail. This research also led to a leap forward in understanding the performance fundamentals for supersonic aircraft, particularly in the areas of minimum time to climb and minimum fuel problems [16].

2.1.2 Bryson's Research

Working through Stanford University, Arthur Bryson published a paper looking at the energy state approximations for supersonic aircraft. Although the focus of the Bryson paper was to look at determining optimum range problems in more detail, the energy equations needed for these problems required him to document slightly on the optimal climb and minimum climb problems as well. The importance of Bryson's research to this study was that he showed that the Rutowski Climb Schedule is a theoretical optimal path. By making this statement, it is realized that an aircraft cannot change its energy state instantaneously as was a primary assumption by the previous research. To illustrate this assumption, Bryson began incorporating details about the approximations that were needed to develop optimal control and optimal performance problems.

Bryson's approximations began by indicating that the aircraft in question, for simple performance problems, can be considered as a point mass. He goes on to discuss how for subsonic aircraft, the effects of acceleration can even be neglected. However, because of the acceleration rate, especially at subsonic speeds, for supersonic aircraft, these effects cannot be ignored. Another important assumption is that once the aircraft reaches supersonic flight, the capability of the air vehicle to trade kinetic energy for potential energy becomes a much more realistic fact. Bryson points out that at subsonic speeds, the available kinetic energy of an aircraft is minimal in comparison to the available potential energy. This information can be verified by reviewing Figure 2.3. Even with a significant drop in altitude, the curves of specific energy are stacked too closely together at subsonic speeds. Substituting altitude for airspeed provides a miniscule benefit to the pilot performing these types of maneuvers.

Using these approximations, Bryson came to an improved set of solutions compared to Rutowski's work that he referred to as the energy-state approximations. Bryson does point out that there is an unrealistic discontinuity in the consideration that kinetic and potential energy can be traded without the lapse of time or total energy, but with the exception of specific performance problems such as a zoom climb, the state variable of total energy can be considered continuous.

From this point, Bryson takes these assumptions and defines his necessary state variables as V for velocity, h for altitude, γ for flight path angle, and m for the mass. Considering α, the angle of attack, as a control variable, all of these variables are combined and Equations 2.10 and 2.11 are developed, the constraint equations for equilibrium parallel and normal to the flight path angle. In Equation 2.11, the constraint equation for normal equilibrium, lift, L, is incorporated instead of drag and the thrust is a function of V and h, but is multiplied by the sum of the angle of attack and the angle between the thrust axis and zero-lift axis, ε. It is important to also note that acceleration was neglected so it can be assumed that the air vehicle is traveling at a steady-level, unaccelerated flight condition.

$$0 \cong T(V,h) - D(\alpha,V,h) - mg \sin \gamma \qquad (2.10)$$

$$0 \cong T(V,h)[\alpha + \varepsilon] + L(\alpha,V,h) - mg \cos \gamma \qquad (2.11)$$

By looking at these equations, the thrust, T, is a function of velocity and altitude, and when drag, D, is subtracted along with the mass of the vehicle, then the equations are approximately zero. Using the small angle approximation and choosing an α to maximize the rate of climb, the two equations from above are constrained to create

Equation 2.12. This equation provides the ability to pick a specific altitude and angle of attack and generate a required velocity and flight path angle. The right hand side of the equation, the equation for specific excess power, now is directly related to velocity and flight path angle providing the capability to determine a negative specific excess power condition based on a dive angle and starting velocity.

$$V \sin \gamma = \frac{V(T-D)}{mg} \qquad (2.12)$$

The relation of specific excess power and flight path angle was crucial to the development of performance characteristics. And the ability to related one aircraft's performance to another was ultimately the primary purpose of this research. Looking at Figure 2.6 and Figure 2.7 shows how an aircraft with differing excess power curves can perform more optimally. In Figure 2.6, the aircraft is assumed to have a fairly typical flight envelope for a supersonic aircraft. Comparing the altitude to the Mach number, the specific excess power curves are shown and the optimum climb path is developed. Note how around the transonic flight region the aircraft can trade altitude for velocity almost in a direct relationship. This relates back to the concept of being able to associate specific excess power with velocity and flight path angle, or dive angle for this case.
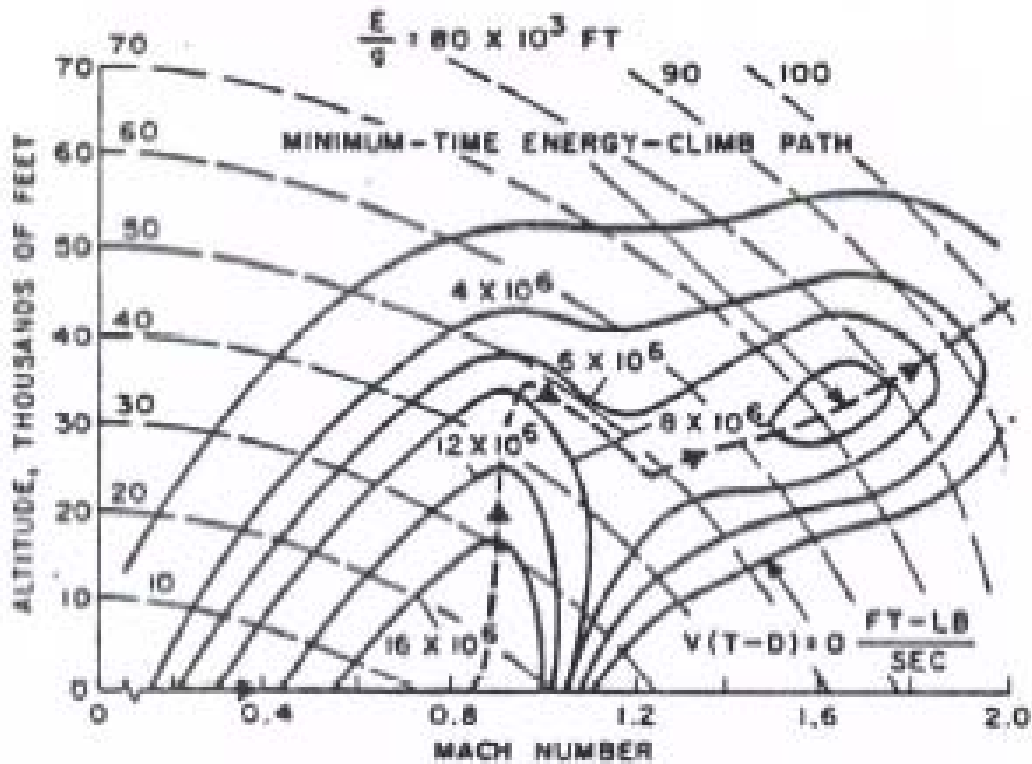
Figure 2.6: Contours of Constant Excess Power and Minimum-Time Energy-Climb Path
for Airplane 1 (taken from [2])

Reprinted with permission of the American Institute of Aeronautics and Astronautics

Aircraft 2, shown in Figure 2.7, is illustrated as an aircraft with a limitless amount of

available power. This aircraft no longer needs to rely on the high-speed dive in order to

progress optimally through the transonic flight realm, but rather can instantly gain both

velocity and altitude. This would be the definition behind having unlimited available

power or negligible power required. Another consideration is that the first aircraft

illustrated in Figure 2.6 must follow the Rutowski Climb Schedule in order to reach the

optimum time to climb. The second aircraft from Figure 2.7 can bypass this climb

schedule and its performance is significantly greater than that of aircraft one, particularly

in acceleration [2].
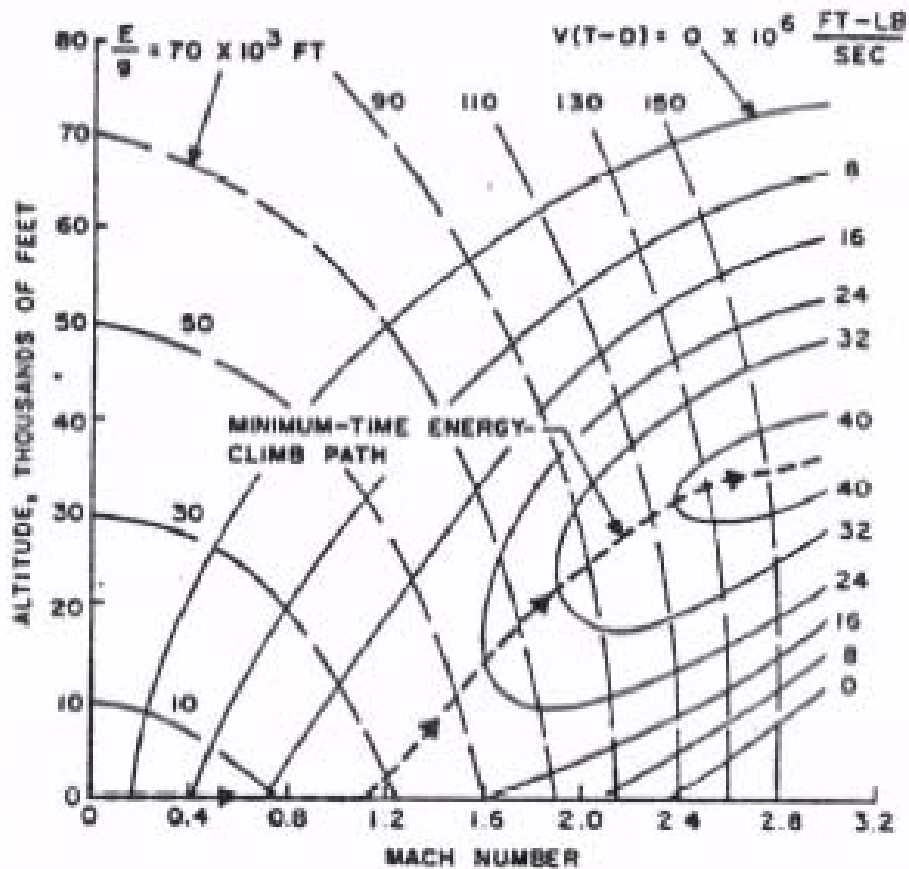
Figure 2.7: Contours of Constant Excess Power and Minimum-Time Energy-Climb Path
for Airplane 2 (taken from [2])

Similarly, Bryson looks at the minimal fuel to climb problem as well using the

same aircraft. Again, it can be seen that in Figure 2.8 and Figure 2.9, the aircraft with the

greater excess power can move more freely through the flight envelope than the aircraft

with specific regions of advantageous excess power. These plots, nearly identical to the

previous two, show the improved performance capabilities of aircraft two in comparison

to aircraft one. Plotted again for altitude versus Mach number, the energy curves are

shown so that, particularly for Figure 2.8, the energy dive through the transonic region is

better illustrated. The minimum fuel path is now shown as the dashed line, but note that

29

the aircraft still must travel through the optimal points of the specific excess power

curves, traveling perpendicular through them to expend the minimal amount of fuel

possible.

For aircraft two, having the unlimited amount of available power (and shown as a

theoretical concept for comparison purposes) is not concerned with a specific dive profile

through the transonic region or a particular climb point through the subsonic region.

Looking at Figure 2.8, aircraft one must climb to its optimal subsonic energy state at a

specific Mach number. Aircraft two has slight greater freedom and does not need to

focus on climbing just before the sound barrier with as much precision in the climb

initialization point [2].
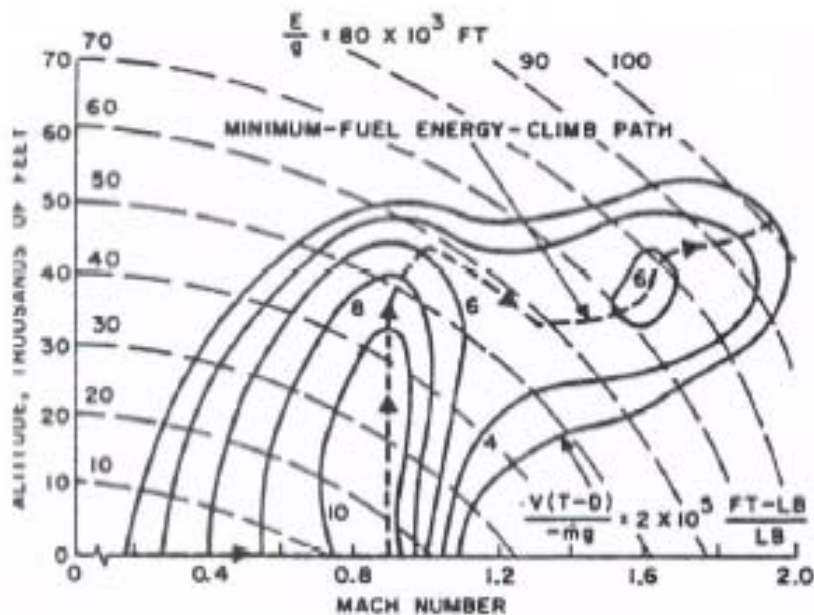
Figure 2.8: Contours of Constant Energy Increase per Pound of Fuel Burned and
Minimum-Fuel Energy-Climb Path for Airplane 1 (taken from [2])

Reprinted with permission of the American Institute of Aeronautics and Astronautics

30
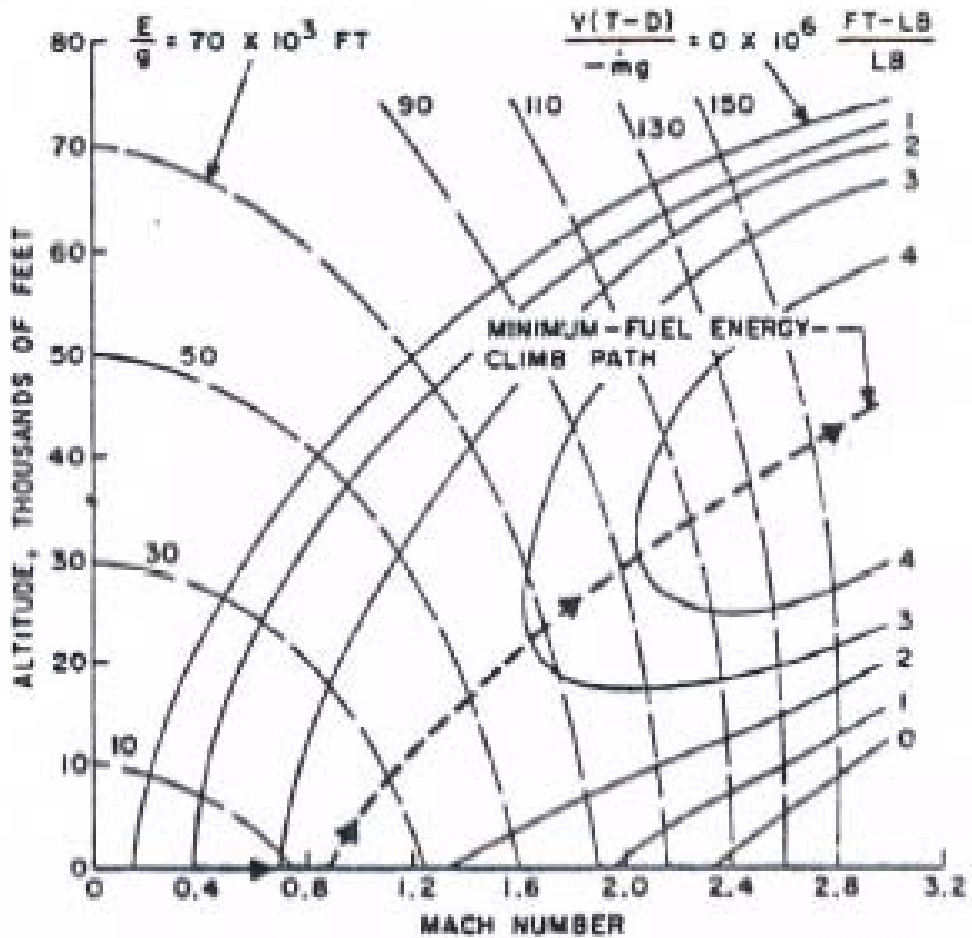
Figure 2.9: Contours of Constant Energy Increase per Pound of Fuel Burned and
Minimum-Fuel Energy-Climb Path for Airplane 2 (taken from [2])

Reprinted with permission of the American Institute of Aeronautics and Astronautics

It is important to make these comparisons between aircraft because when
comparing two fighter aircraft, for instance, the aircraft with the greater excess power at
the time will be able to control the engagement in air-to-air combat more freely. In
retrospect, each aircraft is then ultimately trying to drive the combat engagement to an
area where the pilot knows that their aircraft has the advantage in power and capability.
This fundamental principle is the reason why energy curves and excess power plots are so
carefully discussed when comparing the performance capabilities of one aircraft to

31

another. This information will be illustrated in more detail in a later section of this chapter.

The last important note from Bryson's work was that the optimal problem is not necessarily the exact case. The assumptions made to simplify a problem can sometimes show that the results become slightly skewed. Figure 2.10 shows how the assumptions that Bryson and Rutowski made can prove to provide inaccurate results.
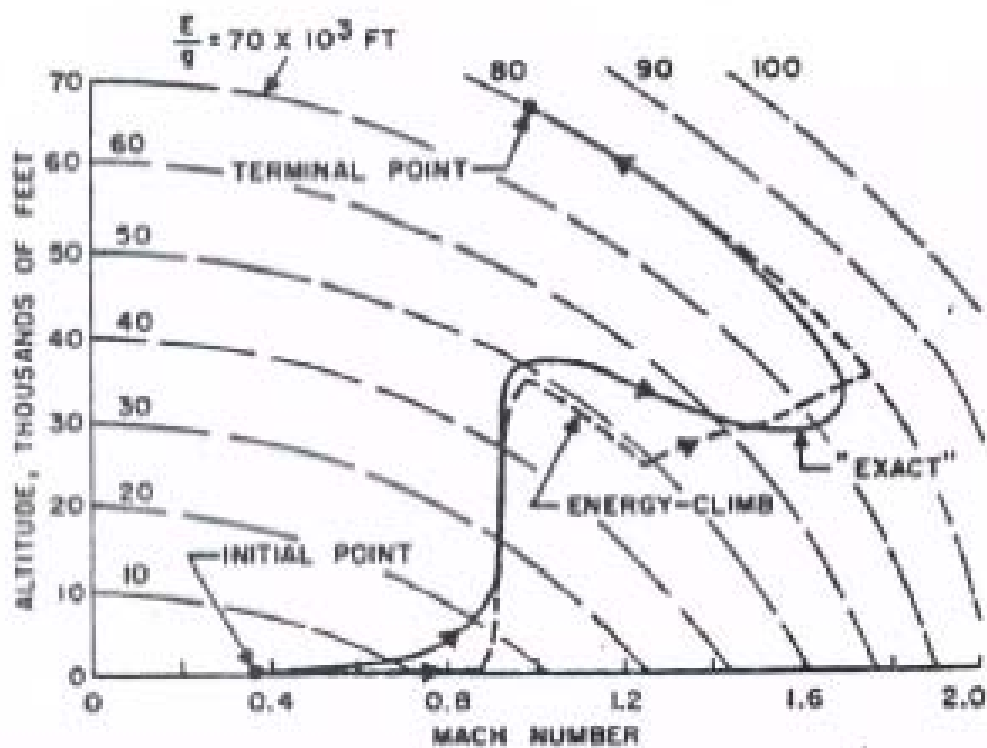
Figure 2.10: Comparison of the Exact and Energy-State Minimum Time-to-Climb Paths for Airplane 1 (taken from [2])

Reprinted with permission of the American Institute of Aeronautics and Astronautics

The primary assumption that is illustrated to be false here is that an aircraft, despite abilities in acceleration, cannot instantaneously accelerate and decelerate or change from climb to descent. There is some response time for the aircraft to make

adjustments in altitude and airspeed. The aircraft and pilot can anticipate an upcoming adjustment to Mach number or changes in altitude, but the aircraft does not in actuality respond instantaneously [2]. It is important that these minute errors, those due to the initial assumptions, are indicated because it is from this foundation that the experiment discussed in latter chapters will be based. The results from that experiment are invaluable without a proper understanding of the assumptions made throughout the programming and the research from which the dive prediction model was derived.

This research done by Rutowski and Bryson was the foundation behind this analysis. Their work provided much of the background mathematics that drove the model that was used for the dive planning sensitivity analysis. The comparison of one aircraft to another allows the users to visualize that one aircraft, possibly with greater engine power, can perform test maneuvers that another aircraft is incapable of attaining. The comparison of performance capabilities to energy curves and specific excess power plots allows for the determination of optimal climb conditions and minimum fuel climbs so that the flight test engineers can improve the efficiency of their flight test programs.

By decreasing fuel costs and the rate at which fuel is burned while the pilot approaches the starting point for a high-speed dive, not only is fuel saved, but the variations in the weight are minimized. By understanding the minimum time to climb problem with some clarity, the conditions of the atmosphere, such as temperature, are now consistent from the planning phase to the testing phase for each test run. The final concepts pointed out in the Bryson paper were important because by illustrating that an aircraft cannot in practicality exchange altitude for velocity instantaneously, the dive profiles that are predicted by the model may not be as accurate. The sensitivity

associated with the mathematics used to determine the dive profiles may cause a drop in
test efficiency as well.

2.2 Energy Height and its Relation to Power

Now that a thorough understanding where the concepts of energy theory
originated, it is important to understand why these notions are important. In order to
grasp this concept fully, it is important to look at several figures that illustrate where the
relationship between excess power and energy theory originates.

It has already been discussed that the total energy an aircraft has is derived from a
combination of its potential and kinetic energy. Referring back to Equation 2.1, the
description of total energy of an aircraft is given. However, by looking at the derivation
of that equation, the units and therefore the commonly accepted name, "energy height",
become apparent. By observing the combination of Equations 2.13 and 2.14, we can
obtain Equation 2.15.

$$P.E. = \frac{mg}{g_c} = W_{S.L.} h_{geopotential} \tag{2.13}$$

$$K.E. = \frac{1}{2}\frac{W}{g}V^2 \tag{2.14}$$

$$T.E. = P.E. + K.E. = Wh + \frac{1}{2}\frac{W}{g}V^2 \tag{2.15}$$

P.E., defined as the potential energy, is defined two ways in Equation 2.13. The
difference between weight, mg, or mass times gravity, and g_c, the gravity change
associated with position above the Earth, and the latter half of the equation is that weight
is now considered a constant at sea level, $W_{S.L.}$, but is corrected by the geopotential

34

altitude, or the altitude decrease as the aircraft is farther away from the center of the

Earth. The kinetic energy, K.E., defined by Equation 2.14 is taken directly from the

energy calculations earlier in this chapter. The total energy, T.E., is a combination of the

potential and kinetic energy, as was previously discussed, and is the definition for the

energy of an aircraft at a given altitude and velocity. Noting that all three of the

equations above are of identical units, dividing through by the weight will provide a new

expression for the total energy that is normalized by the weight of the vehicle. Therefore,

Equation 2.1 is derived and given the name "energy height". It is important to note that

in this field, there are several varying notations for the same terms. For this section,

Equation 2.1 will be rewritten in the form given by Equation 2.16 and with the following

variables:

$$E_h = h_t + \frac{V^2}{2g} \tag{2.16}$$

E_h, defined as the specific energy, or energy height, is a combination of the tape altitude,

h_t, and the velocity over twice the gravitational force of the Earth. The tape altitude is the

combination of the actual geometric altitude above the Earth with a correction factor for

temperature variation from standard day added to it. The equation above has the same

form and definition of Equation 2.1, but now the variables have been simplified so that

energy height is a combination of altitude and velocity squared over two times the

gravitational pull of the Earth. However, the benefit to using this form of the equation is

that it allows a much more simplified approach to understanding where energy curve

profiles originate. Figure 2.11 and 2.12 show examples of energy curves.
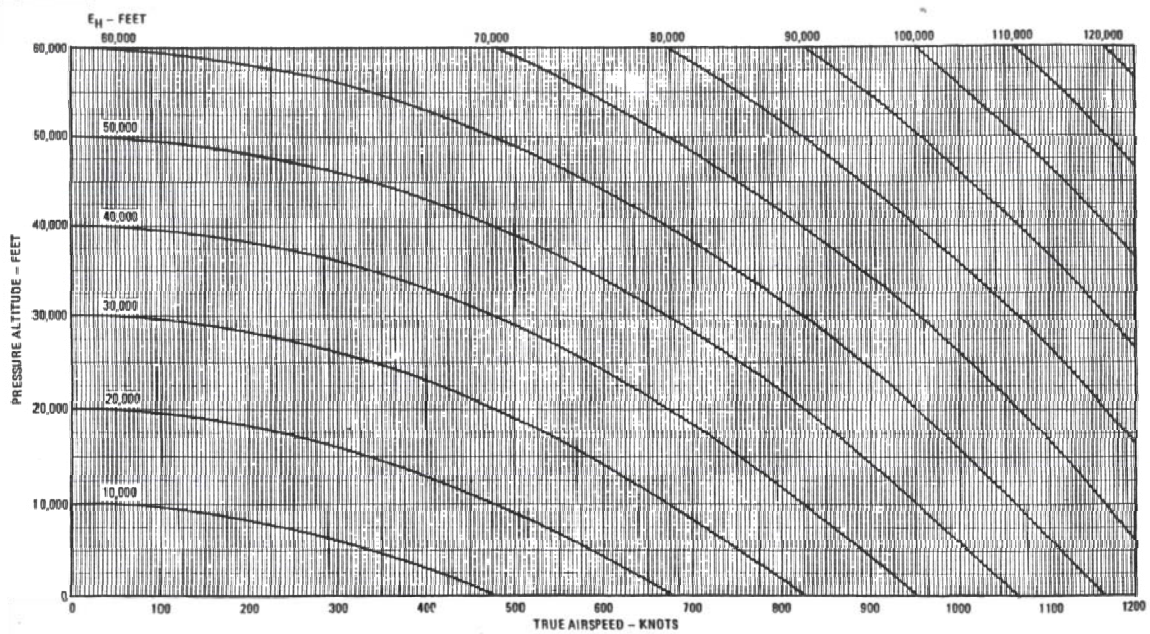
Figure 2.11: Lines of Constant Energy Height Plotted on Altitude versus True Airspeed
(taken from [14])
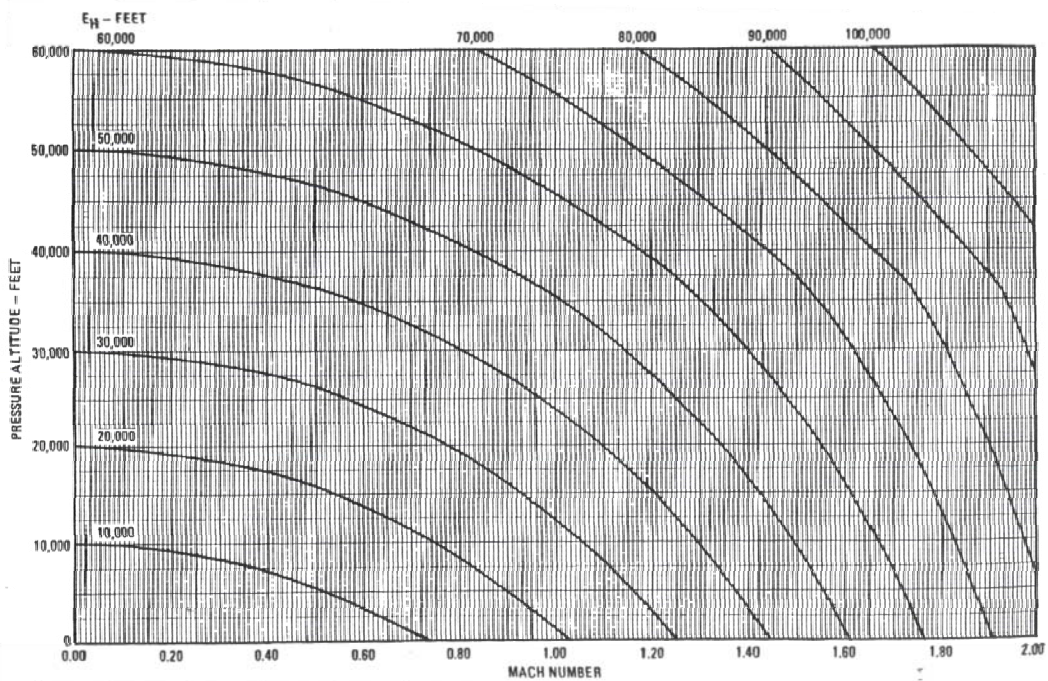
Figure 2.12: Lines of Constant Energy Height Plotted on Altitude versus Mach Number
(taken from [14])

It is important to illustrate here that these lines of constant energy height are parabolic for Figure 2.11. However, when comparing them to Figure 2.12 the lines are parabolic only above 36,089 feet where the standard day temperature remains constant. Note the sharp change in the slope of each curve is much more visible in Figure 2.12 at the higher altitudes and higher Mach numbers. This is caused by the relationship between velocity and Mach number. Equation 2.17 shows this relationship.

$$V \propto M \sqrt{T_a} \tag{2.17}$$

This proportionality is the cause behind this change in the shape of the energy height curves [14].

Once Equation 2.16 is differentiated with respect to time, as Rutowski illustrated, then specific energy is indicated. It was also shown through Rutowski's research that the key function to specific excess power was the difference between thrust available and thrust required. This difference, known as excess power when the velocity is multiplied through, varies for each aircraft based on its specific drag index, the thrust capability of its engines, and other parameters. By multiplying that equation by velocity and developing the relationship shown in Equation 2.18, which is by definition excess power.

$$P_S(W) = V(T - D) = VT - VD \tag{2.18}$$

From here, we can relate this equation back to Equation 2.3 from Rutowski's paper and now illustrate the more common notation for specific excess power once we divide Equation 2.18 by the weight of the aircraft.

$$P_S = \frac{d(E/W)}{dt} = \frac{V(T - D)}{W} = \frac{dh}{dt} + \frac{V}{g}\frac{dV}{dt} \tag{2.19}$$

The key factor to take from Equation 2.19 is that all the quantities are

instantaneous terms. The other important factor of specific excess power, P_S, is that it

can determine how quickly an aircraft can change its energy. This goes back to the

earlier mentioned concept of having an advantage over an adversary's aircraft by having

the ability to change one's energy level more rapidly or by having excess power in a

region where the adversary does not [14]. Figures 2.13 through 2.15 show the difference

in comparing aircraft.
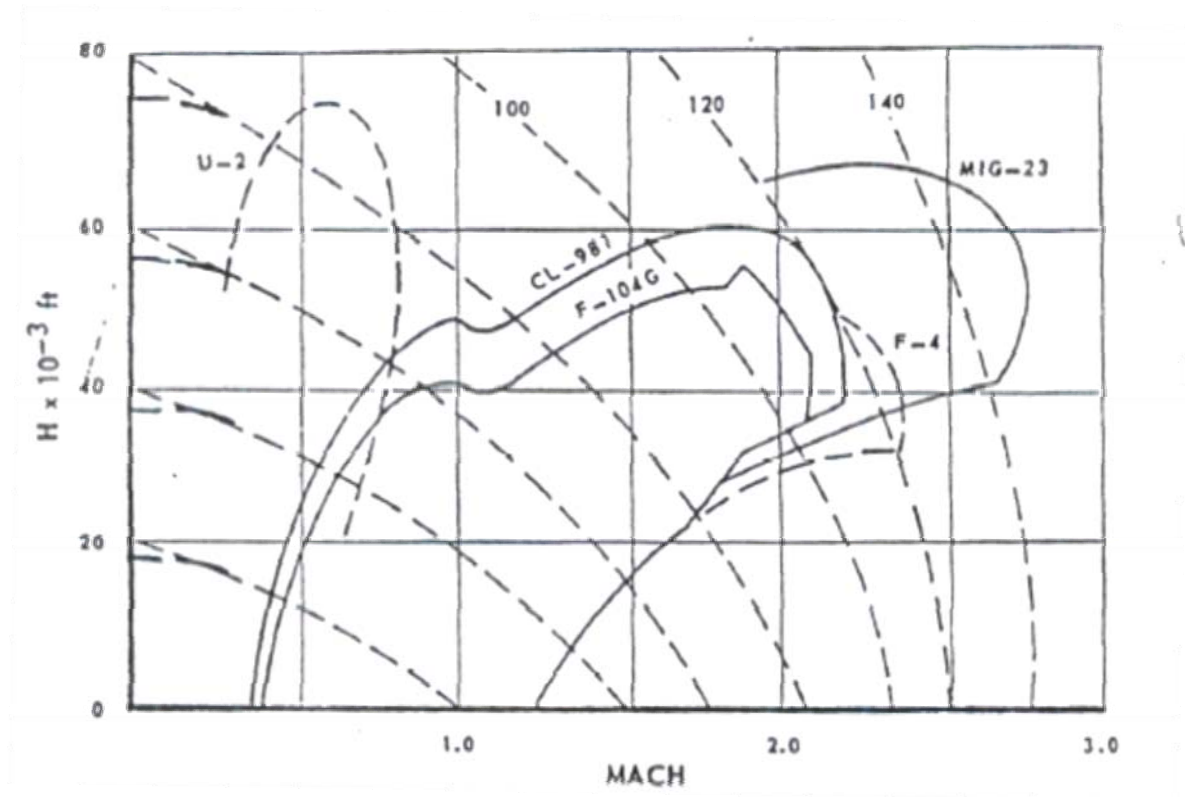
Figure 2.13: Steady State Operating Envelopes for Several Aircraft (taken from [6])

The first figure, Figure 2.13, shows several different aircraft operating envelopes.

Plotted on the axis of altitude versus Mach number, this plot includes the steady-state

performance envelopes for several different aircraft. Also plotted are the constant energy

38

curves shown as the dashed lines moving from the left to the bottom of the graph. This information can be very important in determining regions one aircraft can operate and another cannot. For instance, a U-2 has high altitude but low Mach number operating limits. So in order to avoid a confrontation with an F-4, the U-2 would merely need to climb to a higher altitude and reduce speed to keep the F-4 from having the ability to pursue. In just the opposite effect though, if the F-4 were being chased by a MiG-23, there is very little operating limits in which the F-4 would have an advantage. There are ways to defeat an aircraft that is outside another's performance limits through maneuvers such as a zoom climb, but for the steady-state case, this provides a crude illustration of the point. This leads into the discussion of Figure 2.14.
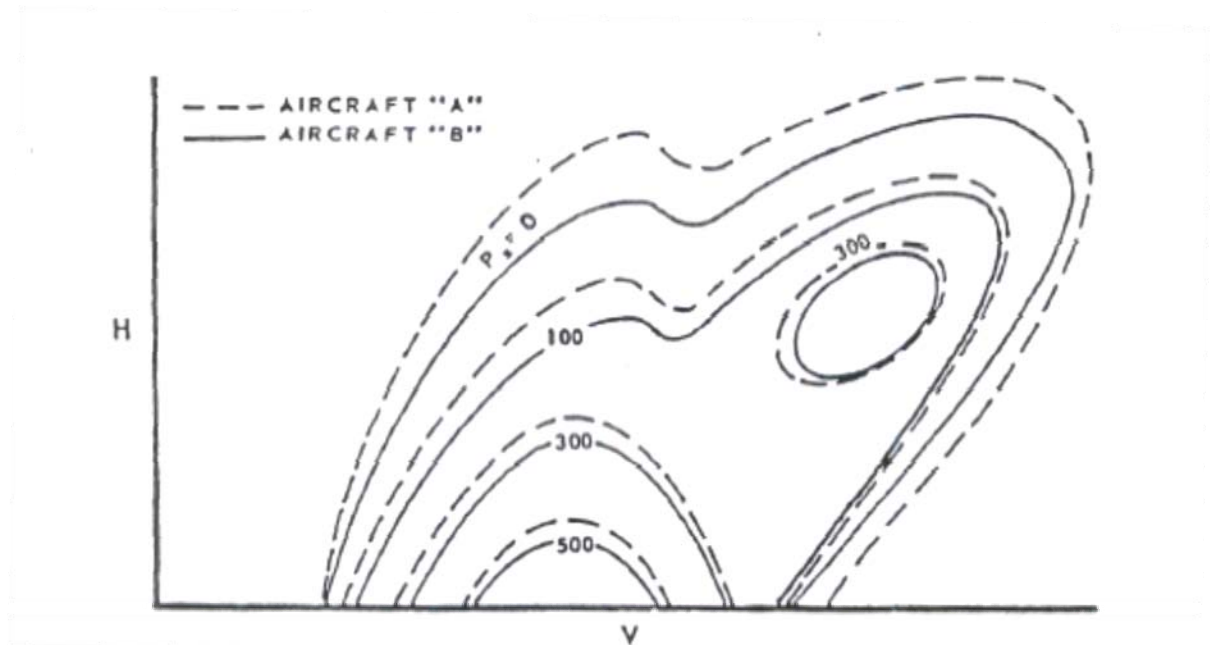
Figure 2.14: Specific Excess Power Overlays for Two Aircraft (taken from [6])

In Figure 2.14, there is an overlay of two aircraft: Aircraft A and Aircraft B. Plotted on a scale of altitude versus velocity, the two different aircraft's specific excess power curves are shown as either a dashed line or a solid line for Aircraft A and Aircraft B respectively. In every region of the flight envelope of Aircraft B, Aircraft A has the advantage. Understanding this information can then provide the pilot of Aircraft A with an understanding of what maneuvers to employ to defeat or overtake Aircraft B.
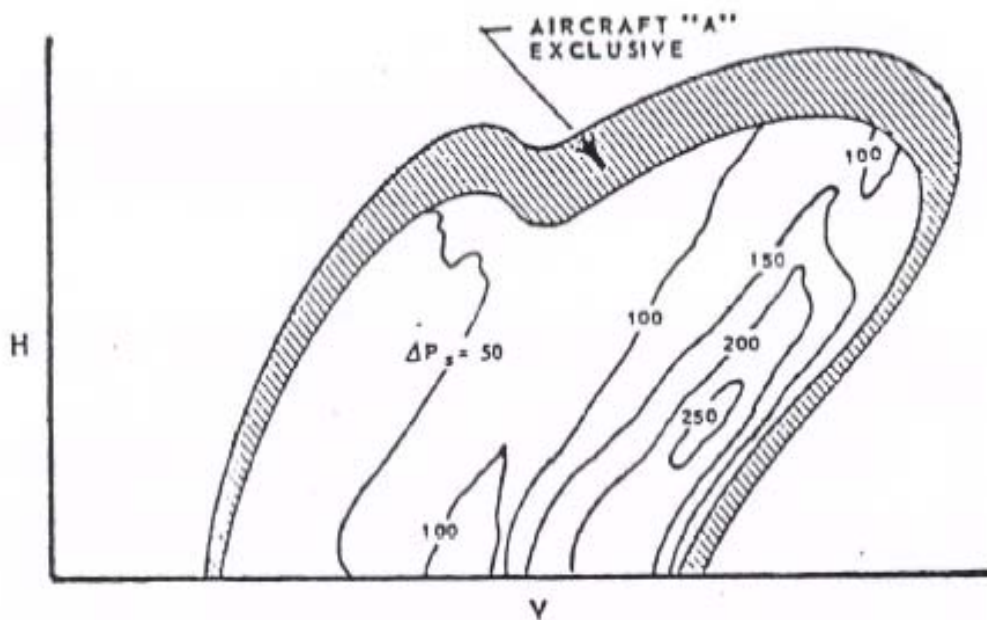
Figure 2.15: Differential Specific Excess Power Contours for Two Aircraft (taken from [6])

An even more efficient way of viewing this exact same information is through Figure 2.15. Here, the differential of the available excess power is contoured. Since there is no area where Aircraft B has the advantage, the pilot must attempt to maintain the combat within the smallest variation between the two aircraft. This will provide the pilot with the greatest chance to maneuver equally to the pilot of Aircraft A. The pilot of Aircraft A theoretically should be attempting to force the air-to-air conflict into the region where

there is the greatest disadvantage to pilot B. The region where the ΔP_S is the 250 feet per second would be pilot A's ideal combat region [6].

Relating specific excess power and specific energy of an aircraft can now be associated with its ability to maneuver. Understanding an aircraft's maneuverability based on its energy and power states, particularly those in a negative excess power region, can provide insight to an aircraft's ability to recover from a high-speed dive. This data can become invaluable toward the development of an accurate predictive model that can be used in flight test planning.

2.3 Relating Excess Power and Energy to Maneuverability

Once a clear understanding of excess power and its importance to flight is established, it is fundamental to relate these concepts to maneuverability of aircraft. The concepts previously mentioned, in particular those that are used to relate one aircraft to another, were organized by Lt. Col. John Boyd (U.S. Air Force) into a topic known as energy-maneuverability. Energy-maneuverability is basically the incorporation of energy management and how manipulations can be performed to maximize the capabilities and performance of a particular air vehicle. This same information can then be used to relate the performance of one aircraft to another using strictly the power and energy data [6].

Energy-maneuverability has since exploded into a vast field and now includes discussions on not only aircraft maneuverability and the comparison to other aircraft, but agility metrics and the establishment of agility metric flight tests. In a paper published in the Journal of Aircraft in 1992, the authors of "Fighter Agility Metrics, Research and Test" [7] indicated that these current metrics for establishing performance criteria for

41

aircraft only test individual energy states. The effort of the authors here was to show that it is crucial to show performance metrics on an aircraft's ability to change energy states as opposed to evaluate solely based on steady-state conditions.

These metrics, when properly applied, encompass more than just the traditional aircraft performance and maneuverability. These new metrics can include the transient capabilities of the aircraft as it maneuvers from one energy state to another. This becomes important in the comparison between two competing airframes. By providing data that would more accurately be representative of a combat maneuver, a fighter pilot in an air-to-air combat scenario can determine what maneuvers would provide the greatest advantage in either a steady-state or instantaneous envelope [7].

2.4 Maneuverability and the Need for Envelope Expansion

So the concepts of maneuverability are a useful tool to pilots and aircraft designers in order to develop the most advantageous aircraft possible. However, in reality, the structures and mechanics of the aircraft may not be able to withstand the aeroelastic principles that govern certain regions of the capable flight envelope. Since even as early as Langley's flights in 1903, flutter has been causing a serious problem for aircraft stability. A combination of the aerodynamic, elastic, and inertial forces, or dynamic aeroelasticity, acting on an airframe yields a flutter, buzz, or buffet type response when in the right combination. As Langley and many other early aircraft designers determined, this can be catastrophic to airframes [22].

2.4.1 Aeroelastic Disturbances and Flutter

Flutter, by definition, is the "unfortunate dynamic interaction between the aerodynamics and the structure of an aircraft" [15]. Similar to the static effects of aeroelastic divergence, flutter is merely the dynamic reaction of these forces. The figure below, Figure 2.16, shows the interaction of these forces and where the aeroelastic areas of concern are.
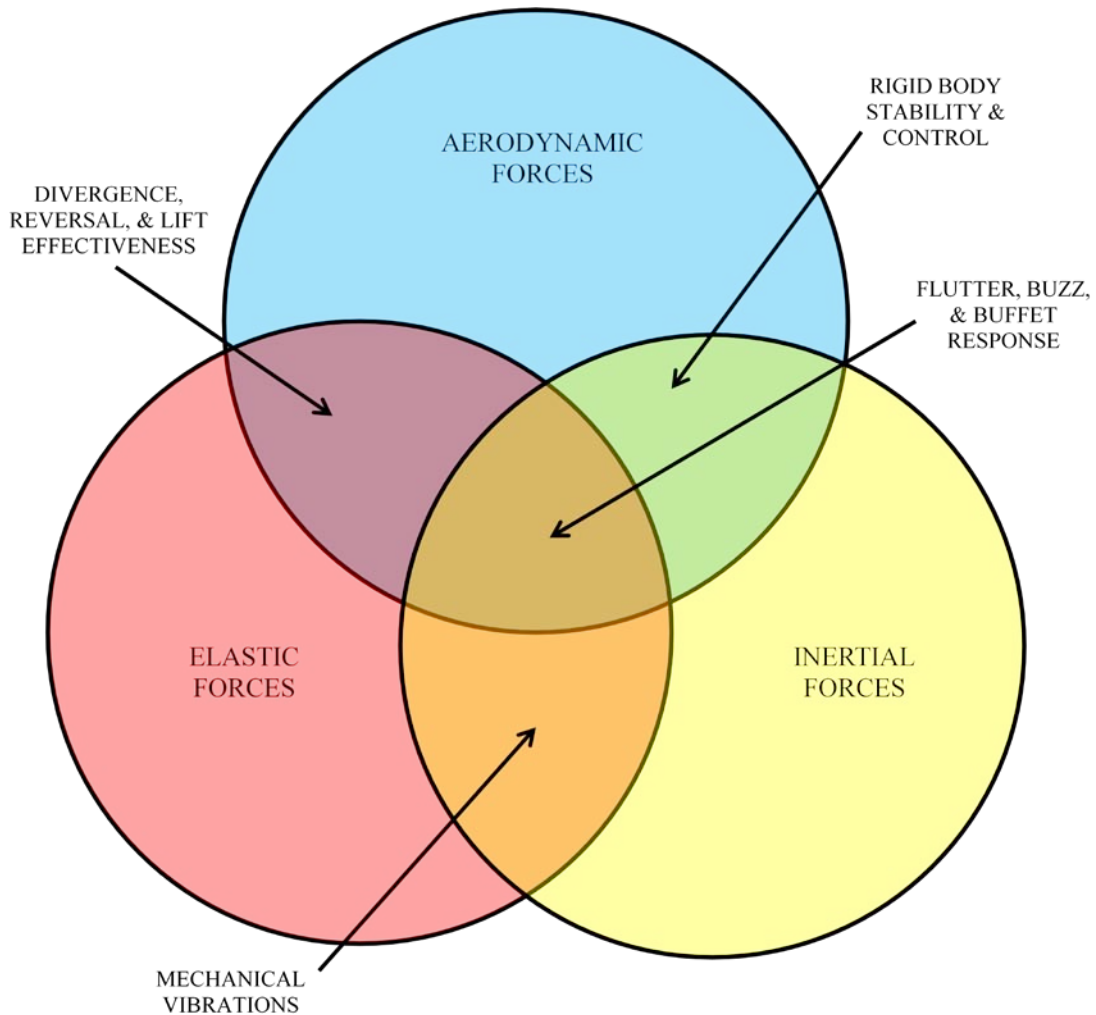
Figure 2.16: Aeroelastic Definitions (taken from [22, 24])

From Introduction to Flight Test Engineering, Vol. II by Don Ward, Thomas Strganac & Rob Niewoehner. Copyright © 2007. Reprinted by permission of Kendall Hunt Publishing Company

The red circle indicates the region of elastic forces, the yellow defines the inertial forces, and the blue circle defines the aerodynamic forces. The orange region is the interaction of the elastic and inertial forces and causes mechanical vibrations in the aircraft. The green region is a combination of aerodynamic and inertial forces and is the region where problems with rigid body stability and control can develop. The purple region defines the interaction between aerodynamic and elastic forces and is related to disturbances such as divergence, control surface reversal, and lift effectiveness changes. The brown region is defined as an interaction of all three forces. In this region, flutter, buzz, and buffet response can cause serious problems for the performance and operation of the aircraft.

The aeroelastic divergence is defined by an increase in the twisting of a surface which proportionally increases the angle of attack. The generated moment from this twisting is then proportional to the square of the flight speed creating a large moment that the elastic restoring forces of the wing are unable to overcome [12]. Flutter is the oscillatory instability is created by these increased moments and is driven into a state of resonance by two or more modes. The airfoil is in theory netting positive energy that has been extracted from the flow field around the structure and is using that energy to develop this self-excited oscillatory instability [22].

Raymer points out that most flutter modes are driven by improper balancing of control surfaces, but these flutter modes can be excited manually in a controlled environment to determine where a control surface may begin to flutter. This flutter, if it occurs in an unexpected flight condition, can quickly, and in some cases without warning, cause a complete structural failure of an aircraft surface [15]. It is because of this

possibility of complete failure that the need to establish an operational flutter boundary is so important to aircraft development.

Figure 2.17 shows how a plot of dynamic pressure (a variable related to equivalent airspeed) and Mach number create an area of safe operational flight.
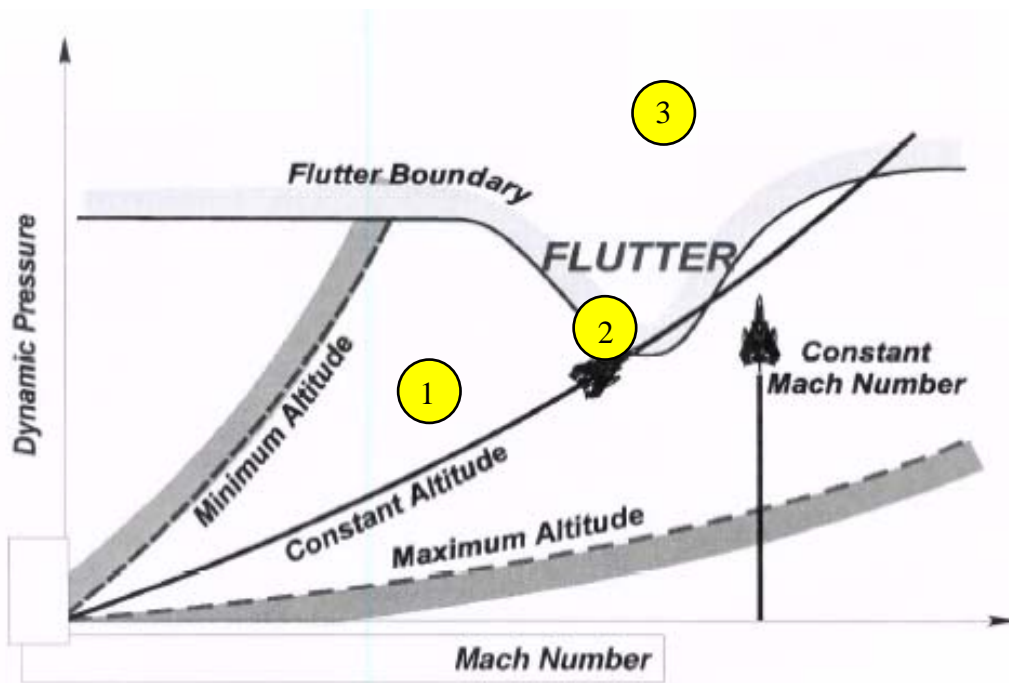
Figure 2.17: Plot of Theoretical Flutter Boundary (taken from [22, 24])

From Introduction to Flight Test Engineering, Vol. II by Don Ward, Thomas Strganac & Rob Niewoehner. Copyright © 2007. Reprinted by permission of Kendall Hunt Publishing Company

Although each aircraft will have its own established flutter boundaries, aircraft designers cannot initially establish these points. This becomes vital to airframe survivability. If a pilot enters a maneuver, whether in testing or operation, the onset of flutter at the any control surface can cause the aircraft performance to quickly deteriorate. Figure 2.17 shows how the lines of constant Mach number and lines of constant altitude are portrayed

on this figure. The flutter boundary, the area of oscillatory instability, is the region of concern. The three points, labeled 1, 2, and 3 on the figure will be discussed with the use of the three figures below.

Figure 2.18 through Figure 2.20 show the computer predictions for the oscillatory effects that an excited mode can have on each region of the flight envelope.
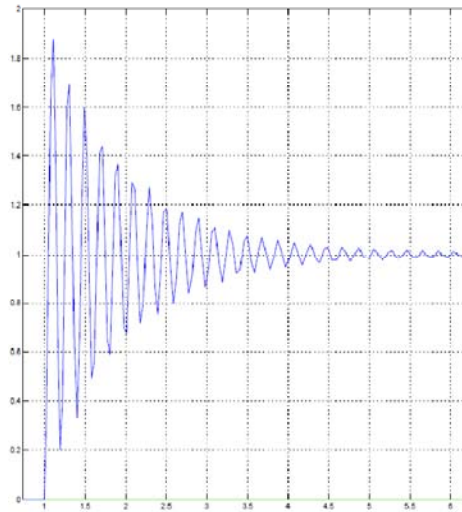
Figure 2.18: Flutter Excitement Response in a Stable Flight Region (taken from [22])
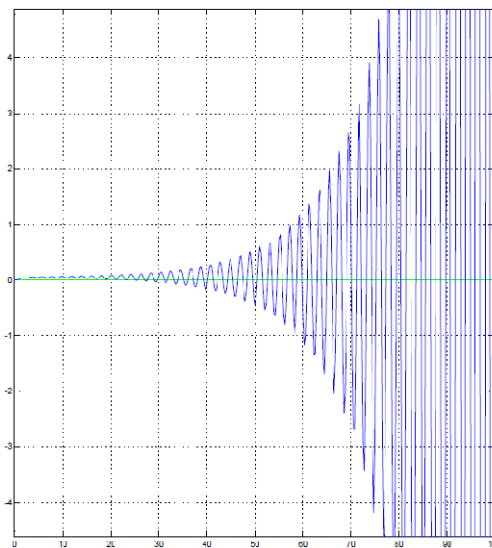
Figure 2.19: Flutter Excitement Response in an Unstable Flight Region
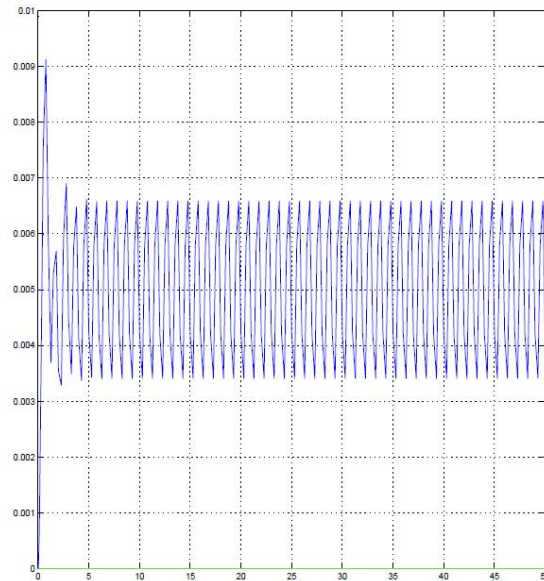
Figure 2.20: Flutter Excitement in the Flutter Boundary Region Causing a Limit Cycle Oscillation (LCO) (taken from [22])

When the aircraft is located in area 1 from Figure 2.17 the response of an excited flutter mode can be illustrated by Figure 2.18. It can be noted that the oscillatory motion still exists, but the elastic forces of the wing can quickly dampen out the excitement. Area 2 on Figure 2.17 relates to Figure 2.19. Here the oscillatory motion, once excited (either by the pilot or by an aerodynamic turbulence), quickly gains amplitude and in most cases will be unrecoverable. Region 3 on Figure 2.17 relates to Figure 2.20. Here is where the pilot would cross the flutter boundary region and transition from the stable to the unstable condition. It is in this transition region that limit cycle oscillations can occur [22].

Limit cycle oscillations in non-linear systems are defined as self-excited oscillations. It is important to make this association of a limit cycle oscillation and a non-linear system because in practical applications, there are no truly linear systems. Although assumptions can be made to linearize the outputs of a particular system, a non-

linear analytical approach is most relevant to obtaining a more accurate solution. These oscillations can be completely independent of the initial disturbance and the amplitude of the oscillation is often independent of the initial conditions. Although flutter is just one type of limit cycle oscillation, they can occur in several different fields of study [20].

Returning the focus to flutter, there is a particular region where flutter excitement is more prevalent than other regions. This region is known as the flutter bucket. Figure 2.21 shows several aeroelastic regions of instability.
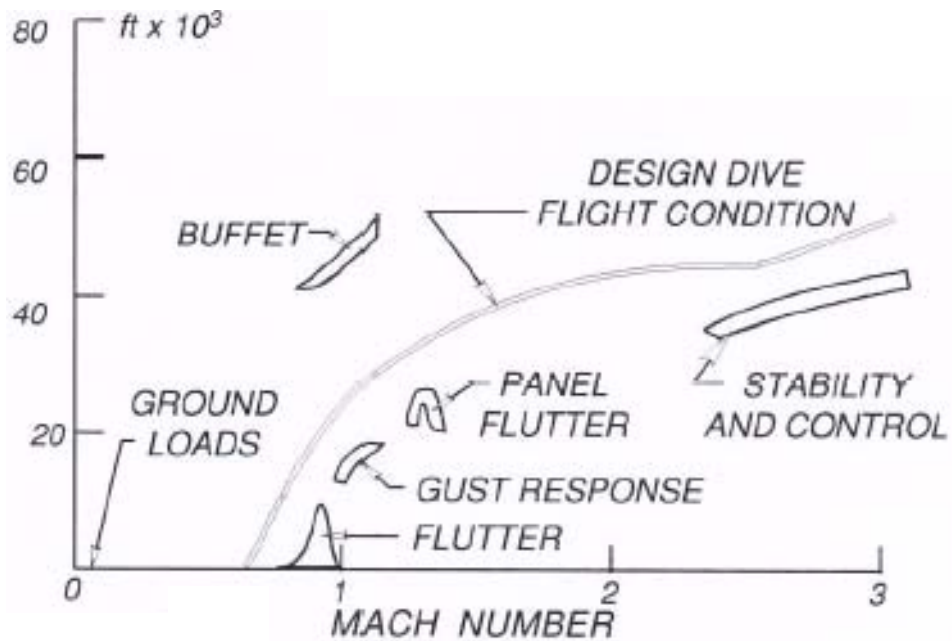
Figure 2.21: Regions of Aeroelastic Instability (taken from [22])

In this figure, plotted on the axes of altitude versus Mach number, the regions of aeroelastic instability are shown. The point of this figure is to illustrate regions in the flight envelope where the instabilities illustrated in Figure 2.16 actually occur. For this discussion, the region of greatest concern is the flutter region located around the Mach

1.0 point. This transonic region of the flight envelope often proves to be the most dangerous area for flight operations because of the increased probability of crossing a flutter boundary. This spike in the flutter boundary is known as a flutter bucket [22].

The flutter bucket is a region of the flutter boundary where there is an extremely high probability at lower altitudes for flutter to occur, in particular around the transonic flight region. Figure 2.17 shows this region when comparing a dynamic pressure to Mach number plot. The dip in the flutter boundary is the area of greatest concern. Figure 2.22, shows a predicted flutter region for the X-29A prototype aircraft [22].
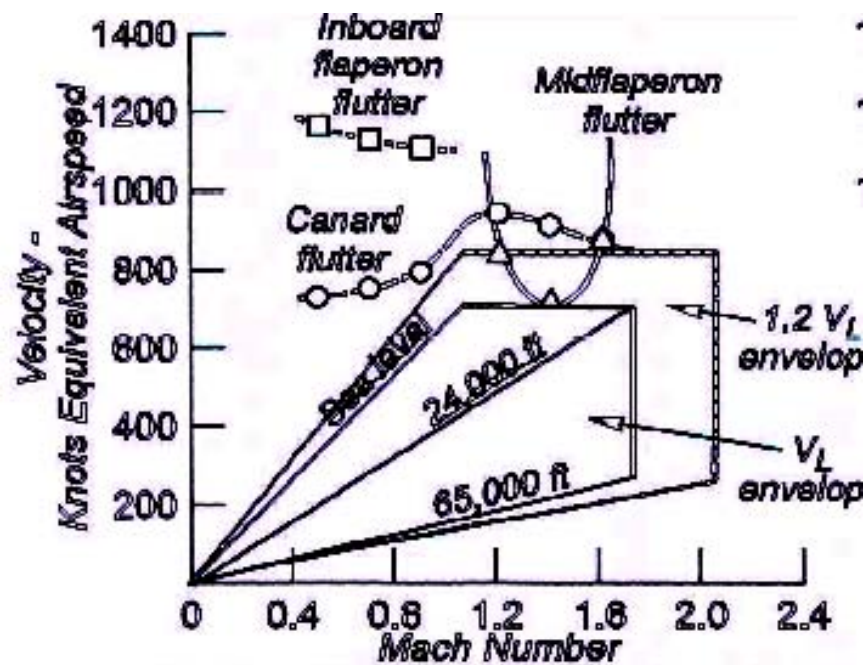
Figure 2.22: Predicted Symmetric Flutter Boundaries for X-29A (taken from [22, 24])

Plotting velocity in knots equivalent airspeed versus Mach number, the flight envelope can be clearly seen as the pyramid extending from the origin. According to the

Federal Aviation Administration Advisory Circulars (AC23-19A: 23.629) and one of the

Military Specification manuals (MIL-A-8870C), a required extension of this envelope of

at least fifteen percent must be cleared as flutter free. This expanded envelope is shown

as the larger pyramid extending from the origin. The curves above and crossing into the

pyramids show the flutter boundaries for different control surfaces on the X-29. This

figure illustrates how different control surfaces can have a greater influence on the flutter

characteristics depending on the given flight conditions. The boxed region bounded by

solid lines indicates the altitude-velocity envelope. The dashed line indicates the flight

envelope with a twenty percent (20%) boundary for an included safety factor. The lines

labeled with a control surface indicate the individual flutter boundaries for each control

surface. Here it can be seen that the most critical flutter boundary for an engineer and

test pilot to be aware of is the mid-flaperon. The other control surfaces all have predicted

flutter boundaries outside the safety envelope.

2.4.2 Requirement for Envelope Expansion Techniques

Because the regions of flutter are so hazardous to aircraft survivability,

particularly in unexpected or high-stress maneuvers (such as air-to-air combat), a method

to determine a safe operational envelope must be established. The aircraft designers can

establish the structural limits in regards to the maximum altitude for the engines to

generate the required thrust and the maximum velocity the airframe structure can

maintain, but these regions may not necessarily take into account the flutter boundary.

However, it is through the method of envelope expansion that a cleared flight envelope

can be established [22].

Envelope expansion techniques start with the predicted flight envelope. Figure

2.23 shows a flight envelope for the F-18 HARV test vehicle. This figure plots altitude

versus knots of calibrated airspeed. The solid line curves running from top to bottom

indicate lines of constant Mach. The hashed line starting on the curve of Mach 2.0

indicates the predicted flight envelope for the F-18 HARV vehicle. The region enclosed

by the dashed lines is illustrating the transonic region of the flight envelope and the area

of most concern for flutter testing, particularly at lower altitudes. The circles indicate

possible test points for flutter envelope expansion and verification.
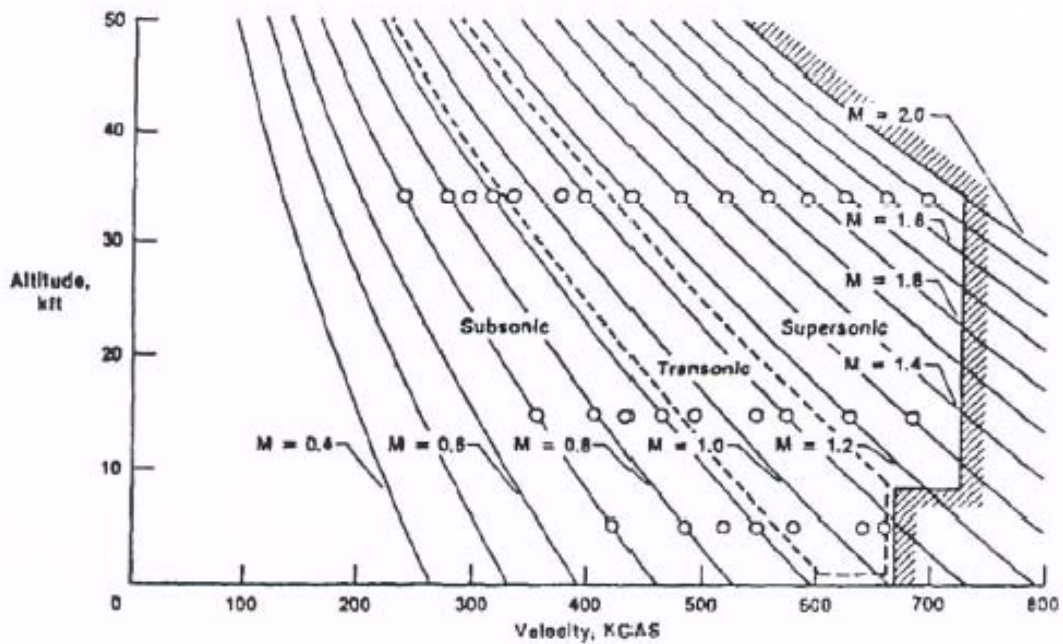
Figure 2.23: Analytically Predicted Flight Envelope Restrictions (taken from [22])

The flight envelope illustrated in the figure above takes into account the

maximum design altitude, maximum design Mach number, and maximum design

airspeed, or KCAS. From this design envelope, the engineers in charge of predictive

flutter modeling place limits on the flight envelope in regions that are most likely prone

to flutter. In Figure 2.23, that restriction is located at the flight envelope bump near 650 KCAS and under 10,000 feet altitude.

From here, it is the responsibility of the flight test team to determine the actual flutter boundary through a rigorous flight test program. Although the ultimate goal is to determine the flutter-free region without ever approaching a flutter boundary, not all predicted flight envelopes will match up with their test profiles. Figure 2.24 shows a typical flutter test profile [24].
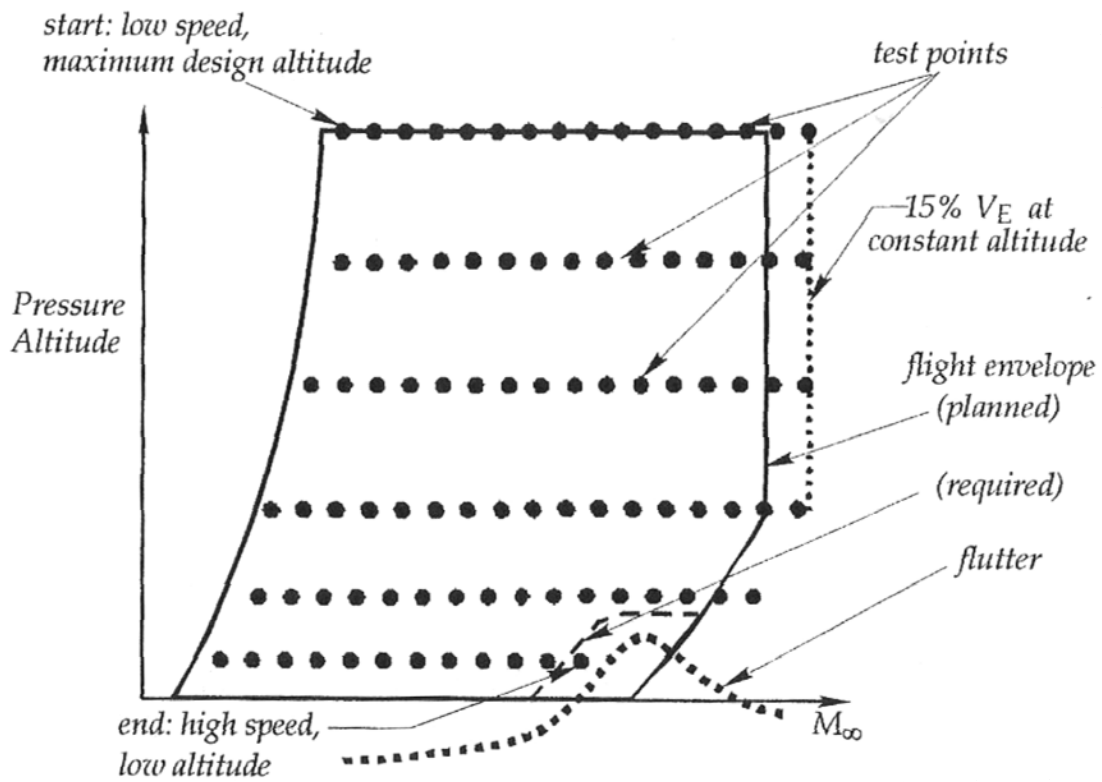
Figure 2.24: Typical Flutter Test Profile (taken from [24])

Moving in incremental steps of increasing Mach number and incremental steps in decreasing altitude, the test program runs several points in regions that are predicted to be of high concern. Based on the information from Figure 2.17, it is understood that the majority of the testing should be conducted near the transonic region. From here, the engineers can establish a "cleared flight envelope" where the pilot is free to perform nearly all maneuvers without fear of causing unexpected flutter oscillations. Figure 2.25 shows this new flight envelope. Notice the shift of the KCAS envelope limit above 10,000 feet as compared to Figure 2.23 [22].
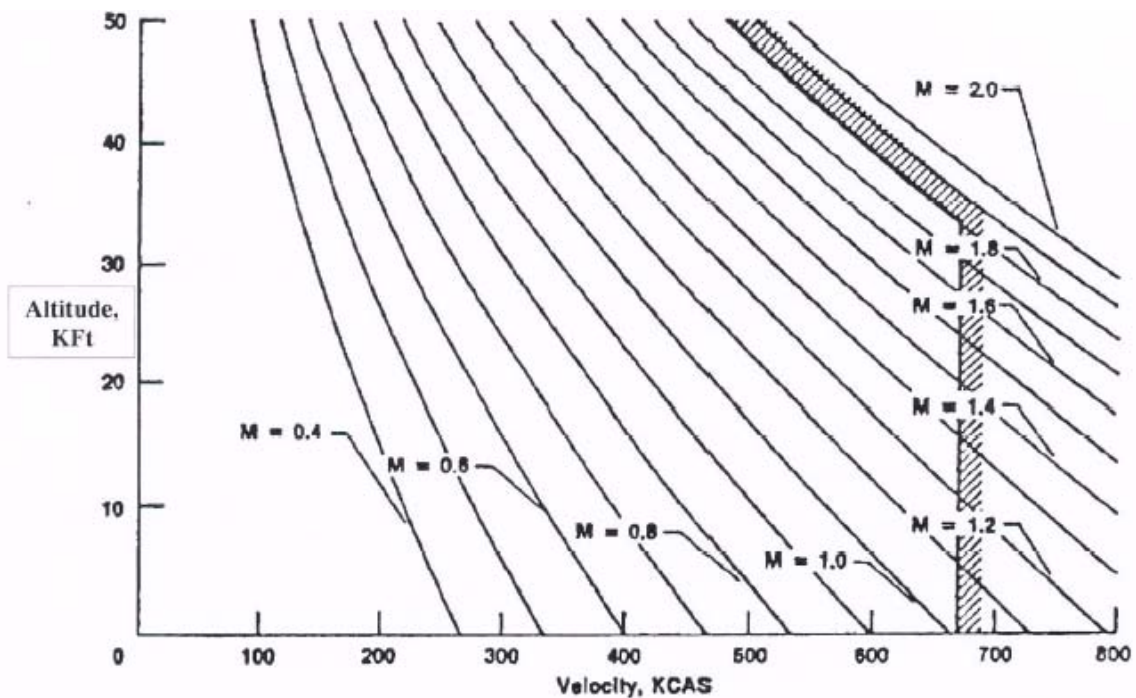
Figure 2.25: F-18 HARV Test Vehicle Clear Flight Envelope (taken from [22])

2.5 Flight Envelope Expansion and Negative Excess Power

In theory, the concept of flight envelope expansion appears straight forward. And for a clean, low drag aircraft, the testing procedures typically will provide little

complications. However, there is an important concern when external stores are added to the aircraft. In military aircraft in particular, certain weapons and fuel stores can completely change the operational flight envelope for the aircraft. The mass added to the wings from different munitions can even change the flutter characteristics.

Therefore, with an increased drag index from external stores and the requirement to still test the aircraft at the fifteen percent (or twenty depending on military or civilian rules) expanded flight envelope, required by military specifications, some flight test points are unobtainable through steady-level flight. Therefore, in order to achieve the required velocity at the required altitude, the pilot must conduct a high-speed dive. These dives are located in the negative excess power region of the flight envelope.

The discussion earlier in regards to the importance of understanding specific excess power now becomes equally significant. All previous discussion has been in regards to positive specific excess power. Negative excess power, still referenced in units of feet per second, is the region of flight where the aircraft will lose energy during a planned maneuver. In order to reach a test point, the pilot must dive through several energy height levels and increase kinetic energy at a faster rate than the potential energy is being lost.

When the pilot reaches the given test point, then the flutter modes can be excited. There are several problems associated with this type of flight testing, however. In many cases, the pilot may not be able to reach the required velocity without an accurate prediction of the necessary dive angle. Since the pilot is starting the dive at zero excess power, meaning the aircraft is traveling at the maximum attainable velocity, V_{max} (typically for fighter aircraft at full afterburner as well), there is a high cost associated

with the burning of fuel and time required to set up a dive. Some test points may require several dives before the test point is reached and useful data can be collected. This is a wasteful use of resources and assets, particularly if there are several test points in the negative excess power region.

Other associated problems with negative excess power flight testing involve high velocity descent rates. If a dive angle is exceptionally steep and the test point is at low altitude (as most concerning flutter envelope expansion test points are), then the pilot is at an extremely high risk to himself/herself and the aircraft. Another issue of concern is in regards to the time spent conducting each test and the variations associated with each test point. An aircraft at full afterburner is consuming massive amounts of fuel very rapidly. This change in the weight of the aircraft, although it will be assumed to be constant for simplification purposes, is anything but consistent from test to test. These inconsistencies require accurate and precise calculations to determine the necessary dive angles and starting conditions to run the fewest number of dives for each required test point [24].

2.5.1 Predicting Flutter Boundaries

One way to eliminate the need for excessive testing and unnecessary test points is by accurately predicting the location of the flutter boundaries that need to be tested. By knowing the location of these boundaries with some precision, test pilots and engineers can start evaluating test points closer where they believe the boundary will start. By eliminating test points, the engineers can save time and resources. There are five primary methods for determining flutter speeds.

55

The first of these methods is based on extrapolating damping trends. This is the most widely used method and requires no consideration of theoretical predictions. This data-based method relies completely on the analysis of flight data from the values of the modal damping ratios. The primary set back is that extraction of the modal damping sometimes contains low signal-to-noise ratios. This aeroelastic flight data must then be filtered using somewhat complicated techniques.

The next method for flutter speed predictions is by using envelope functions. This method, similar to the previous one, uses flight data analysis from impulse excitation. The measurements are made in the time-domain. The primary difference between these first two methods is the envelope function does not directly require estimates of modal damping. Rather, the envelope function method determines the damping from the impulse response and as the damping decreases, the probability of flutter onset increases, thus establishing the flutter boundary. However, the primary set back is that the amplitude used to establish the damping is based on the impulse fed into the system and an inaccurate measurement of that impulse (or an impulse assisted by atmospheric turbulence) can affect the results.

The third method is known as the Zimmerman-Weissenburger Margin. Another data-based method, the flutter margin method uses information about the poles of the transfer functions calculated from the flight data. In short, the method considers the characteristic equation governing the aeroelastic system. Using the Routh stability criterion, it can be determined if the flutter margin of the system is either stable or unstable. Unfortunately, this method may give insight into the flutter margin stability and instability, but it is not necessarily valuable in predicting flutter onset.

The fourth method is by use of a flutterometer. This tool, still under some research as to its effectiveness, approaches the problem in a completely different manner by using a model-based approach to determining the flutter boundary. By comparing both flight data and theoretical models, the flutterometer can predict the onset of flutter. After computing a robust flutter speed for every test point, the flutterometer can take an introduced uncertainty from a theoretical transfer function and produce a realistic flutter speed. This realistic speed is therefore significantly more beneficial than a theoretical prediction because the incorporation of the flight data provides a more accurate flutter speed calculation.

The last method is a discrete-time autoregressive moving average (ARMA) model. This method again uses a data-based approach but takes measurements from the response the system has to random excitation collected by the on-board sensors. The primary benefit of this method is that it does not require an excitation by the user, but the disadvantage of this system is that random atmospheric turbulence may not excite all of the modes of the system leaving some areas unevaluated [8].

2.5.2 Predicting High-speed Dive Angles

Once the flutter speed boundaries have been accurately predicted, the envelope expansion flight testing can begin to take place. Although the scope of this paper focuses on the test points that are located in the negative excess power region of the flight envelope, there are many test points that still are evaluated at steady-level flight conditions. However, when dealing with test points achievable only through an increase

57

in negative excess power, high-speed dive angles and starting flight conditions must be accurately predicted.

Most starting conditions were obtained using energy height analysis to predict a starting energy level so that a theoretical dive could be conducted to achieve the desired test point. Major Douglas Wickert (U.S. Air Force) developed and illustrated in his paper the ability to predict dive starting conditions through flight path angle theory [25]. Using some simple geometry to start, Wickert related flight path angle (or in the case of a high-speed dive the dive angle) to vertical descent rate and true airspeed. By using Figure 2.26, Wickert was able to derive Equation 2.20, shown below.
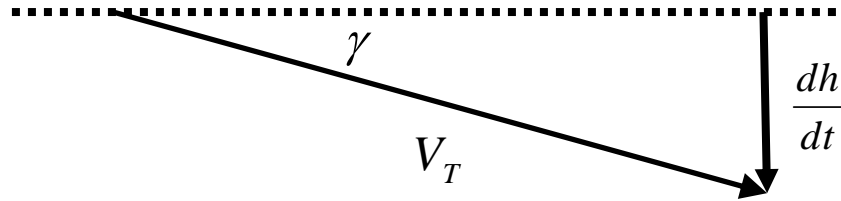
Figure 2.26: Flight Path Angle Geometry (taken from [25])

$$\sin(\gamma) = \frac{1}{V_T} \frac{dh}{dt} \tag{2.20}$$

By taking the equation from Rutowski's work, Wickert was able to relate Equation 2.20 to Equation 2.19. By equating the sine of the flight path angle, γ, to the inverse of the velocity, V_T, multiplied by a differential change in altitude, $\frac{dh}{dt}$, the equation below could be developed.

$$P_S = \frac{dh}{dt} + \frac{V}{g} \frac{dV}{dt} = \frac{dh}{dt}\left(1 + \frac{V}{g} \frac{dV}{dh}\right) = V_T \sin(\gamma)\left(1 + \frac{V}{g} \frac{dV}{dh}\right) \tag{2.21}$$

58

Equation 2.21 is a combination and substitution between the two previous equations. The

specific excess power, P$_S$, is equivalent to the differential change in altitude plus the

velocity over gravity times a differential acceleration, $\dfrac{dV}{dt}$. Through substitution and the

creation of a variable $\dfrac{dV}{dh}$, the differential change of velocity per unit altitude (or a

differential vertical acceleration), can ultimately define the specific excess power as a

function of the flight path angle, vertical acceleration, and velocity. Now, solving for the

flight path angle, Equation 2.22 is derived.

$$\gamma = \sin^{-1}\left(\frac{P_{S_{Test}}}{V_T\left(1 + \dfrac{V_T}{g}\dfrac{dV_T}{dh}\right)} \right) \tag{2.22}$$

Equation 2.22 solves for the flight path angle and defines the test point specific excess

power, $P_{S_{Test}}$. Wickert makes some other simplifications and modifications in his work to

allow him to use the book values of P$_S$, values of specific excess power gathered from

previous calculations and flight tests, by using the ratio shown in Equation 2.23.

$$P_{S_{Test}} = \frac{W_{Book}}{W_{Test}} P_{S_{Book}} \tag{2.23}$$

Creating this relationship allows the calculations for the excess power values much

simpler and does not require previously recorded flight data in order to make predictions

about the necessary flight path angle. The ratio between book weight and test weight,

$\dfrac{W_{Book}}{W_{Test}}$, makes an adjustment to the book values for P$_S$ for the difference between the

listed weight of an aircraft and the weight at the test point. Through this set of equations,

the maximum attainable velocity, or in some cases the desired velocity, can be obtained by solving for the terminal speed given a specific flight path angle.

Once the flight path angle has been determined, Equation 2.20 can be rewritten and the time in the altitude band can be calculated using Equation 2.24 [25].

$$\Delta t_{Band} = \frac{\Delta h_{Band}}{V_T \sin(\gamma)} \tag{2.24}$$

The time spent in the test window is defined as the symbol, Δt_{Band}, and is equivalent to the altitude tolerance, Δh_{Band}, over the velocity times the sine of the flight path angle. Based on standard flight test methods, altitude bands are typically plus or minus 1,000 feet [24].

2.5.3 Flight Path Angle and Negative Excess Power Data

As the analysis for the dive angle, or flight path angle, has been determined, the question is now raised in regards to the determination of the negative excess power data, either at the test point or from a book. Most technical orders include a lot of excess power data when P_S is positive for various configurations, altitudes, and settings. However, when dealing with negative excess power data, the technical orders only provide idle power deceleration data. This data provides little information for entering a high-speed dive at full throttle conditions.

The typical method for obtaining negative excess power data is through a method of extrapolation. Negative excess power data can be extrapolated using theoretical foundations relating drag indices to positive excess power data and understanding that high altitude P_S values are typically greater than lower altitude P_S values. Although using

flight test data is the ideal solution, many airframes do not have enough data in this region of the flight envelope that is publically available for different test programs to utilize. And the last technique that is often used is modeling of flight test performance results from previous aircraft that can be used to generate performance data for the aircraft in question. However, the primary method used by the sponsor is extrapolation [25].

2.6 Current Modeling Techniques

Once all this data is collected and a formula for the prediction of flight path angles in negative excess power regions of the flight envelope is developed, the equations can be written into a program to output desired results. For most high performance aircraft, tables of positive and negative excess power data have been collected from years of testing, both developmental and operational. So for many instances, the modeling technique in use is simply an Excel spreadsheet. A group from the Warfighter Readiness Research Division of the Air Force Research Lab (AFRL) used such a spreadsheet to combine thrust, weight, drag, load factor, wing area, Mach number, and dynamic pressure to output accurate P_S data.

Once this data is collected and organized, it is easy to manipulate changes in configuration and load factors to develop new excess power tables. Table 2.1 shows one of these specific excess power tables [13].

Table 2.1: Sample Specific Excess Power (ft/s) at n=1 (taken from [13])

Mach	Sea Level	10K feet	20K feet	30K feet	40K feet
0.6	-37	-162	-315	-525	-860
0.7	206	65	-65	-213	-420
0.8	405	226	76	-70	-246
0.9	599	376	190	32	-142
1.0	776	532	301	116	-62
1.1	946	691	410	193	6
1.2	1061	831	538	283	78
1.3	1118	966	671	374	149
1.4	1165	1114	843	502	237
1.5	1139	1258	1026	640	330
1.6	1068	1381	1153	807	444
1.7	950	1495	1277	986	566
1.8	834	1515	1361	1078	734
1.9	-1538	1509	1433	1167	832
2.0	-1885	1332	1375	1215	889
2.1	-2281	-1530	1287	1252	940
2.2	-2730	-1829	1217	1201	940
2.3	-3234	-2165	1042	1130	930
2.4	-3798	-2540	-1642	1059	869
2.5	-4424	-2957	-1909	884	827
2.6	-5116	-3418	-2204	528	674
2.7	-5876	-3924	-2528	128	498
2.8	-6709	-4479	-2883	-1807	-1125
2.9	-7617	-5084	-3271	-2047	-1270

These types of charts allow for a visualization of the negative excess power data and the velocities and altitudes where negative excess power conditions exist. The green areas indicate the regions where the specific excess power is negative and a test point at the given Mach number and altitude would require a high-speed dive plan to achieve the test conditions. This sample table is only for a certain engine type and for a load factor of

one. Different load factors will generate different tables and all this data must be present

for the proper determination of flight test conditions.

Once these charts are developed for each necessary flight condition, the

appropriate flight path or dive angle can be interpreted and the starting flight conditions

can be determined.   With this theory and background, now discussed in detail, the set up

for the analysis can begin. Chapter 3 focuses on the initialization of the model and the

procedures for the reproduction of the experiment. Understanding the fundamental

equations driving the model and the methods used to develop the Dive Planning model

were crucial to a successful test and discussion of results. It is important to keep in mind

throughout the next few chapters that the goal of this analysis was for an improvement of

safety and efficiency in flight testing. Determining the parameters responsible for driving

the responses is critical. These results can indicate test runs that have inherent safety or

efficiency concerns based on knowledge of the input variables and their accuracy and

precision, rather than on operator and pilot experience from past flight test trials.

III. Methods for Research

This chapter documents and discusses the experimental design in further detail to include the MATLAB program that was used as well as the method in which the research will be conducted. This chapter will also illustrate changes and modifications that were made to the original program and then discuss some of the inherent uncertainties that drove the research. Those uncertainties will play an important part in the reasoning behind the sensitivity analysis and a section of this chapter will deal with the desired results that the sensitivity analysis will provide.

3.1 Discussion of the Original Model

The concept to take Wickert's research and develop a working model came from Captain Benjamin E. George, U.S. Air Force. George worked to develop the original program using MATLAB, a high-level technical computing language. The software program is designed to solve mathematical computational problems with a more user friendly interface than would be possible using alternative programming languages such as C, C++, and Fortran [9]. George chose to use this software platform for the dive angle prediction software because of its ability to allow a user to build custom graphical user interfaces as well as integrate a variety of mathematical functions to utilize the best visualization of the data computed.

George wrote the original programming in 2006 for use by the Fortieth (40th) Flight Test Squadron (FLTS) operating out of Eglin Air Force Base, Florida. With the help of several other programmers, the dive angle prediction program was updated to its current version, Version 2.2. In 2008, Lieutenant Mark Gabbard, U.S. Air Force,

developed a graphical user interface (GUI) to run over top of the program providing an easier use by future operators. The users have since come to name the program Dive Planning and have developed comprehensive P_S tables and a help file to accompany George's original program.

The program has the P_S data to operate for several different types of aircraft. This gives the users the opportunity to run flutter envelope expansion tests for the F-15C, the F-15E, two variants of the F-16 (based on engine selection), and two variants of the A-10 as well. The primary GUI, shown below in Figure 3.1, allows for the selection of the aircraft type, inputs about the Mission, as well as aircraft information regarding configuration of the external stores, drag index, and gross weight.
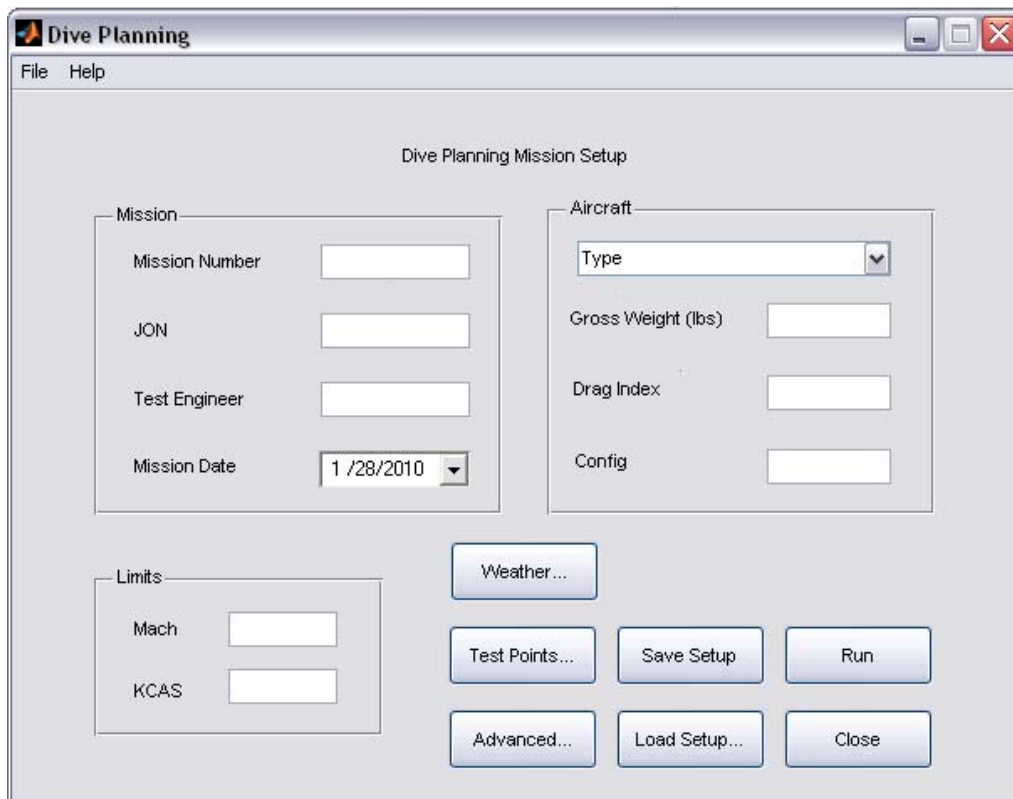
Figure 3.1: Dive Planning Main GUI (taken from [3])

Once the primary data about the aircraft and the aircraft type have been selected,

the user can update the weather information by selecting the "Weather…" button. Figure

3.2 shows this Weather GUI.
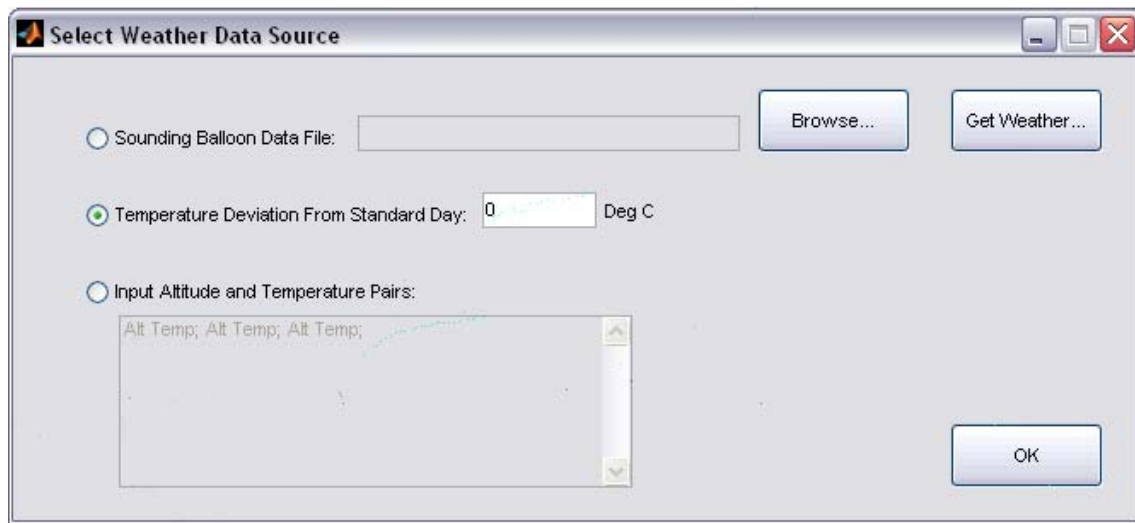
Figure 3.2: "Weather…" Data Source Selection GUI (taken from [3])

This GUI allows the user to either select the data from sounding balloon data that was

previously recorded and then developed into a ".txt" file, set the deviation from the

standard day temperature, or input altitude and temperature pairs manually. For this

experiment, the second option, "Temperature Deviation from Standard Day" was used.

This allowed for a computer generated temperature lapse rate that would be a consistent

control throughout all of the tests.

The next tab should be selected is the "Test Points…" button. Figure 3.3 shows

what this GUI provides.
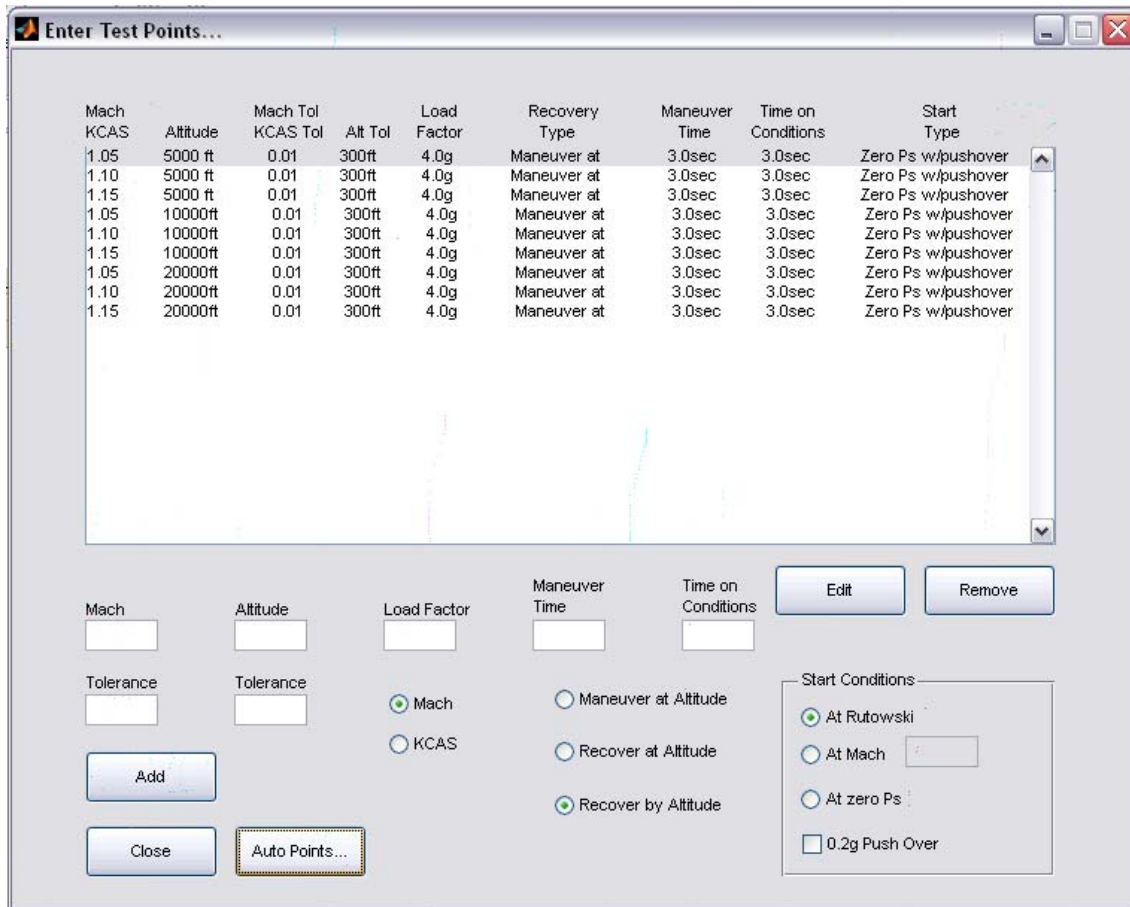
Figure 3.3: "Test Points…" GUI with Nine (9) Selected Test Points (taken from [3])

The "Test Points…" GUI allows the user to either enter each point manually or select the points using an automatic test point generator. By selecting the "Auto Points…" button, a new GUI opens, shown in Figure 3.4, that was used to generate the nine (9) test points shown in Figure 3.3 and that were used in this experiment.
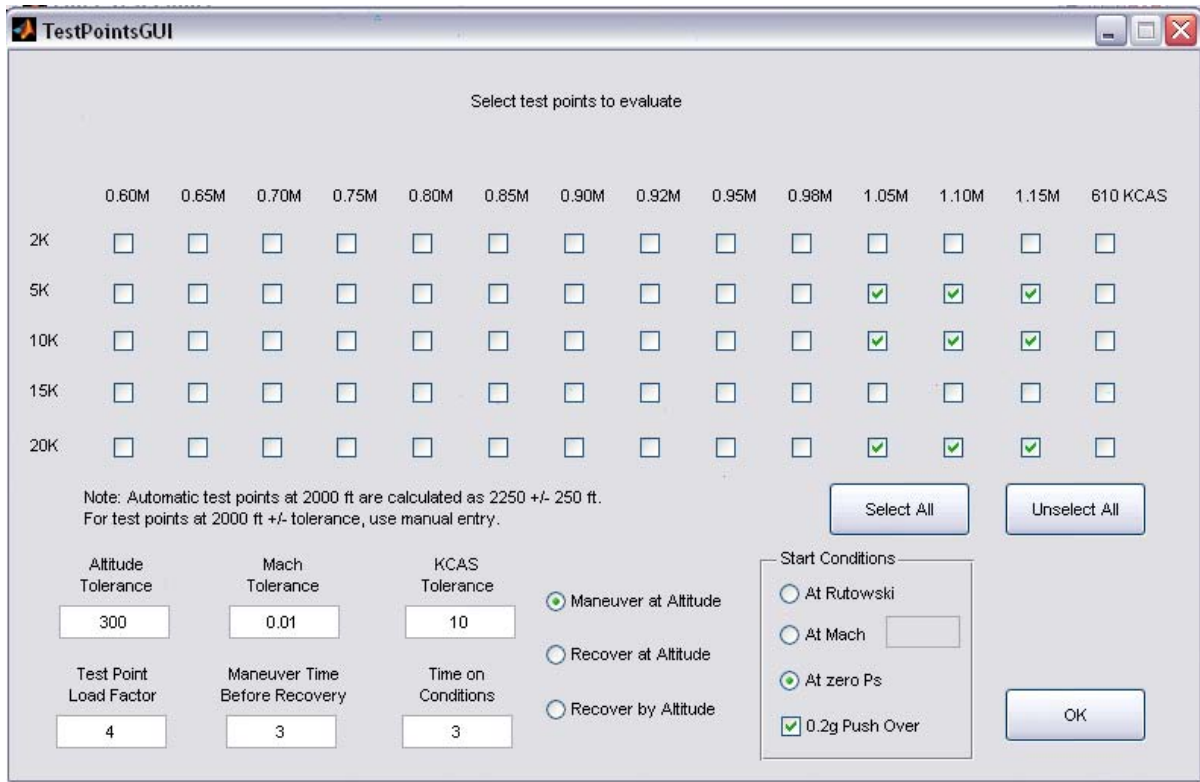
Figure 3.4: "Auto Points…" GUI with Test Points Selected (taken from [3])

This GUI allows the user to select points using constant tolerances and load factors for a variety of commonly used altitudes and Mach numbers. If a point is needed that is not available during the envelope expansion test, then the user can enter the point manually from the GUI shown in Figure 3.3. Again, it can be shown that the nine test points used for this experiment were selected and determined using the "Auto Points…" generator and GUI.

The program then saves the data to a Mission folder in the same directory that the folder containing the MATLAB code files and saves a text document containing the information presented in the MATLAB window as well as any figures that the model produces. Those figures can be seen after running the Dive Planning model for any of

the test points used throughout the experiment [3]. A sample from the first set of test points can be seen in Figure 3.5 and Figure 3.6. These figures correspond directly to the data shown in Table 3.1, located on page 74.
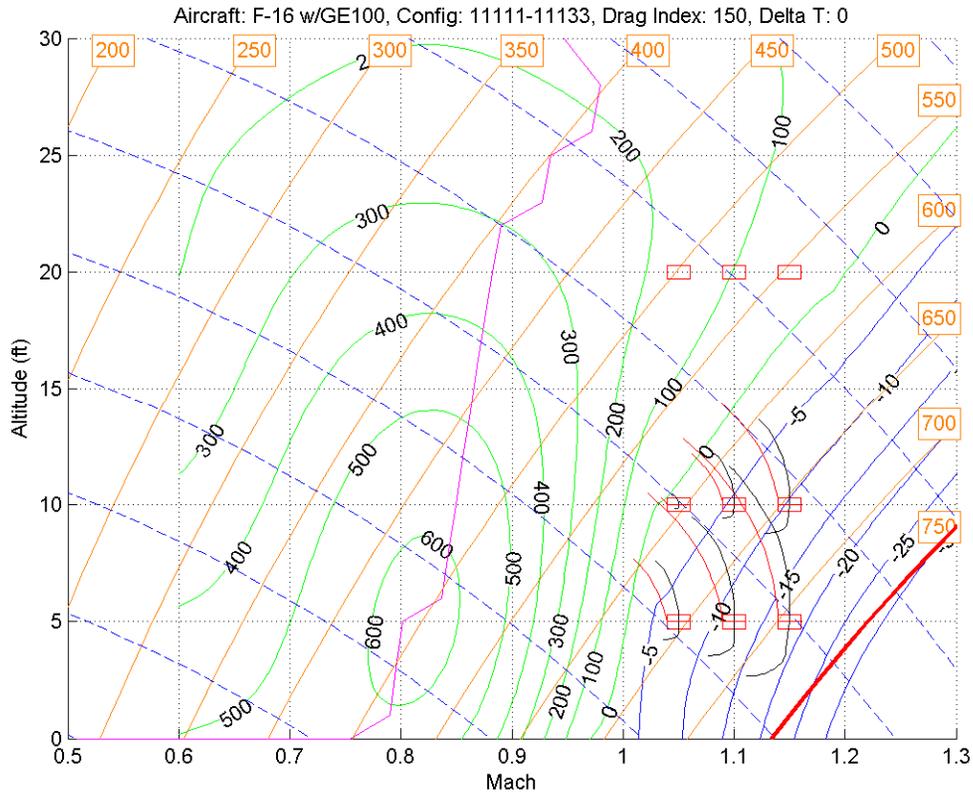
Figure 3.5: Dive Planning Sample Output Showing Energy Curves

A quick description of this figure will help develop an understanding of the information contained within it. Figure 3.5 shows a large collection of information. The orange lines with labels around the top and side ranging from 200 to 750 are indicating lines of constant knots calibrated airspeed (KCAS). The blue dashed lines that run from the left side of the plot to the bottom are the energy height curves that were discussed in

Chapter 2. The green lines indicate excess power curves. Each labeled (ranging from 0 to 600) indicate the amount of excess power available in each region in units of feet per second. The zero (0) P_S curve indicates where the test pilot would begin a dive profile. The solid blue lines, representing lines of constant excess power, are labeled here in terms of dive angle required to achieve that level. Although this is not a typical method for labeling, the 40th FLTS found this labeling to be the most useful. The solid red line indicates a limit and in this example is a KCAS limit. The pink line is a representation of the Rutowski climb schedule that was also discussed in Chapter 2.

Looking at Figure 3.6, the plot from Figure 3.5 has been zoomed in to show the nine test points of interest for this trial. From this zoomed in view, the test points from the sample are shown as red boxes. The boxes include the tolerances set up initially for the test point in both Mach number and altitude tolerance. The black lines indicate the actual dive profile required to obtain each test point. Notice how the model predicts the maneuver at the test point as was initialized and then performs the recovery function after the maneuver time has elapsed. From this understanding, it can now be illustrated how dangerous these maneuvers can be. A recovery altitude from an easily attainable test point (such as the point at Mach 1.15 and 5,000 feet altitude) requires several thousand feet of recovery altitude. Aircraft configurations with higher drag indexes and increased deviations from standard temperature can cause an even greater required recovery altitude.
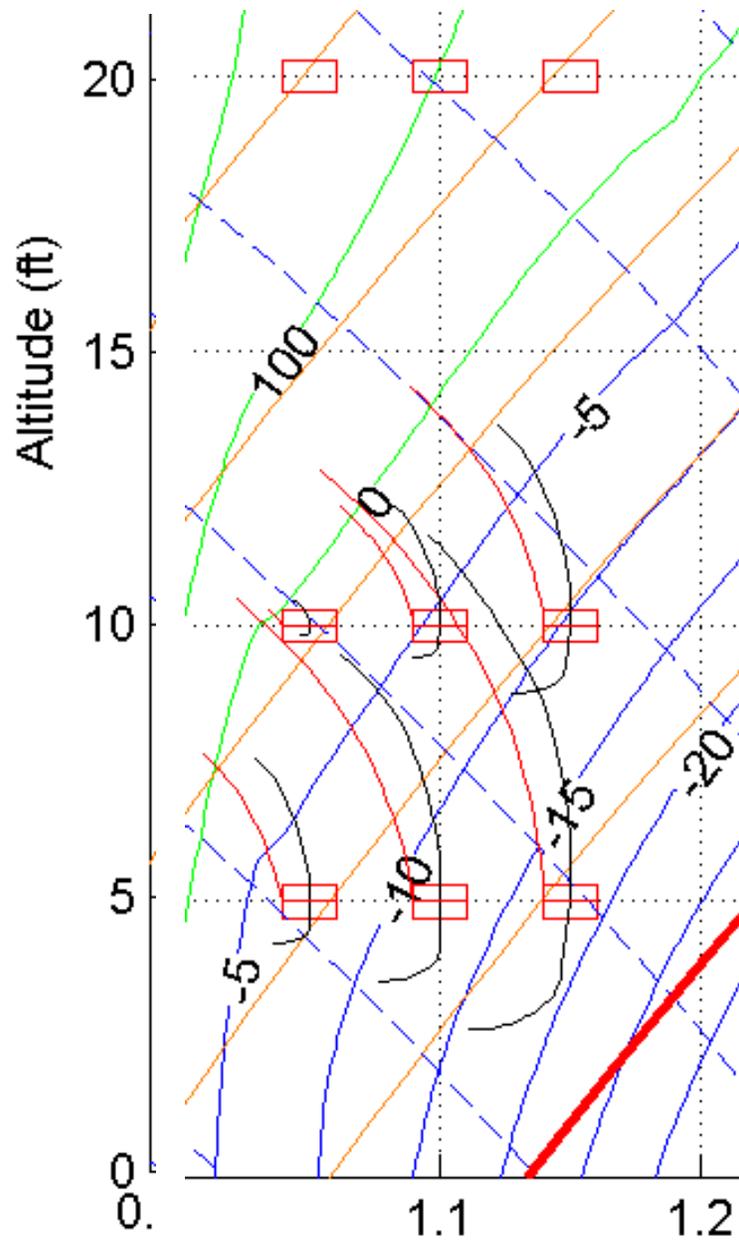
Figure 3.6: Zoomed View of Test Points from Sample
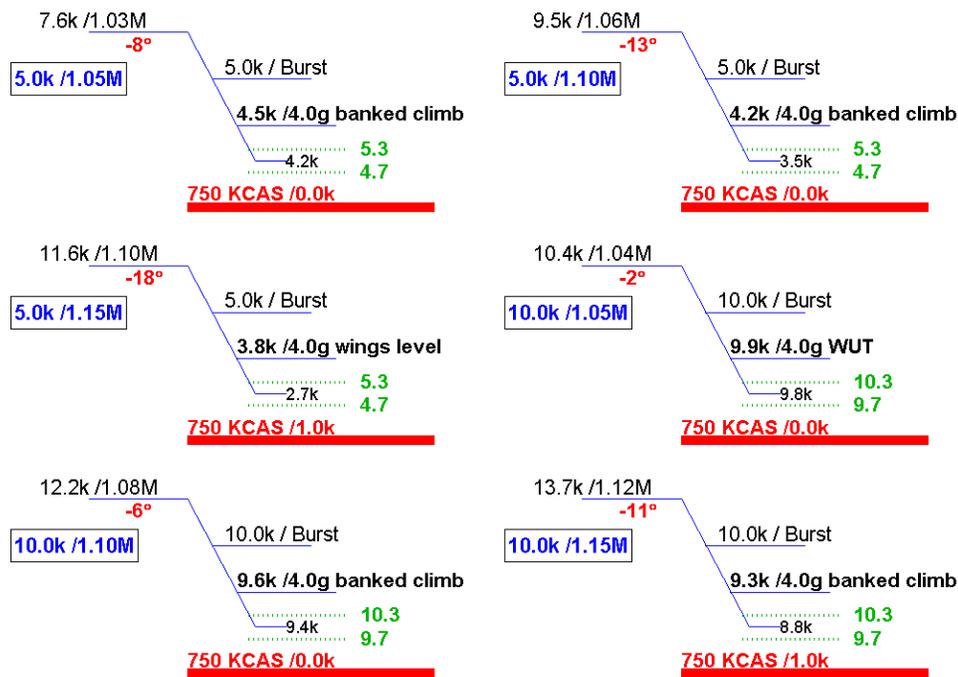
Figure 3.7: Dive Planning Sample Output Showing Computed Dive Profiles

Looking at Figure 3.6, this sample actually shows each dive profile for each test point. There are only six (6) test points shown here because as will be explained by Table 3.1, the three high altitude test points were attainable without the use of a high-speed dive. Looking at each dive individually from Figure 3.7, the boxed in numbers indicate the test point location. The starting altitude and Mach number are shown at the top of the illustration and the required dive angle is shown just below in red text. The data indicating burst shows the point at which the excitement for flutter testing is to occur prior to the maneuver. In the case of this analysis, all trials were done as maneuver at

altitude. It is for this reason that the trials show a burst altitude located at the test point altitude.

The maneuver data is shown below the burst data, indicating the altitude and load factor for each maneuver. Note that the type of maneuver, based on the conditions and altitudes, is also shown. For example, the first test point in the top left of Figure 3.6 shows a 4.0 g banked climb where the same Mach number but at a higher altitude uses a windup turn (WUT) maneuver instead. The last data that can be taken from this chart is the recovery altitude. The last number, located in between the two green lines indicates the recovery altitude. As was previously mentioned, for the third test point at Mach 1.15 and 5,000 feet altitude, the recovery altitude is becoming extremely hazardous. The green numbers indicate the altitude band surrounding the location of the test point.

When looking at the coding, the MATLAB file itself was broken down into a series of functions that are all called from the main m-file. The script m-file that is the primary execution file is saved under the title "DivePlanning.m". When executed, this file generates the GUI from Figure 3.1 and then calls a series of functions to execute each following GUI until the "Run" button is selected. Once selected, the program executes the functions and generates the text file, the two (or more depending on the number of test points) figures, and then also outputs the information to the MATLAB command window.

The output in the MATLAB command window appears in a similar fashion to that of the text file data. Table 3.1 shows an example from the first set of test points required for the sensitivity analysis.

Table 3.1: Sample Text File Output

Test Planning File For Config 11111-11133 Msn   for JON 0001.
This File was created on 28-Jan-2010 by Schneider

Based on the following configuration:
Aircraft: F-16 w/GE100
Drag Index: 150
Weight: 33000
Limits Based on 2.05 Mach Limit 750 KCAS Limit
Atmosphere: 0 degrees C above standard day.

MACH TEST POINTS

Test Point			Starting			Maneuver		Recovery			Limit	
#	Mach	Alt	Mach	Alt	Angle	Alt	Time	Alt1	g	Alt2	Alt	KCAS
1	1.05	5	1.03	7.6	-8	5	3	4.5	4	4.2	0	750
2	1.1	5	1.06	9.5	-13	5	3	4.2	4	3.5	0	750
3	1.15	5	1.1	11.6	-18	5	3	3.8	4	2.7	1	750
4	1.05	10	1.04	10.4	-2	10	3	9.9	4	9.8	0	750
5	1.1	10	1.08	12.2	-6	10	3	9.6	4	9.4	0	750
6	1.15	10	1.12	13.7	-11	10	3	9.3	4	8.8	1	750
7	1.05	20	Positive Ps - Achievable Straight and Level									
8	1.1	20	Positive Ps - Achievable Straight and Level									
9	1.15	20	Positive Ps - Achievable Straight and Level									

The entire set of text file outputs were combined into a single table and sorted. That table can be found in Appendix A of this document.

3.2 Uncertainties with Model

However, even with the benefits of this model, there are certain problems associated with its calculations. The first noted problem is that the model does not incorporate data from any source associated to the equations of motion for a specific aircraft. It does use the excess power tables that are specific to each aircraft, but that is

basically only providing the program with engine data rather than data about the movement of a particular air vehicle. For example, the F-16 actuators that control elevator movement and allow for the alteration of flight path angle, or dive angle, are very different from those of an A-10 or F-15. Therefore during a windup turn, it is quite possible that actual turn performance (or any maneuvering performance for that matter) may be inaccurately modeled or increase the level of uncertainty to the model's results. The results of the model have been validated to provide an indication of accuracy, but when conditions change, the effects on the responses are driving the uncertainties of concern within the model.

Another key area where uncertainty is incorporated is in the way that the program runs its calculations. The Dive Planning model relies heavily on interpolation of data between two data points in order to accurately predict an appropriate dive angle and starting dive conditions. Interpolation, since it is not using exact data, can sometimes add a small amount of uncertainty to the model's predictions. Also adding uncertainty to the calculations is the method that the computer uses for indicating standard day. A temperature increase over standard day at sea level is greatly varied from a temperature increase over standard day at 30,000 feet. Typically, this is why weather balloon sounding data is used over a standard indication because it provides much more realistic temperature data. A constant bias for temperature variation from standard day is not the most accurate prediction for temperature variations. For the purposes of this analysis, the temperature was controlled using the average increase over a standard day temperature lapse rate. The reasoning behind using this constant bias was that using weather balloon sounding data would provide skewed results. The solutions would be based on a

particular day's weather conditions. The results could not be duplicated if the analysis was to be repeated unless identical weather balloon data was used. Since the standard day variation is already incorporated into the model as a constant bias, this will allow for consistency of future analysis and tests.

3.3 Need for a Sensitivity Analysis

These uncertainties, while only providing a small variation in the data individually, can compound to provide a vast variation in the final result when all are operating together. This combination of uncertainties drives up the overall uncertainty in the model. It is for this reason that a need for a sensitivity analysis of the model's predictions is required. A sensitivity analysis can provide a realistic understanding for the variables (weight, temperature variation, drag index, etcetera) that carry the most weight throughout the program's calculations. The results that come from a sensitivity analysis can then be used to indicate to the user which variables carry the most significance and when the value of those particular variables contains possible error, a useless dive test can be avoided.

3.4 Method for Sensitivity Analysis

Using a program called JMP, a Design of Experiments and sensitivity analysis software platform, data from several trial runs of the Dive Planning program will be evaluated. Using the full factorial calculation program within JMP, the JMP software will indicate the number of trials needed based on the data provided for the range of each variable. Once the number of trials is determined, the trials will be sorted into a method

that allows the experimenter to run a systematic set of tests covering all of the required test points for later analysis.

For the data associated with this experiment, the Dive Planning program will be calculating nine (9) test points each time that the program operates. By determining the results from several test points simultaneously, it will improve the consistency in the results as well as speed up the experimentation time. The nine test points that are being used are shown in Table 3.2.

Table 3.2: Test Points Used for Data Collection

Test Point	Altitude (ft)	Mach Number	Altitude Tolerance (ft)	Mach Tolerance	KCAS Tolerance (kts)
1	5,000	1.05	± 300	± 0.01	± 5
2	5,000	1.10	± 300	± 0.01	± 5
3	5,000	1.15	± 300	± 0.01	± 5
4	10,000	1.05	± 300	± 0.01	± 5
5	10,000	1.10	± 300	± 0.01	± 5
6	10,000	1.15	± 300	± 0.01	± 5
7	20,000	1.05	± 300	± 0.01	± 5
8	20,000	1.10	± 300	± 0.01	± 5
9	20,000	1.15	± 300	± 0.01	± 5

As can be seen above, three Mach numbers for each altitude of 5,000, 10,000, and 20,000 feet were used. The reasoning behind using such a small variation in the Mach numbers was associated with the constraints of the Dive Planning program. Referencing Figure 3.4, the only three Mach values that were supersonic were the three that were chosen for the experiment. The last available selection for velocity is in KCAS and using inconsistent measurements for velocity would remove that control from the analysis. The test points in the transonic region (specifically Mach 0.95 and 0.98) can cause other

inconsistencies associated with the inability to accurately model aerodynamic properties under those flight conditions. The subsonic test points were also neglected because with the exception of extremely high drag indexes, most of the points would be attainable at steady-level flight. Having all positive P_S test points would invalidate the results. The tolerances were held as a constant for all three values to maintain control in the experiment. These tolerances allow for some variation in the operation of the Dive Planning program in order to cut down on computation time. These tolerances are those that are typically used by the 40th FLTS at Eglin Air Force Base in Florida.

Once the test points are selected, the variation in the remaining parameters must be determined. In other words, the JMP program needs to know the level of each factorial so that it can compute all the required trials to conduct the sensitivity analysis. Table 3.3 shows these variations for the remaining variables.

Table 3.3: Level and Variations for Remaining Variables

Variable	Level	Range of Values	Increment of Values	Units of Variable
Weight	3	29,000 - 33,000	2,000	pounds
Temperature	5	0 - 20	5	° C
Drag Index	3	150 - 200	25	[dimensionless]

This table shows the remaining variables that were used in the full factorial calculations by the JMP program. The level indicates the number of values for each variable. For example, weight is a level three variable. This variable has a range of 29,000 pounds to 33,000 pounds which is incremented every 2,000 pounds. Therefore the values used in the JMP table will be 29,000, 31,000, and 33,000 pounds. When the level of the weight is computed with the level three drag index, the level five temperature, and the level three

test altitude and test Mach number, the JMP program will compute a 3 x 5 x 3 x 3 x 3 factorial computation. That will be the number of required trials for the sensitivity analysis. Once the trials have been executed and the data reentered into the JMP software, the "Fit Model" analysis will be run to determine the sensitivity of each variable. Chapter four will discuss this analytical method in more detail.

3.5 Setting up JMP 8.0

JMP is listed as a program that allows a user to interactively explore data, instantly visualize it, and use powerful analytics to provide the best results and visualizations to the user possible [18]. The set up for this experiment used JMP version 8.0. The "statistical discovery" software is developed by SAS Institute Inc. Using the Design of Experiments tool in the JMP Starter window, shown in Figure 3.8, the most logical experimental design type was chosen, the "Full Factorial Design".

This is the most logical choice because the other options do not provide the resources that this experiment needs. For instance, the Screening design only allows level two and level three factors. Since temperature is a level five factor, this approach will not work. The Response Surface design provided the user with a set of predetermined response designs. This is not applicable here because the user already knew the number and type of responses. The Choice design involves human probabilistic predictions. Since this is a computer model generating the results and not a human response, this design will not provide a relevant analysis of the data. The Nonlinear design was not appropriate because the parameters or terms were not nonlinear within themselves. Although the model was nonlinear, the parameters themselves were not.

The Space Filling design is for deterministic systems and the Taguchi array is associated

with signal and noise factors. The terms in this experiment were not associated with

having noise directly, although noise was present within the model. After eliminating

these other choices for design, the Full Factorial design becomes the most appropriate.

The JMP program can take any number of parameters of multiple levels and creates all

possible combinations for those factors. This allowed the table presenting the trials

needed to be as accurate as possible for this experiment.
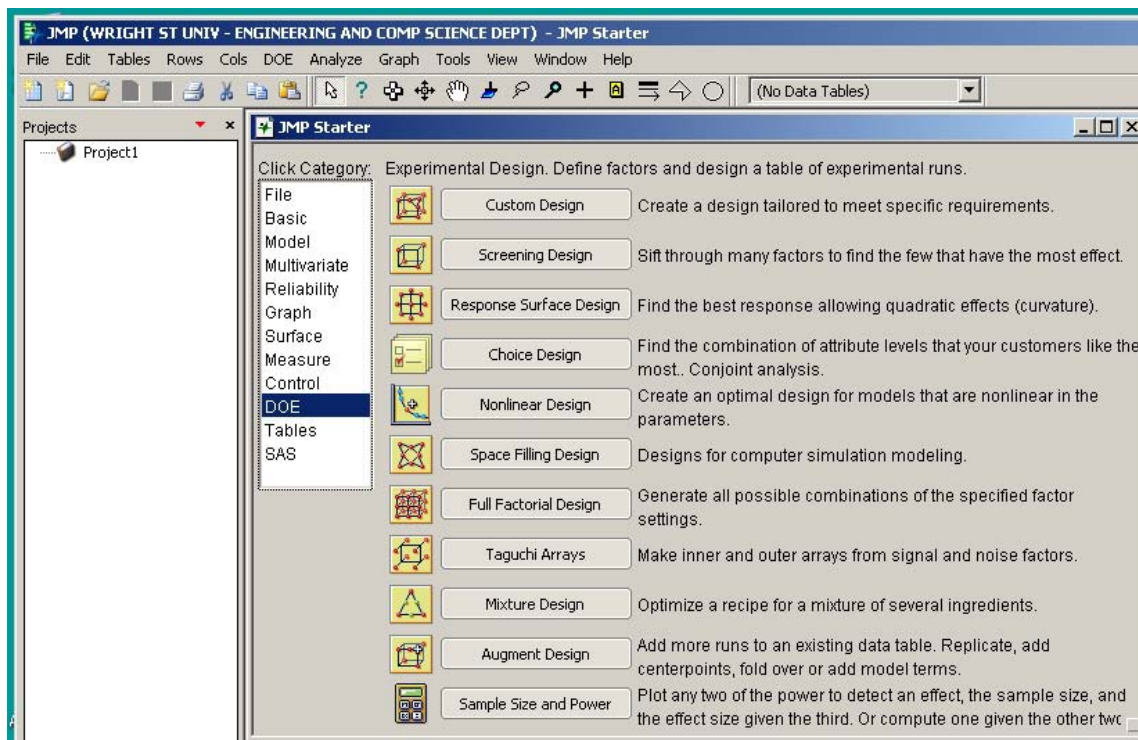
Figure 3.8: JMP Starter Window (taken from [18])

Once the full factorial design type is selected, the design criteria can be entered.

For this experiment there were five (5) responses and five design factors. The responses,

titled Starting Altitude, Starting Mach Number, Dive Angle, Recovery Altitude 1, and

Recovery Altitude 2, were chosen as a goal of either maximum or minimum, depending on the variable itself. For example, the Dive Angle response should be the least negative number possible, and therefore is classified as a maximum. The Starting Altitude is a minimal response because the test pilot does not want to waste excess fuel and time climbing to an unnecessarily high starting point.

The design factors were the Weight, Temperature, Drag Index, TP (Test Point) Altitude, and TP Mach Number. All of these factors are continuous values and are assigned to be either three (3) or five level factors. All of the factors with the exception of Temperature were level three since only three weights, drag index values, altitudes, and Mach numbers were chosen. Temperature, as is shown in the table above, had five levels. Figure 3.9 shows the set up for the factorial design. It is also important to note that the program automatically determines that there are 405 possible test runs for the given design factors.
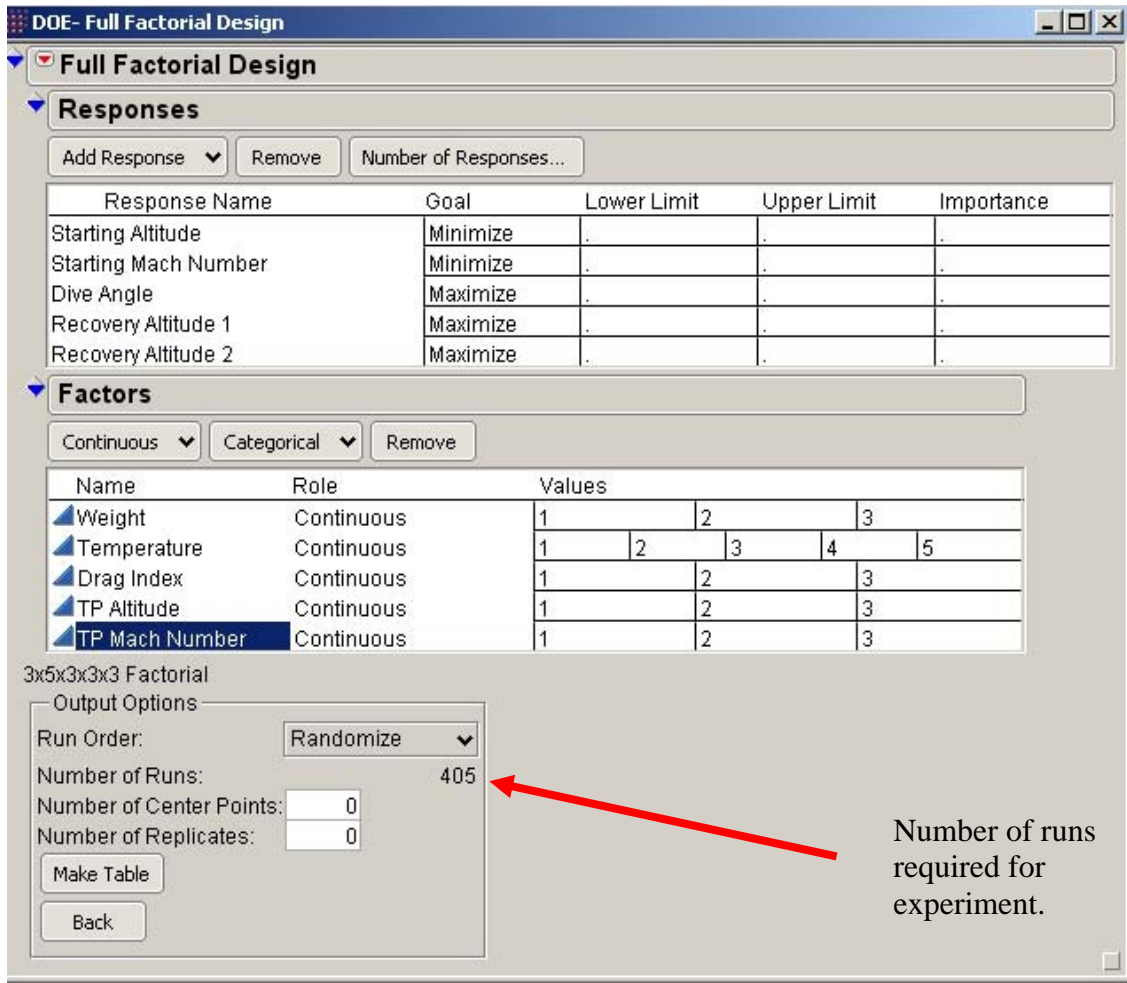
Figure 3.9: Full Factorial Design Set Up Window (taken from [18])

JMP can then generate the table that will provide an entry point for each run

necessary for the analysis. A small sample of the table is shown in Figure 3.10.

	Pattern	Weight	Temperature	Drag Index	TP Altitude	TP Mach Number	Starting Altitude	Starting Mach Number	Dive Angle	Recovery
1	32233	3	2	2	3	3	.	.	.	
2	31132	3	1	1	3	2	.	.	.	
3	34122	3	4	1	2	2	.	.	.	
4	33331	3	3	3	3	1	.	.	.	
5	12332	1	2	3	3	2	.	.	.	
6	34113	3	4	1	1	3	.	.	.	
7	13133	1	3	1	3	3	.	.	.	
8	24132	2	4	1	3	2	.	.	.	
9	21221	2	1	2	2	1	.	.	.	
10	21123	2	1	1	2	3	.	.	.	
11	22133	2	2	1	3	3	.	.	.	
12	24111	2	4	1	1	1	.	.	.	
13	14222	1	4	2	2	2	.	.	.	
14	23133	2	3	1	3	3	.	.	.	
15	31312	3	1	3	1	2	.	.	.	
16	14323	1	4	3	2	3	.	.	.	
17	15223	1	5	2	2	3	.	.	.	
18	13111	1	3	1	1	1	.	.	.	
19	31311	3	1	3	1	1	.	.	.	
20	21313	2	1	3	1	3	.	.	.	
21	13113	1	3	1	1	3	.	.	.	
22	13132	1	3	1	3	2	.	.	.	
23	23321	2	3	3	2	1	.	.	.	
24	11123	1	1	1	2	3	.	.	.	
25	21231	2	1	2	3	1	.	.	.	
26	24131	2	4	1	3	1	.	.	.	
27	25221	2	5	2	2	1	.	.	.	
28	24222	2	4	2	2	2	.	.	.	
29	15232	1	5	2	3	2	.	.	.	
30	23122	2	3	1	2	2	.	.	.	
31	13332	1	3	3	3	2	.	.	.	
32	11231	1	1	2	3	1	.	.	.	
33	14321	1	4	3	2	1	.	.	.	
34	22132	2	2	1	3	2	.	.	.	
35	34123	3	4	1	2	3	.	.	.	
36	11332	1	1	3	3	2	.	.	.	
37	25332	2	5	3	3	2	.	.	.	
38	24113	2	4	1	1	3	.	.	.	
39	13311	1	3	3	1	1	.	.	.	
40	34321	3	4	3	2	1	.	.	.	

Figure 3.10: Randomized Table Developed by Factorial Design (taken from [18])

The data in this table can then be sorted into a format that is set up to ease the process of importing data. Once the data has been collected, the completed table can be used for the sensitivity analysis. A sample of the completed table is shown in Figure 3.11 and the complete table can be found in Appendix A.

JMP (WRIGHT ST UNIV - ENGINEERING AND COMP SCIENCE DEPT) - [DivePlanning]

File Edit Tables Rows Cols DOE Analyze Graph Tools View Window Help

DivePlanning
Design 3x5x3x3x3 Factorial
Screening
Model

Pattern	Weight	Temperature	Drag Index	TP Altitude	TP Mach	Starting Mach	Starting Altitude	Dive Angle	Start Recovery	End Recovery
11111	33000	0	150	5000	1.05	1.03	7.6	-8	4.5	4.2
11112	33000	0	150	5000	1.1	1.06	9.5	-13	4.2	3.5
11113	33000	0	150	5000	1.15	1.1	11.6	-18	3.8	2.7
11121	33000	0	150	10000	1.05	1.04	10.4	-2	9.9	9.8
11122	33000	0	150	10000	1.1	1.08	12.2	-6	9.6	9.4
11123	33000	0	150	10000	1.15	1.12	13.7	-11	9.3	8.8
11131	33000	0	150	20000	1.05	1.05	20	0	20	20
11132	33000	0	150	20000	1.1	1.1	20	0	20	20
11133	33000	0	150	20000	1.15	1.15	20	0	20	20
11211	33000	0	175	5000	1.05	1.02	8.7	-11	4.3	3.9
11212	33000	0	175	5000	1.1	1.05	10.8	-16	4	3.1
11213	33000	0	175	5000	1.15	1.05	14.9	-23	3.5	1.8
11221	33000	0	175	10000	1.05	1.03	11.6	-4	9.8	9.7
11222	33000	0	175	10000	1.1	1.08	12.8	-9	9.4	9.1
11231	33000	0	175	20000	1.05	1.05	20	0	20	20
11232	33000	0	175	20000	1.1	1.1	20	0	20	20
11233	33000	0	175	20000	1.15	1.15	20	0	20	20
11311	33000	0	200	5000	1.05	1.02	9.5	-12	4.3	3.8
11313	33000	0	200	5000	1.15	1.03	15.6	-26	3.3	1.2
11321	33000	0	200	10000	1.05	1.04	11.4	-6	9.6	9.5
11322	33000	0	200	10000	1.1	1.07	13	-11	9.3	8.8
11323	33000	0	200	10000	1.15	1.08	16.3	-17	8.9	7.9
11331	33000	0	200	20000	1.05	1.05	20	0	20	20
11332	33000	0	200	20000	1.1	1.1	20	0	20	20
11333	33000	0	200	20000	1.15	1.15	20	0	20	20
12111	33000	5	150	5000	1.05	1.03	8	-8	4.5	4.2
12112	33000	5	150	5000	1.1	1.06	10.4	-13	4.2	3.5
12113	33000	5	150	5000	1.15	1.09	12.6	-19	3.8	2.5
12121	33000	5	150	10000	1.05	1.04	11.1	-3	9.8	9.8
12122	33000	5	150	10000	1.1	1.08	12.7	-8	9.5	9.2
12123	33000	5	150	10000	1.15	1.11	14.6	-13	9.2	8.5
12131	33000	5	150	20000	1.05	1.05	20	0	20	20
12132	33000	5	150	20000	1.1	1.1	20	0	20	20
12133	33000	5	150	20000	1.15	1.15	20.1	-1	19.9	19.9
12211	33000	5	175	5000	1.05	1.02	9	-11	4.3	3.9
12212	33000	5	175	5000	1.1	1.05	11.3	-17	3.9	2.9
12221	33000	5	175	10000	1.05	1.03	12.1	-5	9.7	9.6
12222	33000	5	175	10000	1.1	1.08	13.6	-10	9.4	9
12223	33000	5	175	10000	1.15	1.1	15.5	-16	9	8
12231	33000	5	175	20000	1.05	1.05	20	0	20	20
12232	33000	5	175	20000	1.1	1.1	20	0	20	20
12233	33000	5	175	20000	1.15	1.14	20.7	-2	19.9	19.8
12311	33000	5	200	5000	1.05	1.02	9.9	-12	4.3	3.7
12313	33000	5	200	5000	1.15	1.03	16.6	-27	3.3	0.9

Columns (11/1): Pattern, Weight ✱, Temperature ✱, Drag Index ✱, TP Altitude ✱, TP Mach ✱, Starting Mach ✱, Starting Altitude ✱, Dive Angle ✱, Start Recovery ✱, End Recovery ✱

Rows: All rows 386, Selected 1, Excluded 0, Hidden 0, Labelled 0

Ready

Figure 3.11: Completed JMP Table Ready for Analysis (taken from [18])

At this point, there were two types of analysis conducted. The first analysis conducted was aimed at determining the sensitivity of all variables. Using the Fit Model Analysis under the Analyze drop-down menu, a sensitivity study is conducted automatically by the software. The second analysis was done using the Fit Model analytical technique again, but the data was restricted.

For the second study, the analysis was restricted to only test points at the 20,000 foot altitude. The reason that this study was done separately was in order to draw conclusions on one of the uncertainties that was previously discussed. This is the uncertainty that higher altitude test points may possibly have a greater significance than

the test points at lower altitudes. In theory, the effects of temperature variation and weight variation on the energy and power curves differs greatly as the potential energy and kinetic energy increase with altitude and Mach increases proportionally to temperature. Figure 3.12 shows a sample of the modified table that was used for this secondary analysis. This second table can also be found in its entirety in Appendix A.

	Pattern	Weight	Temperature	Drag Index	TP Mach	Starting Mach	Starting Altitude	Dive Angle	Start Recovery	End Recovery
1	11131	33000	0	150	1.05	1.05	20	0	20	20
2	11132	33000	0	150	1.1	1.1	20	0	20	20
3	11133	33000	0	150	1.15	1.15	20	0	20	20
4	11231	33000	0	175	1.05	1.05	20	0	20	20
5	11232	33000	0	175	1.1	1.1	20	0	20	20
6	11233	33000	0	175	1.15	1.15	20	0	20	20
7	11331	33000	0	200	1.05	1.05	20	0	20	20
8	11332	33000	0	200	1.1	1.1	20	0	20	20
9	11333	33000	0	200	1.15	1.15	20	0	20	20
10	12131	33000	5	150	1.05	1.05	20	0	20	20
11	12132	33000	5	150	1.1	1.1	20	0	20	20
12	12133	33000	5	150	1.15	1.15	20.1	-1	19.9	19.9
13	12231	33000	5	175	1.05	1.05	20	0	20	20
14	12232	33000	5	175	1.1	1.1	20	0	20	20
15	12233	33000	5	175	1.15	1.14	20.7	-2	19.9	19.8
16	12331	33000	5	200	1.05	1.05	20	0	20	20
17	12332	33000	5	200	1.1	1.1	20	0	20	20
18	12333	33000	5	200	1.15	1.14	21.2	-3	19.8	19.7
19	13131	33000	10	150	1.05	1.05	20	0	20	20
20	13132	33000	10	150	1.1	1.1	20	0	20	20
21	13133	33000	10	150	1.15	1.13	21.9	-3	19.8	19.7
22	13231	33000	10	175	1.05	1.05	20	0	20	20
23	13232	33000	10	175	1.1	1.09	20.4	-1	19.9	19.9
24	13233	33000	10	175	1.15	1.12	22.9	-5	19.7	19.5
25	13331	33000	10	200	1.05	1.05	20	0	20	20
26	13332	33000	10	200	1.1	1.09	21	-2	19.9	19.8
27	13333	33000	10	200	1.15	1.12	23.8	-6	19.6	19.4
28	14131	33000	15	150	1.05	1.05	20	0	20	20
29	14132	33000	15	150	1.1	1.09	21.4	-2	19.9	19.8
30	14133	33000	15	150	1.15	1.12	23.5	-6	19.6	19.4
31	14231	33000	15	175	1.05	1.05	20.1	-1	19.9	19.9
32	14232	33000	15	175	1.1	1.07	22.8	-4	19.8	19.7
33	14233	33000	15	175	1.15	1.1	25.2	-8	19.5	19.2
34	14331	33000	15	200	1.05	1.04	20.6	-2	19.9	19.8
35	14332	33000	15	200	1.1	1.06	24.4	-5	19.7	19.6
36	14333	33000	15	200	1.15	1.07	27.2	-10	19.4	18.9
37	15131	33000	20	150	1.05	1.04	20.6	-2	19.9	19.8
38	15132	33000	20	150	1.1	1.07	23	-5	19.7	19.5
39	15133	33000	20	150	1.15	1.11	24.6	-9	19.4	19
40	15231	33000	20	175	1.05	1.02	22.6	-4	19.8	19.7
41	15232	33000	20	175	1.1	1.06	24.9	-7	19.6	19.3
42	15233	33000	20	175	1.15	1.09	27	-11	19.3	18.8
43	15331	33000	20	200	1.05	1.01	23.4	-5	19.7	19.6
44	15332	33000	20	200	1.1	1.03	26.7	-9	19.4	19.1

Figure 3.12: Sample of Modified Table for Secondary Analysis (taken from [18])

Once the data table has been completed, the method for analysis can be chosen. JMP provides several different types of modeling. The Fit Model technique was chosen because it provides the most complete set of data for a sensitivity analysis. Several of the

other analytical methods do not provide the necessary information to determine the

sensitivity or significance of one variable over another. Once the Fit Model technique

was selected from the Analyze drop-down menu within the JMP program, a set up

window was activated. Figure 3.13 shows the set up window.
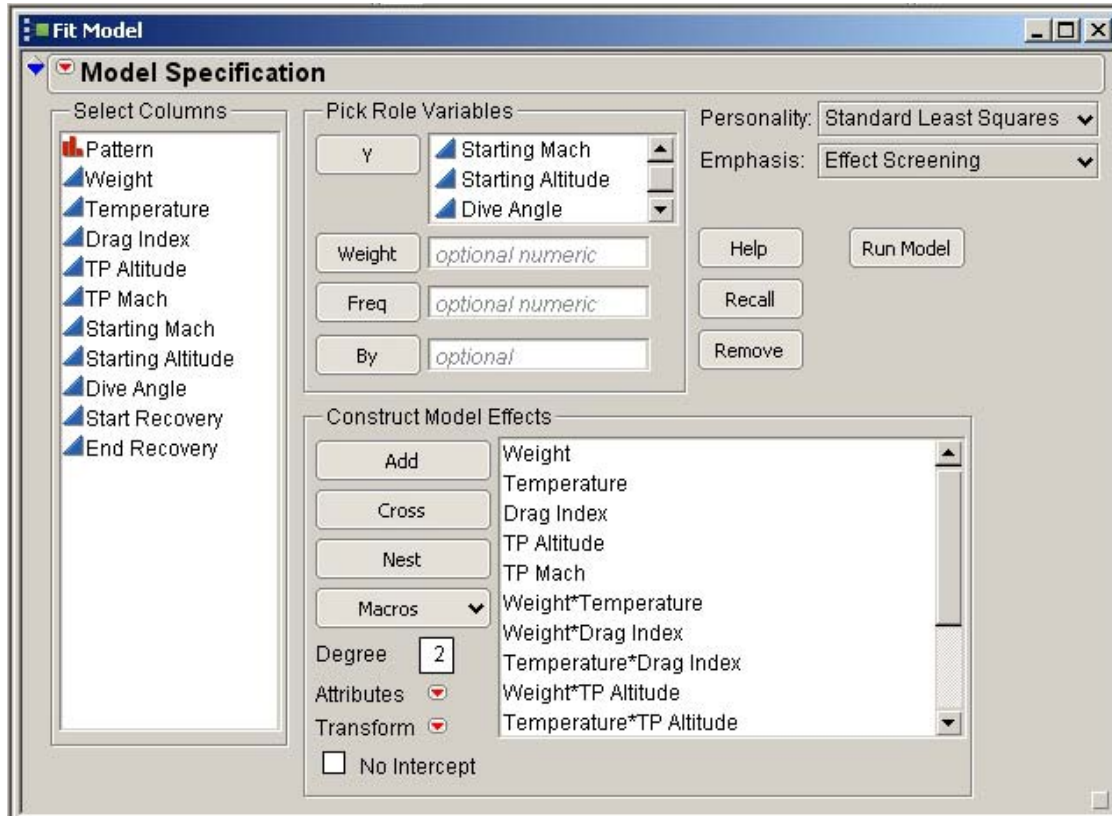
Figure 3.13: Fit Model Set-up Window (taken from [18])

In this window, the user was required to determine the type of modeling, the role

variables, and then verify the model effects that were to be tested. The standard least

squares personality is the method chosen due to the type of data entered. This method

was the most practical choice based on the data presented. The other options in the JMP

program are a Manova approach, the Generalized Linear Model, and Loglinear Variance

method. The Loglinear Variance method does not compute because the fitting

personality did not match the data presented. The Generalized Linear Model did not

provide any results because the JMP software allows only one response for this

personality type. The Manova method provided results for multivariate analysis for

multiple responses. In contrast, the standard least squares approach looked at each

response individually. This was useful for this experiment because the goal of this

experiment was to evaluate the sensitivity of each response independently, not the set of

them as a whole as the Manova method does. Therefore, the least squares personality

provides the most data relating the sensitivity of one variable to another and the

interaction of those variables. The "Pick Role Variables" are the responses that are being

evaluated. Those are the same responses that were chosen earlier in the initial factorial

design set-up. The model effects that were chosen are the design factors and the

interactions between each one. For example, weight is paired with temperature, drag

index, and both test point conditions in order to show whether the interaction of these

variables is important or just the variables independently. It is possible for several

variables to be insensitive to the results independently, but the interaction of two

variables may have a fundamental significance to all of the results. A discussion of the

results that were computed by the software is laid out in Chapter 4 of this thesis.

IV. Results and Discussion

The results that the JMP software computed can be broken down into two segments. The first segment analyzes the entire set of data. The second set of data focuses on an analysis with the uncertainty at high altitude that was discussed earlier and only involves the test points at the 20,000 foot altitude. The results from this data set will be first analyzed separately from the original results and then comparisons will be made about the differences between the two solutions and the possible explanation for those differences.

It is important to note that the original data set required 405 test runs. Due to the Dive Planning model computational limitations, only 386 points were used for the evaluation. Nineteen points caused the simulation to terminate unexpectedly and therefore were not included in the statistical analysis. The nineteen (19) points that failed may introduce a minor error to the results, but since less than five percent (5%) of the data has been omitted, it was assumed that this error is negligible. The assumption behind the failing of these particular points may be associated with a lack of accurately modeled P_S data for those test points and conditions. Since the software is using a cubic spline interpolation, this assumption was derived. The solutions were being interrupted by the inability to interpolate the specific P_S value required at that test point and test conditions. The reasoning for the failure can be estimated, but the sponsor has been made aware of the area and is conducting further research into the coding to determine the true cause behind the point failures. However, this data can be omitted without significant error introduction because it is well dispersed throughout all of the trial runs. There was no specific set of points or patterns that failed.

An effort to calculate the missing data points was made, but it appeared to be an interpolation problem within the Dive Planning code itself. The program was running for over twelve (12) hours and still could not yield a solution to a single dive prediction. It is possible that some of these points have interpolation requirements that are too convoluted for the current versions of MATLAB to calculate. Another possibility is that the P_S tables for these points were not well behaved. The results for this modified set of data will now be discussed below.

4.1 Definitions for Results Presented

The Fit Model Analysis in the JMP program provides a large collection of data. Several results that will be discussed use unique definitions and calculations to determine results. This section will provide these definitions so that later sections can focus on the presentation of the data.

4.1.1 Summary of Fit Definitions

The first set of data that will be presented for each response is based on a plot of the predicted versus the actual responses. The JMP software first determines the mean of the particular response and then compares the data for each observation. The data is then plotted and the mean line is represented for both the data in its entirety and a mean line is presented for the actual response as well. This plot is known as a Leverage Plot. In some cases, particularly for the entire set of data, this result is not necessarily relevant, particularly the average for the entire response. The reasoning behind this irrelevance is that because of the varying Mach numbers required for the nine (9) different test points, a

mean value is not truly representative of the mean for each altitude. A breakdown of the data would be required to really obtain valuable information from this plot. For this reason, this data will only be presented for the 20,000 foot altitude condition results in section 4.3.

The data that corresponds to the plot described above is indicated by the Summary of Fit Table. This table provides information on the variation of the data, provides an adjusted variation, and provides a standard deviation from that error. The adjusted variation is used to compensate for different responses so that the response can be compared with some consistency despite the type of response. The same table also provides the mean values and lists the number of patterns or observations that were used to determine the results.

The variation of the data from the mean line is defined by the R^2 value. This value is listed by definition as the "proportion of the variation in the response around the mean that can be attributed to terms in the model rather than to random error" [19]. R^2 is calculated by dividing the Sum of the Squares of the model by the corrected total (C. Total) Sum of the Squares. In short, R^2 is the correlation between the actual response and the predicted response from the earlier described plot.

The R^2 Adjusted value modifies the R^2 value to make it comparable to models with a different number of parameters. In order to make this calculation, the software includes the degrees of freedom in the calculations. The R^2 Adjusted value is therefore a ratio of the mean squares instead of the sum of squares. Most of these values (sum of squares and mean squares) are found in the Analysis of Variance table which will be discussed in the next section.

The next line of data is the Root Mean Square Error. This value is simply an estimation of the standard deviation in the random error. Often defined by the symbol σ, the root mean square error is calculated by taking the square root of the mean square error for the model error. The mean of the response, the next value in the data tables, is the overall mean of the response values. Because of the variance in the test points chosen for this experiment, these values, as previously mentioned, are only relevant for discussion in the 20,000 foot altitude study. The mean response is a critical value for prediction because all the other models are compared to this mean value.

The last category in the summary of fit table is Observations. This value merely indicates the number of patterns or test points. As long as the data is complete and no rows are excluded, this number is equivalent to the number of data points.

4.1.2 Analysis of Variance Definitions

The Analysis of Variance table is used to make the basic calculations for the linear model. As was stated in the previous section, many of the values in this table are directly used in calculating the summary of fit for the given response. The Source column indicates the source of the data provided. The three categories are Model, Error, and C. Total (the definition for C. Total was previously defined). The DF column indicates the associated degrees of freedom for each source of variation. Because there is only one degree of freedom used in the calculation for the variation, the degree of freedom of the C. Total will always be one number less than the number of observations for that response. The degrees of freedom for the Model and Error can be summed to equal the degrees of freedom of the C. Total. The Model degrees of freedom are the

91

number of parameters used to fit the model and the remaining degrees of freedom are partitioned to the Error. The Sum of Squares and Mean Square columns are merely used for the calculations for the Summary of Fit table previously described.

The important values in the Analysis of Variance table for this experiment are the F Ratio and the Prob > F. The F Ratio is a simple computation of the model mean square divided by the error mean square. This ratio tests a hypothesis that the two mean squares have the same expectation and that all the regression parameters are zero (0). If the model contains a significant effect, then the F Ratio is higher than expected by chance alone.

The Prob > F value indicates the presence of significant regression factors within the model. If the probabilities are lower than 0.05, then this is considered evidence of significance. This is a quick way for analysts to check and see if there is significance in the system for one or more factors before delving into the information and the details of the analysis.

4.1.3 Parameter Estimates Definitions

The parameter estimates table shows the estimates for each parameter in the linear model. This table is broken down into several columns as well. The first column names the estimated parameter. The parameters are sorted based on their t-Ratio which will be discussed later in this section. The estimate column lists the actual estimate for each parameter for the given response. These estimates are the coefficients of the linear model determined using the least squares method. The standard error column is the measure of

the standard deviation for the distribution of that particular estimate. It is used for t-tests and to determine confidence intervals.

The t-Ratio is the ratio of the estimate to its standard error. Ideally, the t-Ratio should be zero indicating that the true parameter is equal to the estimate. This relates directly to the next column, the Prob > |t| column. This term is the probability of obtaining a greater t-statistic (under the hypothesis that the parameter is zero as was mentioned earlier). Probabilities that are less than 0.05 indicate significance for that term. In other words, the samples share the same mean when they are significant. The t-Ratio will provide the strength of significance in regards to the other test points and the Prob > |t| will indicate which parameters are significant to the response. The hypothesis shows that when the inputs are significant, then the null is valid. If the parameters are significant, then the null of the hypothesis (that certain parameters are significant) is rejected.

The figure that is typically associated with the Parameter Estimates Table indicates the significance of each parameter in relation to the other. Since the table is already presorted according to the absolute value of the t-Ratio, the most significant effects are also located on the top of this figure. The lines running top to bottom indicate the 0.05 significance level. Terms contained inside the lines entirely have low significance and terms that extend farther beyond the significance lines indicate greater impact of that parameter on the response.

4.1.4 Interaction Plots

The last type of figure that will be presented is the interaction plots. These plots show the interaction of the different variables and how they correspond to other parameters for that response. Lines that are parallel indicate little to no interaction between the design factors in determining the solution to the response. Lines that are shown as non-parallel indicate high interactions between those variables. In some cases, the interactions can be so great that they can actually mask the effect of the primary parameter. This masking effect is also described as over shadowing of one variable versus another. This overshadowing can be described as the concealment of the interaction of one variable in regards to another. For example, if the interaction of weight and temperature produced non parallel lines, then it is possible that either the weight or the temperature results are skewed. This misrepresentation of the data could lead to an inaccurate discussion of the results, hence the importance of including such an analysis for each response. This indicates why some parameters have greater reactive significance than significance of individual parameters.

4.2 Analysis Using Complete Data Set

For this portion of the analysis and results, the first table in Appendix A was used. This data table contains the information for all 386 trials that were run using the Dive Planning program. As previously noted, the information that will be discussed in this section will be the Parameter Estimates and the Interaction Plots. Reference may be made to the Analysis of Variance table and those tables will be included in Appendix B for each response.

4.2.1 Analysis of Starting Mach Response

The first step in the analysis was to ensure that there are significant factors present in the system. Based on the Analysis of Variance Table, Table B.1.1, there are one or more significant factors in the system. At this point it is important to move to the parameter estimates table. This table, Table 4.1, shows the each term or pair of terms, the estimate, standard error, t-Ratio, and Prob > |t| value. The parameter estimates are the estimates calculated by the computer for each term in the linear model. The estimate divided by the standard error provides the t-Ratio. These values are important, because higher t-Ratios indicate a greater significance and higher sensitivity within the model.

Table 4.1: Sorted Parameter Estimates for Starting Mach Response

Term	Estimate		Standard Error		t-Ratio	Prob > |t|
TP Mach	0.5376		0.0137		39.25	<0.0001
TP Altitude	3.31	E-06	9.00	E-08	36.72	<0.0001
Temperature	-0.0018		7.96	E-05	-22.59	<0.0001
Drag Index	-0.0004		2.75	E-05	-14.68	<0.0001
(TP Altitude)*(TP Mach)	3.12	E-05	2.18	E-06	14.27	<0.0001
(Drag Index)*(TP Mach)	-0.0055		6.67	E-04	-8.26	<0.0001
(Temperature)*(TP Mach)	-0.0117		1.93	E-03	-6.05	<0.0001
(Temperature)*(TP Altitude)	-6.83	E-08	1.27	E-08	-5.36	<0.0001
(Drag Index)*(TP Altitude)	1.69	E-08	4.40	E-09	3.85	0.0001
(Weight)*(TP Altitude)	-1.76	E-10	5.47	E-11	-3.22	0.0014
(Temperature)*(Drag Index)	-1.13	E-05	3.89	E-06	-2.9	0.0039
Weight	9.74	E-07	3.43	E-07	2.84	0.0048
(Weight)*(TP Mach)	1.88	E-05	8.38	E-06	2.24	0.0255
(Weight)*(Drag Index)	1.76	E-08	1.68	E-08	1.05	0.2937
(Weight)*(Temperature)	-3.06	E-08	4.86	E-08	-0.63	0.5293

From observing the data in this table, it is apparent that nearly all the parameters and their combinations are significant. It is obvious to assume that TP Mach and TP

Altitude will have significance with every data point based on the assumption that each result is focused around each test point. However, the original assumption was that Weight would be a factor of primary concern. Although it is still significant to the data (i.e. 0.0048 < 0.05), the interaction of Temperature and Drag Index carry a greater importance. If all of the TP interactions and values were removed, we perhaps can even see more precise results. Table 4.2 shows this relation.

Table 4.2: Sorted Parameter Estimates without TP Interactions

Term	Estimate		Standard Error		t-Ratio	Prob > |t|
Temperature	-0.0018		7.96	E-05	-22.59	<0.0001
Drag Index	-0.0004		2.75	E-05	-14.68	<0.0001
(Temperature)*(Drag Index)	-1.13	E-05	3.89	E-06	-2.9	0.0039
Weight	9.74	E-07	3.43	E-07	2.84	0.0048
(Weight)*(Drag Index)	1.76	E-08	1.68	E-08	1.05	0.2937
(Weight)*(Temperature)	-3.06	E-08	4.86	E-08	-0.63	0.5293

From this simplified table, the results are much clearer.

Looking at the sorted estimates figure, it can be seen more clearly which parameters are significant and which parameters are not. For the Starting Mach number response, Figure 4.1 shows this result. Comparing Table 4.1 and Figure 4.1 provides some additional insight into which parameters carry more consequence. Although all of them provide significance, the parameters that appear to be the most sensitive to adjustment would be Temperature and Drag Index. The blue lines indicate the point of significance (0.05) and show that although all three primary inputs are important, temperature changes and miscalculations in the drag index number will cause a much

greater shift in the outcome of the starting Mach number. Note that this analysis above is only for the starting Mach number system response.
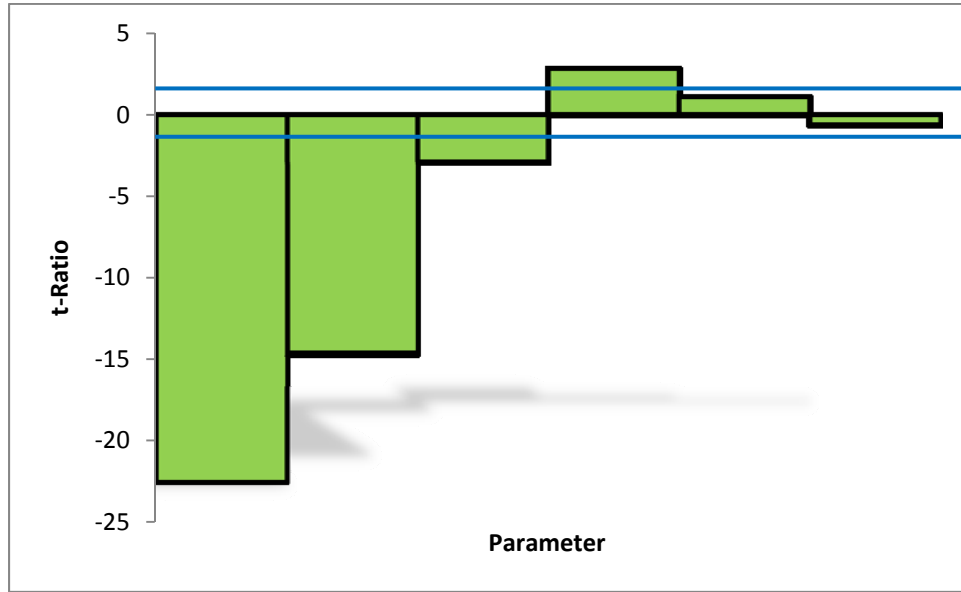
Figure 4.1: Starting Mach Response Sensitivity Probability Plot

Another consideration for this response is the interaction of the variables. From Table 4.1 and Table 4.2, there is an important interaction in regards to sensitivity between temperature and drag index, but another uncertainty must be accounted for. This

uncertainty is whether or not one interaction is shadowing a single parameter. Figure 4.2 shows these interactions.
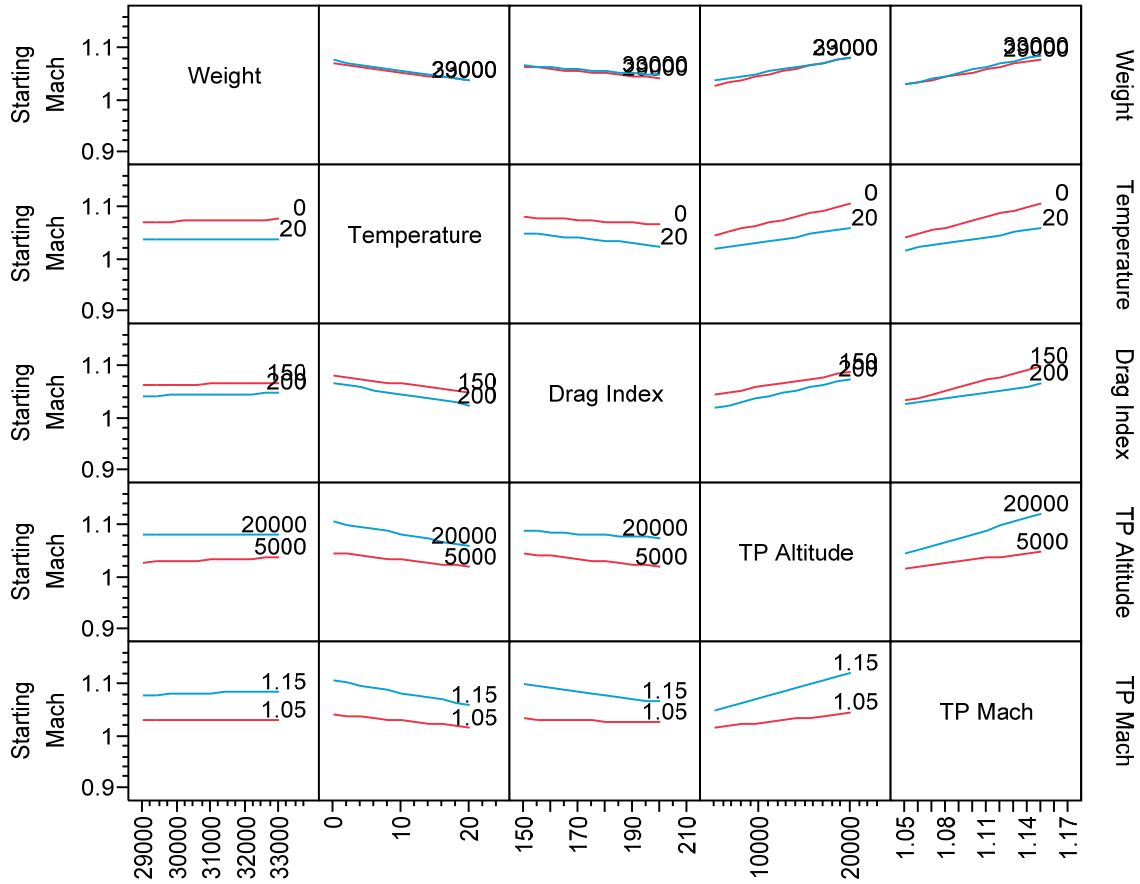
Figure 4.2: Interaction Profiles for Starting Mach Response

As was stated in the beginning of Chapter four, the interactions can be over shadowing of individual parameters as the lines become less parallel. And based on the analysis already conducted (the determination that the weight was surprising less important than the other variables), we must consider its interactions foremost. However, focusing on the first column and row from Figure 4.2, it can be seen that nearly all the lines are exactly parallel. This indicates that there is minimal over shadowing of the weight variable and it can be assumed that the sensitivity analysis for this response is

accurate. The key behind this figure is determining where the two interaction lines are non parallel for each set of interactions. In this case, the lines for all twenty interaction plots are parallel (in general) and do not have any over shadowing effects over the other variables.

In summary, the Starting Mach response is fundamentally affected by changes in the temperature and the drag index. The weight is actually insignificant to this particular response. The interaction of temperature and drag index also can play a significant role in the outcome of the Dive Planning model. From here, the next step is to evaluate the other responses. The next response of interest is the Starting Altitude response.

4.2.2 Analysis of Starting Altitude Response

Repeating the same process as before, the observation of the Analysis of Variance Table, Table B.1.2 in this report, must be done first. Since the Prob > |t| value is less than 0.0001, then a significant variable must be present in the system. Since at this point it is understood that each response will have at least one significant variable, this step can now be skipped for future analysis. Now, moving to the parameter estimates table, Table 4.3, assumptions can be made about variables that will be the most sensitive to the starting altitude response.

Table 4.3: Sorted Parameter Estimates for Starting Altitude Response

Term	Estimate		Standard Error		t-Ratio	Prob > |t|
TP Altitude	0.0006		7.29	E-06	83.39	<0.0001
TP Mach	45.6532		1.108787		41.17	<0.0001
Temperature	0.2204		0.006443		34.22	<0.0001
Drag Index	0.0333		0.0022		14.99	<0.0001
(TP Altitude)*(TP Mach)	-0.0025		0.0002		-14.07	<0.0001
(Temperature)*(TP Mach)	1.3981		0.1560		8.96	<0.0001
(Drag Index)*(TP Mach)	0.3025		0.0540		5.61	<0.0001
(Temperature)*(TP Altitude)	3.42	E-6	1.03	E-06	3.31	0.0010
(Temperature)*(Drag Index)	0.0008		0.0003		2.65	0.0084
(Drag Index)*(TP Altitude)	-6.17	E-7	5.56	E-07	-1.73	0.0839
(Weight)*(TP Altitude)	7.06	E-9	4.43	E-09	1.59	0.1117
Weight	-4.20	E-5	2.78	E-05	-1.51	0.1325
(Weight)*(Temperature)	4.95	E-6	3.93	E-06	1.26	0.2087
(Weight)*(TP Mach)	-0.0007		0.0007		-1.01	0.3111
(Weight)*(Drag Index)	-2.05	E-7	1.36	E-06	-0.15	0.8798

Using a similar analytical method as previously, the trend on the significance of results remains fairly unchanged. There is some rearrangement of the terms, but the primary note here is that six (6) of the terms are now insignificant to the response. It may be more realistic, however, to make another table as was done in the previous section. Table 4.4 shows the removal of terms assumed to be significant such as the test point criteria.

Table 4.4: Sorted Parameter Estimates without TP Interactions

Term	Estimate		Standard Error		t-Ratio	Prob > |t|
Temperature	0.2204		0.006443		34.22	<0.0001
Drag Index	0.0333		0.0022		14.99	<0.0001
(Temperature)*(Drag Index)	0.0008		0.0003		2.65	0.0084
Weight	-4.20	E-5	2.78	E-05	-1.51	0.1325
(Weight)*(Temperature)	4.95	E-6	3.93	E-06	1.26	0.2087
(Weight)*(Drag Index)	-2.05	E-7	1.36	E-06	-0.15	0.8798

Looking at this second table, and comparing the order of terms to the first table, it can be observed that the only difference is that the last two terms have been switched (the interaction of weight and temperature is now more significant than the interaction of weight and drag index. The order of importance has remained virtually unchanged since the only two terms that were switched were both insignificant. It is important to point out again that the weight parameter is not significant in the determination of the starting altitude condition. Figure 4.3 will illustrate that result.
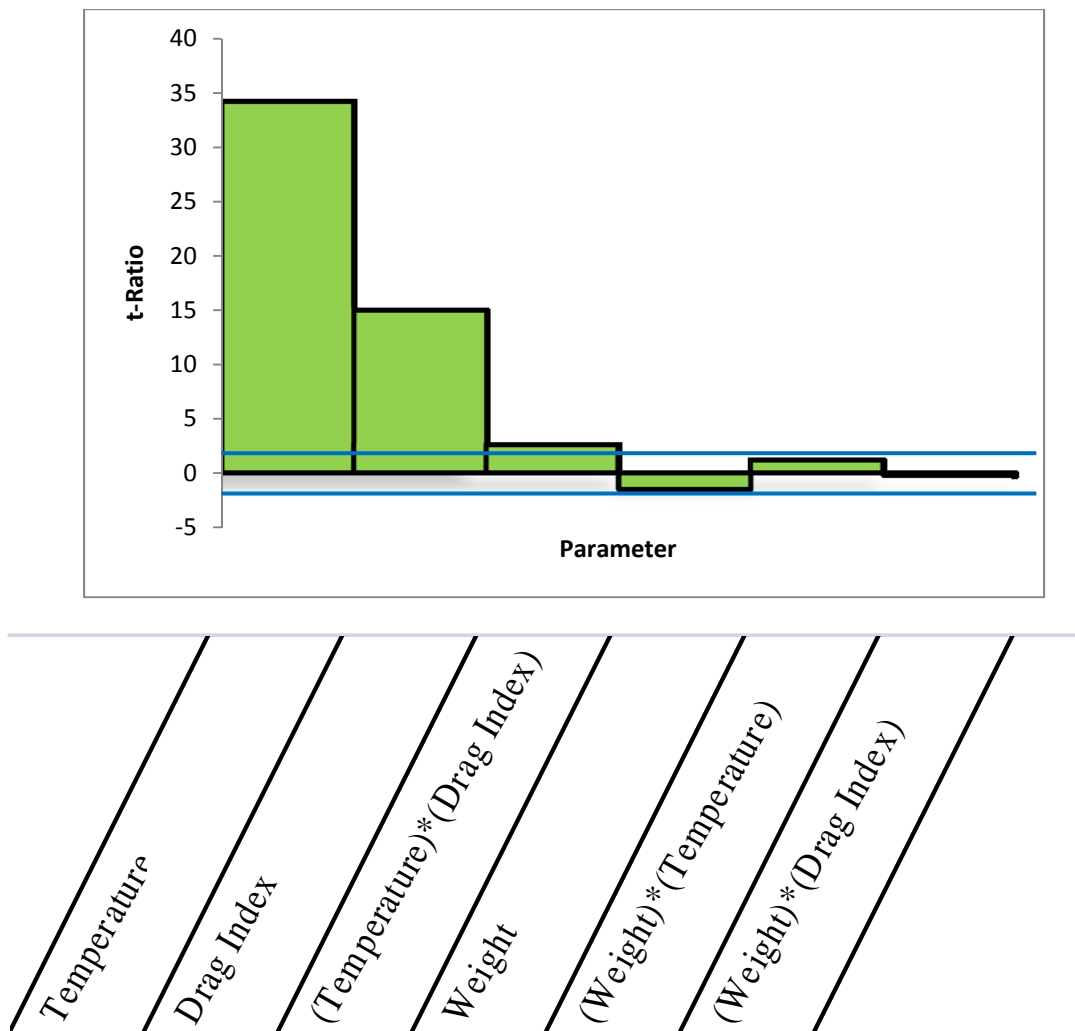
Figure 4.3: Starting Altitude Response Sensitivity Probability Plot

The verification of the importance of weight can be verified from an observation of the above figure. Since the weight parameter is completely enclosed within the blue sensitivity lines, it can be documented that weight has no significance on the determination of starting altitude conditions. The temperature and drag index still carry heavy significance over many of the other interactions, but not nearly to the degree that both parameters did in the determination of the starting Mach condition.

The last step to verify the results from this analysis for the starting altitude response is to ensure that no parameter or interaction of parameters is over shadowing the weight and reducing its significance inaccurately. Figure 4.4 shows the interaction plot for the starting altitude response.
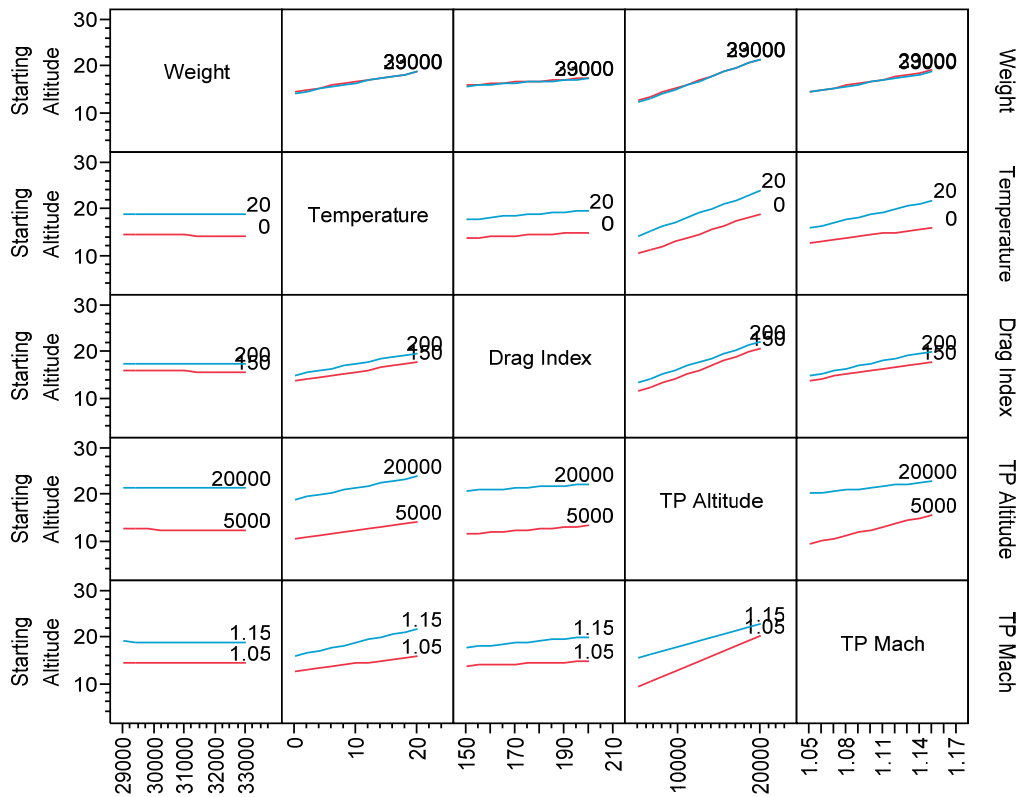
Figure 4.4: Interaction Profiles for Starting Altitude Response

Focusing again on the first row and column as was done previously to verify the preceding analysis it can be observed that the interaction lines are nearly parallel once again. In fact, in several instances the lines actually are overlaid on top of one another. This information continues to illustrate that weight may not a primary factor sensitive to variations during the flight test planning. The lack of over shadowing of one variable over another creates an important conclusion that can be used for the final analysis. The interaction plots that contain only parallel lines verify that the data being analyzed has some consistency and is not inaccurately represented or distorted by the interactions of multiple variables.

This response had a very similar result as compared to the Starting Mach response. There is no over shadowing of the variables and the temperature and drag index are the driving parameters for the predictive model. In essence, the starting conditions for the dive profile are primarily controlled by the temperature, the drag index, and the interaction of temperature and drag index. This is consistent with the understanding of the model. The next response, Dive Angle response, is evaluated in a similar manner to determine if this output is affected by a different set of parameters.

4.2.3 Analysis of Dive Angle Response

With the significance already assumed to be present in at least one variable, the initial step of checking the Analysis of Variance Table becomes redundant. However, the table is located in Appendix B as Table B.1.3 for referencing if necessary. With that step aside, the next procedure is to make observations about the parameter estimates. Table

103

4.5, shown below indicates the estimates, the standard error, the t-Ratio, and establishes

the sensitivity of each term with the Prob > |t| value.

The information that can be obtained from looking at the sensitivity values is that

all but two of the terms are significant, and those two terms are weight interactions,

which have typically been insignificant in past discussions. Table 4.5 is shown here.

Table 4.5: Sorted Parameter Estimates for Dive Angle Response

Term	Estimate		Standard Error		t-Ratio	Prob > |t|
TP Altitude	0.0010		8.35	E-06	118.51	<0.0001
TP Mach	-101.6981		1.2697		-80.10	<0.0001
Temperature	-2.583		0.0074		-35.00	<0.0001
Drag Index	-0.0873		0.0025		-34.27	<0.0001
(TP Altitude)*(TP Mach)	0.0066		0.0002		32.76	<0.0001
(Temperature)*(TP Altitude)	-1.77	E-05	1.18	E-06	-14.97	<0.0001
(Drag Index)*(TP Altitude)	6.06	E-06	4.08	E-07	14.86	<0.0001
(Temperature)*(TP Mach)	-2.1925		0.1786		-12.27	<0.0001
Weight	0.0003		3.18	E-05	10.44	<0.0001
(Drag Index)*(TP Mach)	-0.4845		0.0618		-7.85	<0.0001
(Weight)*(TP Altitude)	-3.03	E-08	5.07	E-09	-5.98	<0.0001
(Weight)*(TP Mach)	0.0032		0.0008		4.15	<0.0001
(Temperature)*(Drag Index)	-0.0010		0.0004		-2.91	0.0038
(Weight)*(Drag Index)	2.05	E-06	1.56	E-06	1.32	0.1880
(Weight)*(Temperature)	5.13	E-06	4.50	E-06	1.14	0.255

Once the significant values are identified initially it again is convenient to observe

the same data table with the test point terms removed. Table 4.6 shows this information

for the dive angle response.

Table 4.6: Sorted Parameter Estimates without TP Interactions

Term	Estimate		Standard Error		t-Ratio	Prob > |t|
Temperature	-2.583		0.0074		-35.00	<0.0001
Drag Index	-0.0873		0.0025		-34.27	<0.0001
Weight	0.0003		3.18 E-05		10.44	<0.0001
(Temperature)*(Drag Index)	-0.0010		0.0004		-2.91	0.0038
(Weight)*(Drag Index)	2.05 E-06		1.56 E-06		1.32	0.1880
(Weight)*(Temperature)	5.13 E-06		4.50 E-06		1.14	0.255

Once the test point terms are removed, a startling discovery can be made. It can be seen that weight has actually increased in significance and sensitivity to the model in terms of the dive angle response. Although in Table 4.5, weight was still a middle category variable, it carries a probability of less than 0.0001. Its interaction with the other two terms is still insignificant; however, the temperature and drag index interaction still carries some weight in the determination of the response.

The next important comparison that needs to be made is in regards to Figure 4.5 shown below. Figure 4.5 shows that temperature and drag index have nearly identical importance in the determination of dive angle from the model. The weight, while still dramatically more relevant in the determination of this response, is only a fraction of the importance and significance carried by the other two primary terms. When compared to the previous sorted parameter figure, Figure 4.3, it can be observed that all of the variables carry a greater significance in comparison to the reactions with the starting altitude response.

This determination can be made by the distance between the two blue lines. Although in the figure below there appears to be only one thicker blue line, it is in fact

indicative of a very important set of variables that all play a crucial role in the determination of the dive angle response. This is an important observation because it provides insight as to the sensitivity of these variables.
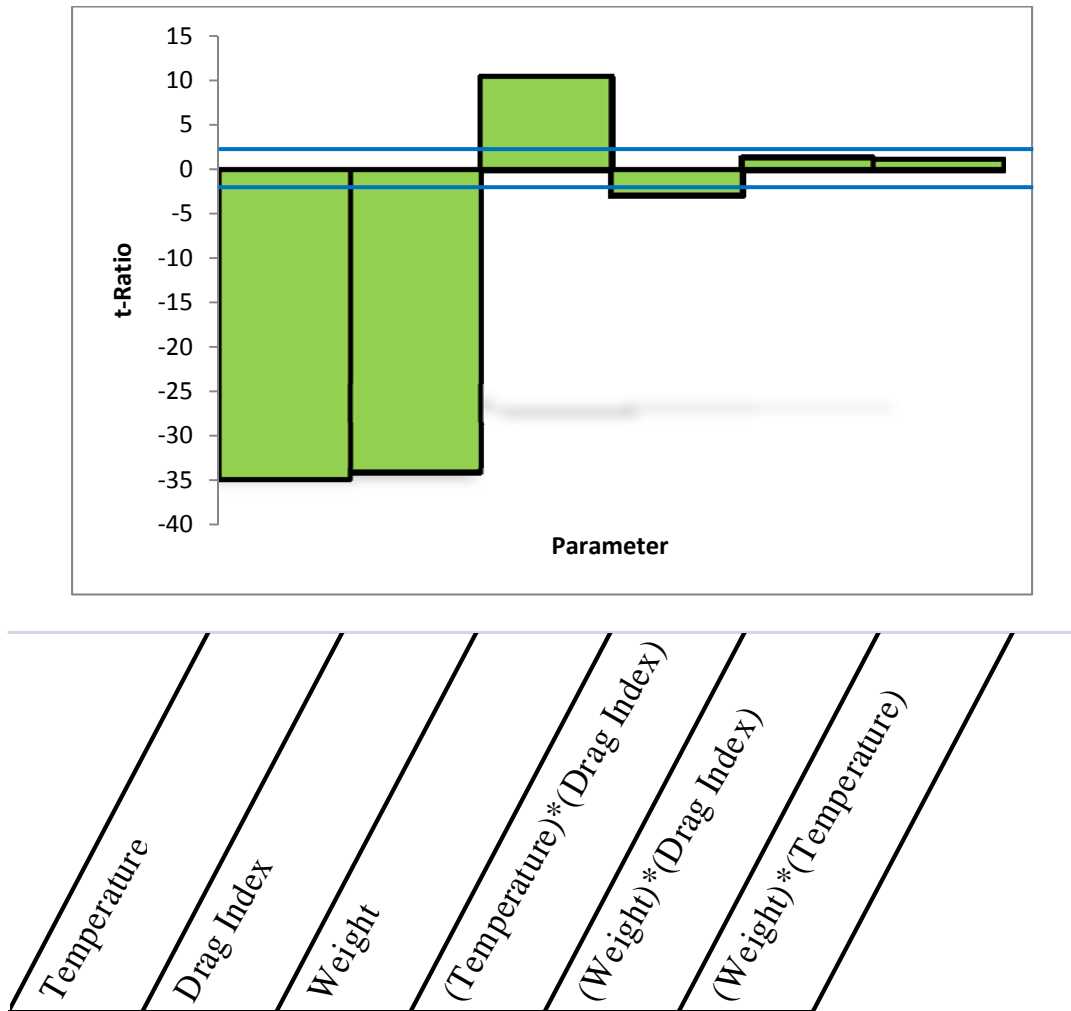
Figure 4.5: Dive Angle Response Sensitivity Probability Plot

The last figure that needs to be observed for this response is the interaction plot. This plot provides information about how one variable may be overshadowing another.

The ideal situation is that the lines are perfectly parallel indicating that there are no adverse interactions between the variables. By looking at Figure 4.6 shown below it can be seen that most of the interactions are nearly parallel. There are no cross-over points between the data results and this is consistent when considering that all three of the primary terms discussed are in fact significant to the determination of the dive angle response.
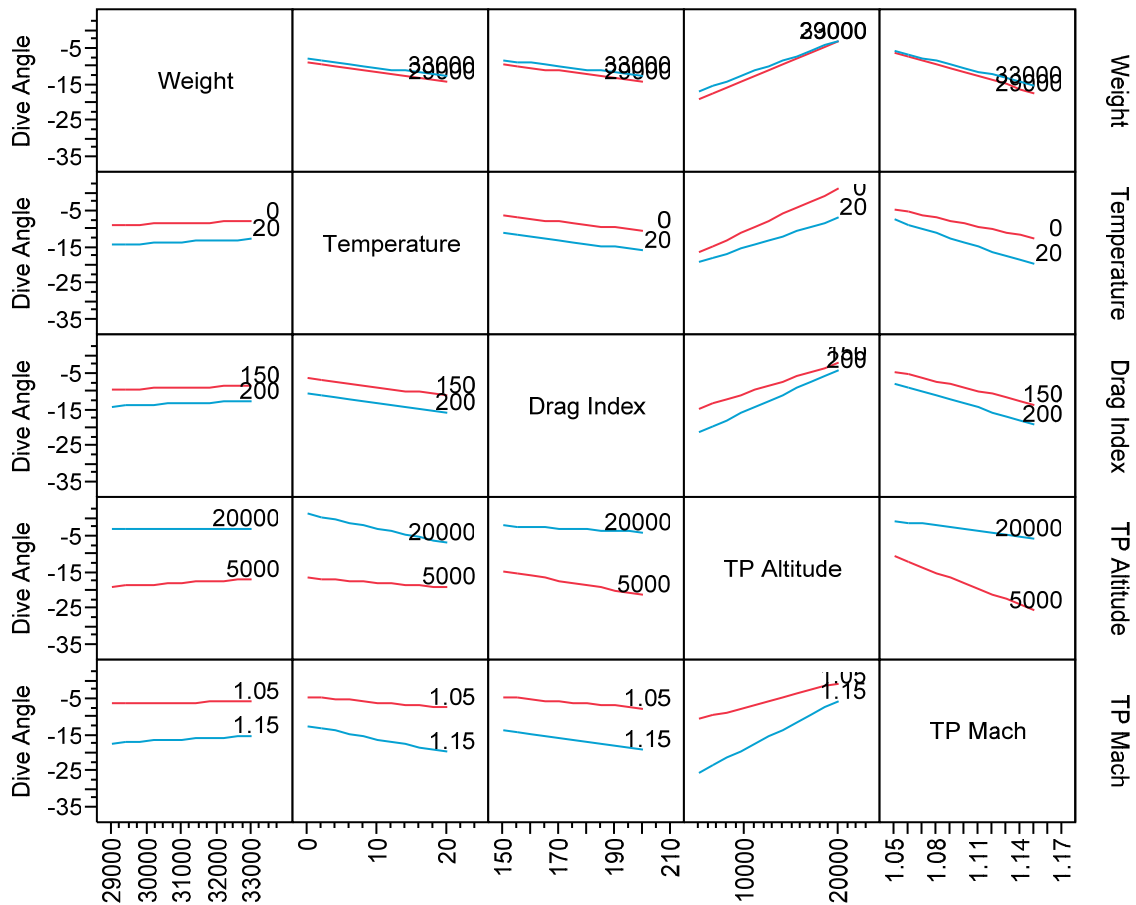
Figure 4.6: Interaction Profiles for Dive Angle Response

From the analysis of the Dive Angle response, the important conclusion is that weight now carries significance and the model is sensitive to changes in weight. This conclusion is important because the first two responses were insensitive to the weight parameter and its interactions. Understanding that the starting conditions are driven by temperature and drag index and that the dive angle is driven by weight, temperature, and drag index provide insight into the Dive Planning model's sensitivities. The next two responses deal directly with the recovery from the high-speed dive.

4.2.4 Analysis of Start Recovery Response (Recovery Altitude 1)

The start of the recovery is the condition after the completion of the maneuver that the pilot would need to begin to reestablish steady-level flight. There will later be discussion of a "Recovery Altitude 2" or "End Recovery" response. The difference is that the Start Recovery response is the point at which the test pilot should begin to exit the maneuver at the test point and begin a recovery procedure. The second recovery point or End Recovery response is the predicted altitude where the pilot should have regained steady-level and controlled flight of the aircraft. This is the point at which the aircraft can resume normal flight. Understanding the sensitivity of the terms affecting this response is critical to the safety of the mission, particularly at low altitude test points. Table 4.7, shown below, gives a list of the sorted parameter estimates so that the significance of each interaction and term can be analyzed.

Table 4.7: Sorted Parameter Estimates for Recovery Altitude 1 Response

Term	Estimate		Standard Error		t-Ratio	Prob > |t|
TP Altitude	0.0010		5.76	E-07	1845.1	0.0000
TP Mach	-6.8195		0.0877		-77.79	<0.0001
Temperature	-0.0170		0.0005		-33.46	<0.0001
(TP Altitude)*(TP Mach)	0.0005		0.00001		32.59	<0.0001
Drag Index	-0.0053		0.0002		-30.26	<0.0001
(Drag Index)*(TP Altitude)	3.73	E-07	2.81	E-08	13.25	<0.0001
(Temperature)*(TP Mach)	-0.1568		0.0123		-12.71	<0.0001
(Temperature)*(TP Altitude)	-9.67	E-07	8.15	E-08	-11.86	<0.0001
Weight	1.94	E-05	2.20	E-06	8.81	<0.0001
(Drag Index)*(TP Mach)	-0.0303		0.0043		-7.10	<0.0001
(Weight)*(TP Altitude)	-1.56	E-09	3.50	E-10	-4.45	<0.0001
(Weight)*(TP Mach)	0.0002		5.37	E-05	3.90	0.0001
(Temperature)*(Drag Index)	-6.25	E-05	2.49	E-05	-2.51	0.0124
(Weight)*(Drag Index)	1.35	E-07	1.07	E-07	1.25	0.2103
(Weight)*(Temperature)	3.40	E-07	3.11	E-07	1.09	0.2748

This table has a similar look to the dive angle response table, Table 4.5. When eliminating the test point data to obtain a clearer look at the results, the sensitivity of the parameters can be more readily comprehended. Table 4.8 contains this reduction of data.

Table 4.8: Sorted Parameter Estimates without TP Interactions

Term	Estimate		Standard Error		t-Ratio	Prob > |t|
Temperature	-0.0170		0.0005		-33.46	<0.0001
Drag Index	-0.0053		0.0002		-30.26	<0.0001
Weight	1.94	E-05	2.20	E-06	8.81	<0.0001
(Temperature)*(Drag Index)	-6.25	E-05	2.49	E-05	-2.51	0.0124
(Weight)*(Drag Index)	1.35	E-07	1.07	E-07	1.25	0.2103
(Weight)*(Temperature)	3.40	E-07	3.11	E-07	1.09	0.2748

Once the test point data has been removed, Table 4.8 looks nearly identical to

Table 4.6. It is because of this nearly similar result that analyzing the results in Figure

4.7, the sensitivity probability plot, becomes vital to a clear understanding of the differences in the data presented for each response.
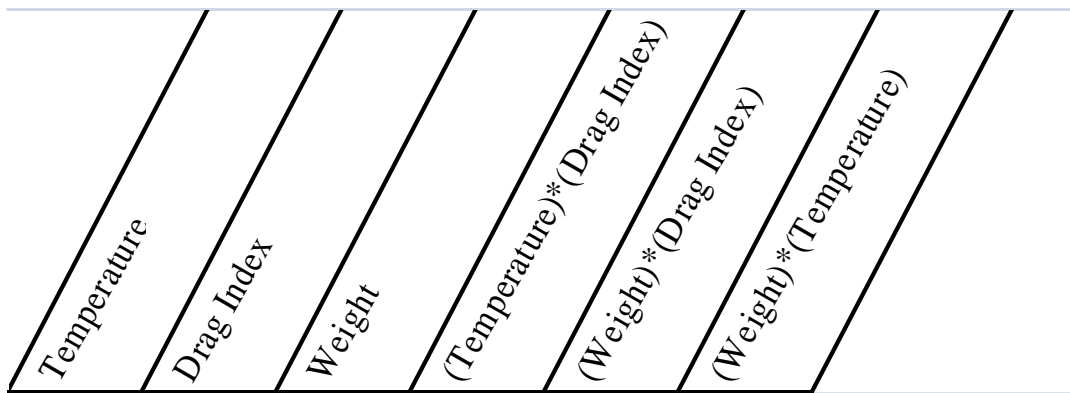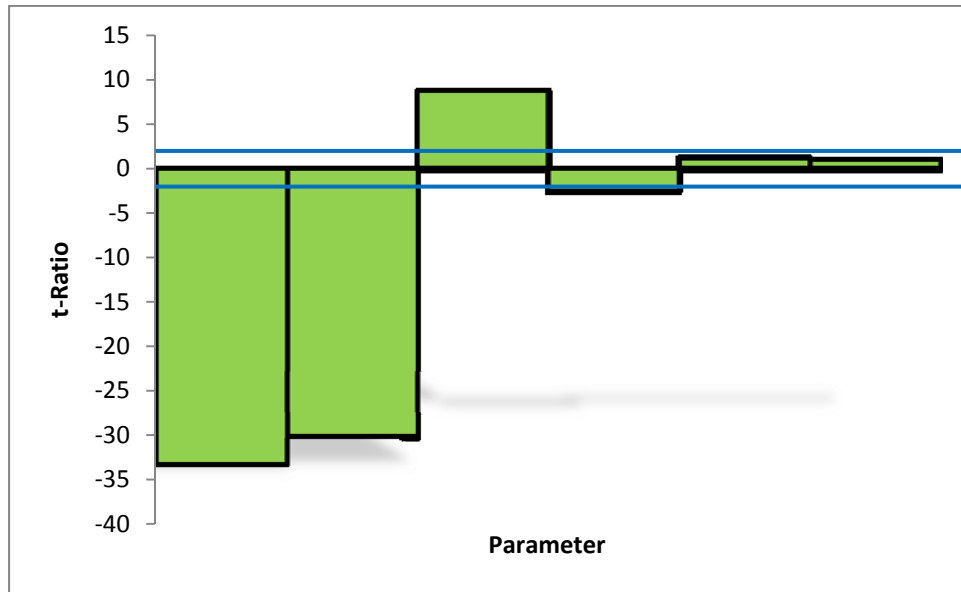
Figure 4.7: Start Recovery Response Sensitivity Probability Plot

Looking at the results presented in Figure 4.7, it can be seen that with respect to the primary parameter of the test point altitude, that the others are of minimal importance. Looking at the t-Ratio values for TP Altitude in Table 4.7 particularly illustrates this point since the value is on the order of two magnitudes higher than the next most

significant term. All of the data appears to be significant with the exception of the last two interactions with weight and drag index and temperature respectively. But because of the over powering effect of the test point altitude, the information must be derived from observation of the t-Ratios and the sensitivity probability values contained within the tables.

The interaction profile is the next piece of information that must be considered. This ensures that no probabilities are being dominated by another parameter. Looking at the interaction profiles for the starting recovery response, Figure 4.8, there are no interactions at all that are disrupting the results. The lines are nearly parallel in all cases and in some instances sit directly on top of one another. See Figure 4.8 below.
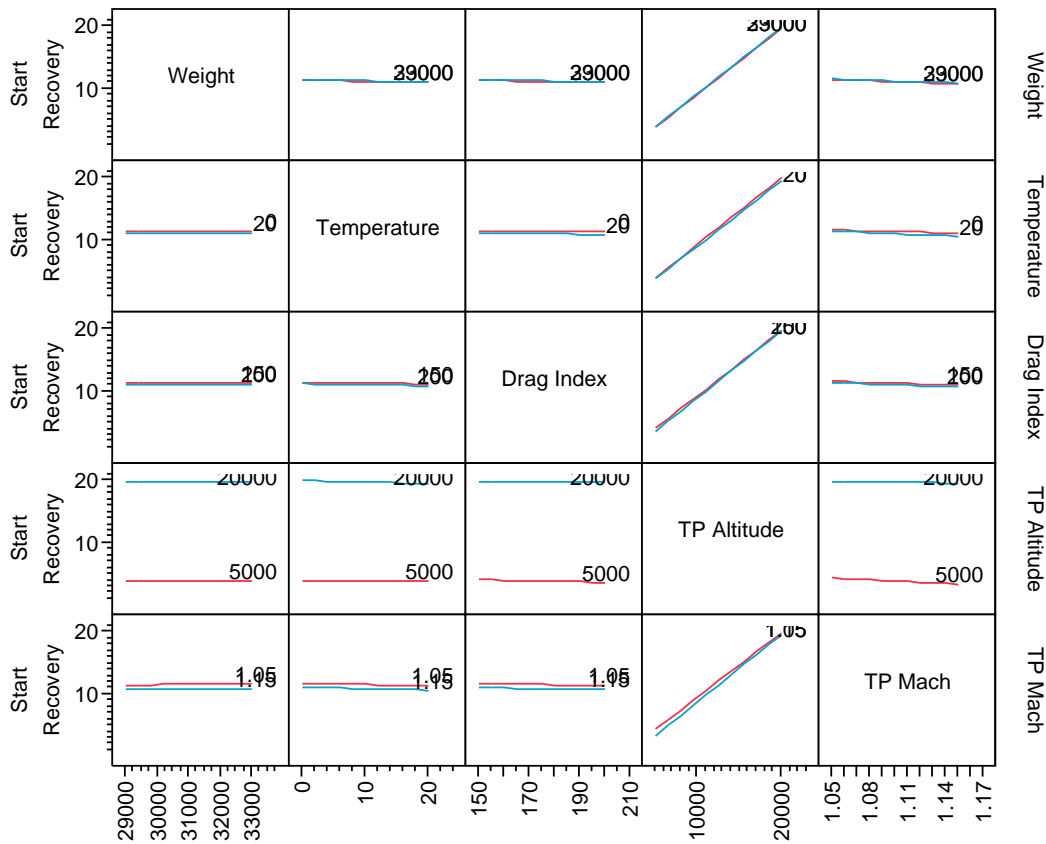
Figure 4.8: Interaction Profiles for Starting Recovery Response

111

Similar to the Dive Angle response, the starting recovery altitude output is controlled by the temperature, weight, and drag index. The interaction of temperature and drag index also plays a vital role, but the three independent parameters are the primary drivers for the model. Knowing that weight is a primary variable of concern at the Start Recovery response increases the need to accurately model the weight of the aircraft throughout the entire flight test, particularly since the weight may change significantly between the start of the dive and the start of the recovery. The End Recovery response is the most critical for understanding its sensitivities. This is because of the possibility of low altitude recovery points that can increase risk for the test run.

4.2.5 Analysis of End Recovery Response (Recovery Altitude 2)

The last analysis from the first set of results is the end recovery response. This response is the final altitude at which the test pilot regains a steady-level flight condition with the aircraft. The analysis of the sensitivity of this response carries the most weight of any of the results. The reasoning behind this is that if the table in Appendix A is carefully observed, it can be seen that some recovery altitudes are at 100 feet above sea level. Any minor deviation in the conditions could possibly result in a fatal accident and cost the sponsor millions in damages. The concept of mitigating risk becomes critical here. These points would typically be thrown out or adjustments made such that the final recovery altitude was much higher.

For this reason, the data in this section must be analyzed with the utmost consideration. The first step of the analysis will be to look at the sorted parameter estimates for this response. Table 4.9 contains this information.

Table 4.9: Sorted Parameter Estimates for Recovery Altitude 2 Response

Term	Estimate		Standard Error		t-Ratio	Prob > |t|
TP Altitude	0.0011		1.50	E-06	755.19	0.0000
TP Mach	-16.4206		0.2287		-71.80	<0.0001
(TP Altitude)*(TP Mach)	0.0014		3.65	E-05	38.57	<0.0001
Drag Index	-0.0131		0.0005		28.60	<0.0001
Temperature	-0.0349		0.0013		-26.25	<0.0001
(Drag Index)*(TP Altitude)	-1.17	E-06	7.34	E-08	15.90	<0.0001
(Temperature)*(TP Mach)	-0.4036		0.0322		-12.54	<0.0001
(Drag Index)*(TP Mach)	-0.1275		0.0111		-11.45	<0.0001
Weight	5.31	E-05	5.73	E-06	9.27	<0.0001
(Weight)*(TP Altitude)	-5.47	E-09	9.13	E-10	-5.99	<0.0001
(Weight)*(TP Mach)	0.0007		0.0001		4.85	<0.0001
(Temperature)*(TP Altitude)	-9.73	E-09	2.13	E-07	-4.58	<0.0001
(Temperature)*(Drag Index)	-0.0002		6.49	E-05	-2.80	0.0054
(Weight)*(Drag Index)	4.22	E-07	2.80	E-07	1.51	0.1322
(Weight)*(Temperature)	7.95	E-07	8.11	E-07	0.98	0.3276

The first information that can be pulled from this data table is in regards to the order of the significance of the terms. This is the first table where an interaction of test point parameters outweighs the primary parameters of drag index and temperature. The other consideration that can be noted is that weight is once again more significant than any other set of parameters. Table 4.10 will illustrate this information better by removing the test point terms.

Table 4.10: Sorted Parameter Estimates without TP Interactions

Term	Estimate		Standard Error		t-Ratio	Prob > |t|
Drag Index	-0.0131		0.0005		28.60	<0.0001
Temperature	-0.0349		0.0013		-26.25	<0.0001
Weight	5.31	E-05	5.73	E-06	9.27	<0.0001
(Temperature)*(Drag Index)	-0.0002		6.49	E-05	-2.80	0.0054
(Weight)*(Drag Index)	4.22	E-07	2.80	E-07	1.51	0.1322
(Weight)*(Temperature)	7.95	E-07	8.11	E-07	0.98	0.3276

With the additional information removed about the test point parameters, the table above is beginning to take a familiar form. Once again it can be seen that the three primary factors in significance are the independent terms of drag index, temperature, and weight. The important note that can be made here, however, is that drag index becomes the most significant parameter with the test point interactions removed. This provides insight into the sensitivity of this information in regards to the final recovery altitude.

There is one major positive and one major negative associate with the drag index being the primary factor affecting the final recovery altitude response. The positive is that drag index, during flutter envelope expansion flight testing, typically remains unchanged. Unless a store breaks free or the test involves the release of munitions at low altitudes, the test will typically cease if the drag index changes. This eliminates the risk of a miscalculation in the recovery responses from the model. The negative side of this is that the drag index may be difficult to determine exactly for a given aircraft configuration. This problem may lead to an undershoot or overshoot of the data and cause the model predictions to present a significant amount of error and increasing the risk to personnel and equipment.

The next analysis should come from the information contained in Figure 4.9 shown below.
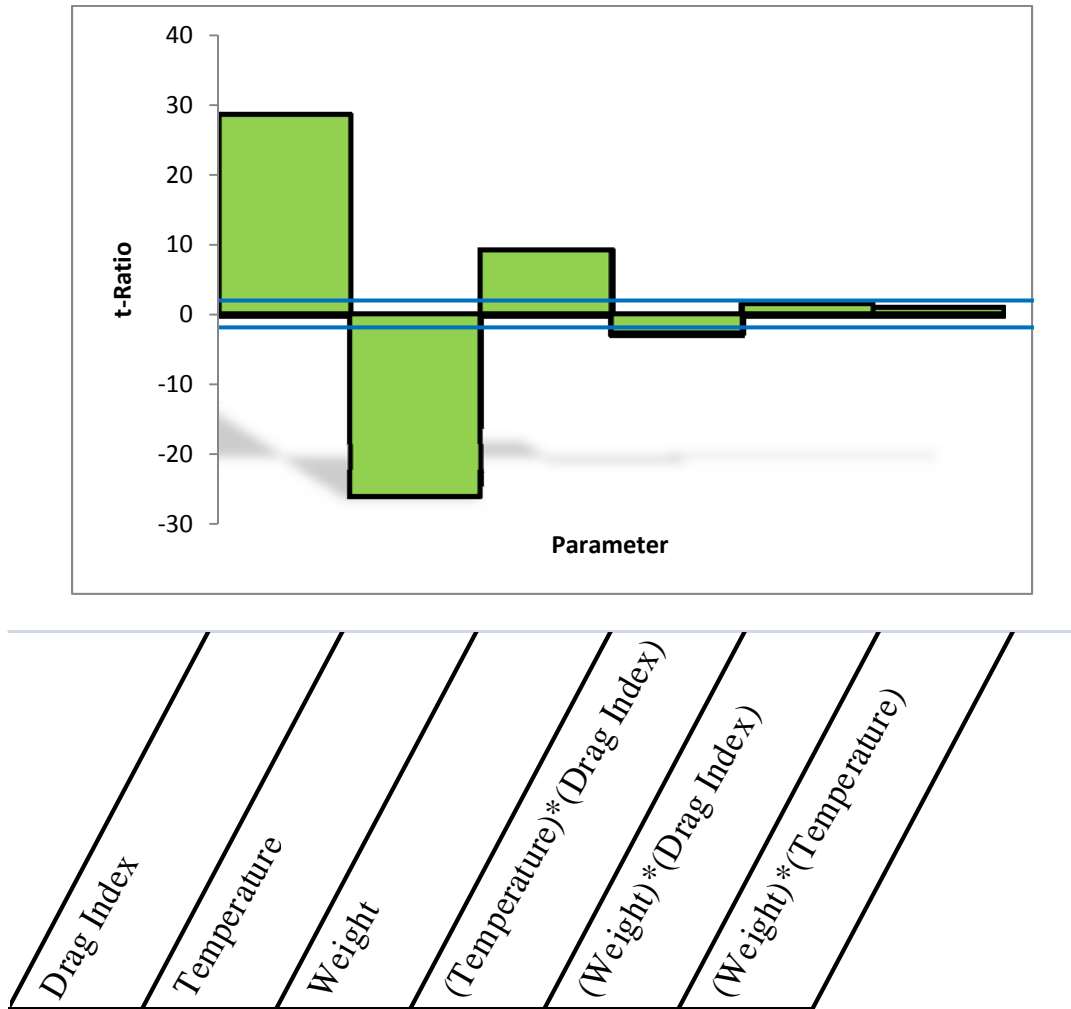
Figure 4.9: End Recovery Response Sensitivity Probability Plot

Once again, as in Figure 4.7, there is a single overpowering term that drives the sensitivity probability plot. The test point altitude term carries a t-Ratio one order of magnitude higher than the other terms. It can be noted, though not necessarily visible in the figure, that all the parameters carry significance with the exception of the weight

interactions once again. However, in this case, those interactions are not nearly as insignificant as they have proven to be throughout the previous analysis of this data set.

The final observation that must be made for this section involves the interactions plot, Figure 4.10.
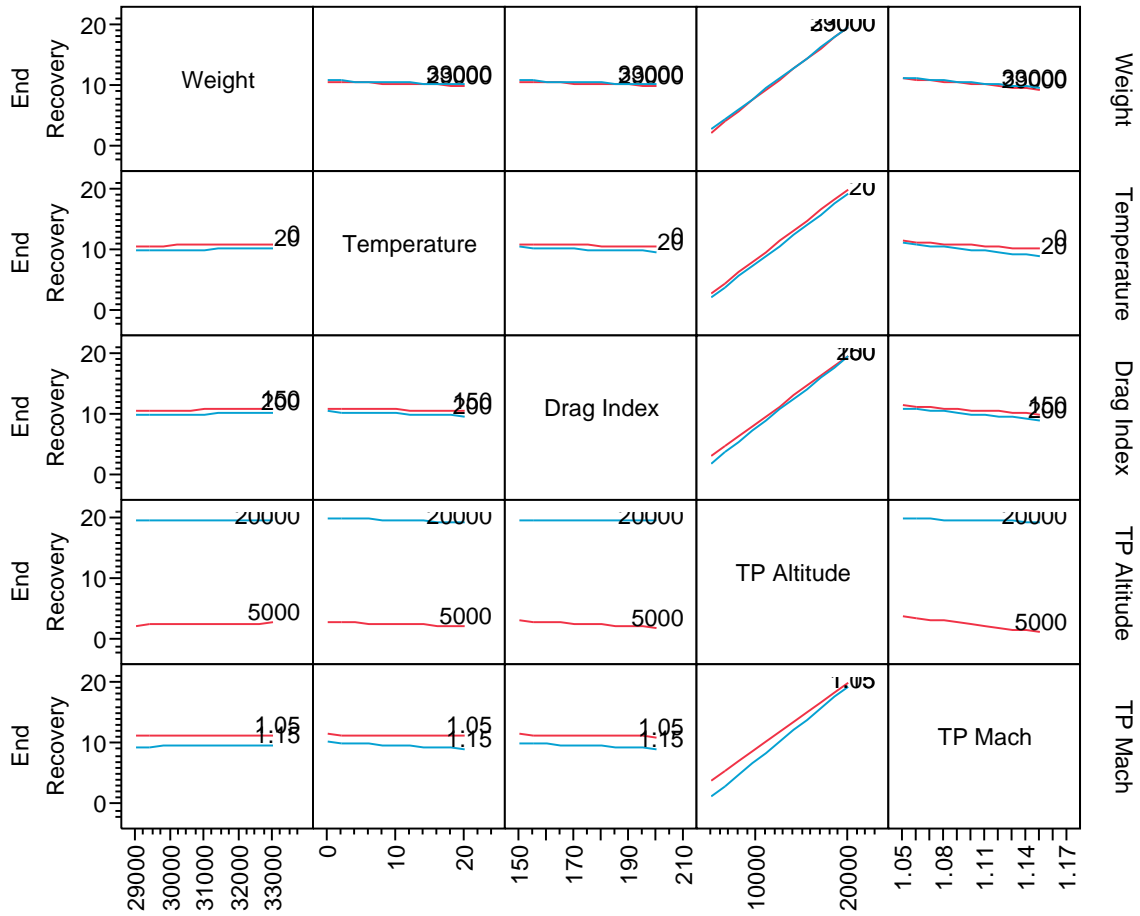
Figure 4.10: Interaction Profiles for Ending Recovery Response

Similar to the previous results, the interaction profiles for the ending recovery response show no over shadowing. The lines in each block are nearly parallel indicating a consistent trend that the data of each parameter is accurately represented in the sorted parameter estimates table and figures presented above.

Looking at all of the data for the initial analysis, several conclusions can be drawn. The first is that the dive model has a sensitivity concern primarily with the temperature and the drag index variables. The weight parameter becomes a critical variable towards the model's sensitivity when dealing with the predictions for the dive angle and the recovery of the aircraft. The interaction of temperature and drag index also plays a contributing role in the determination of the dive model responses. The interactions of the weight and the other parameters were considered insignificant to the responses for all cases.

From these results, the important conclusion about the determination and proper modeling of the temperature variation from standard day, aircraft drag index, and aircraft weight changes can be made. That conclusion is that these three variables are the driving parameters behind the dive model for all test conditions. In general, the temperature variation and drag index are the primary factors of concern, and weight is primarily driving the outcome associated with dive angle determination and recovery conditions. The Dive Planning model operator can take into consideration the responses produced by the model and determine the possible error with the variables to scratch certain flight test runs and increase the safety of the flight test program. The other benefit is that the operator can also know that variations in temperature and drag index calculations will drive the model's responses. Knowing these drivers, the operator can improve the efficiency of the test program by running flight tests when the conditions and calculations are optimal.

However, it is important to look at a specific case as well. In theory, the test points at high altitude will have a stronger association with variations in temperature and

117

weight. To verify that hypothesis, the high altitude test points were evaluated independently to determine any trends. Those results are identified in the next section.

4.3 Analysis Using 20,000 Foot Altitude Test Point Data Set

Due to the uncertainties that have been previously discussed, it is important to do an identical comparison of data for a high altitude sample of the previous data. Although the numbers and response values are identical to the application portion of the entire data set, by selecting the high altitude conditions, the analysis on the significance and sensitivity should be amplified due to the discussed energy differences and temperature variations that carry greater effect at increased altitudes.

4.3.1 Analysis of High Altitude Starting Mach Response

The high altitude analysis has a slight variation in the type of analysis that should be conducted. As was previously mentioned at the beginning of the chapter, there will be additional information reviewed in this section. The first information that is added is the Leverage plot, shown in Figure 4.11.
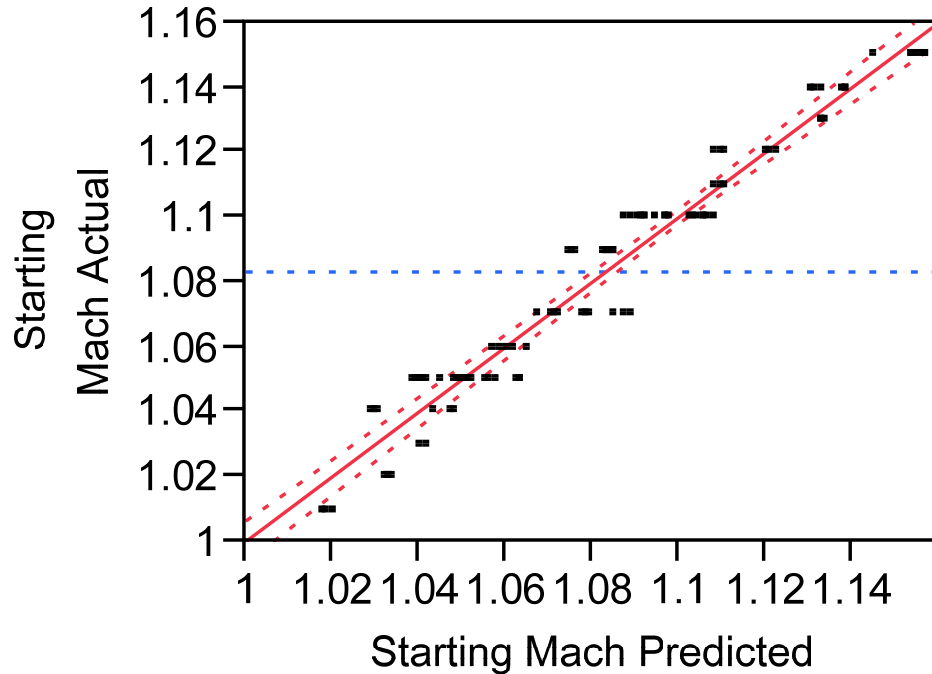
Figure 4.11: Leverage Plot for Starting Mach Response

The Leverage plot shows a plot of the actual starting Mach numbers versus the predicted starting Mach numbers. These predictions are the drivers behind the parameter estimates. The figure above shows that response values are located in bands running horizontally across the graph. The average and variances for the high altitude starting Mach numbers can be seen in Table 4.11. Between the figure above and the table below, the t-Ratios gain new meaning. By definition, the R^2 values and the Root Mean Square Error provide information about the deviation of the data from the mean. This is relevant in the high altitude case because there is another control that can drive these values. The control, being a constant test altitude, eliminates the variability across the data and the data fits a much closer regression curve. See the numbers in Table 4.11 below.

Table 4.11: Summary of Fit Table for Starting Mach Response

R^2	0.962
R^2 Adjusted	0.959
Root Mean Square Error	0.008
Mean of Response	1.082
Observations	135

As was discussed earlier, the difference between the R^2 values and the adjusted values are that the adjusted values can be compared across all of the responses. This adjustment shows that in general, the starting Mach response data has a ninety-six percent (96%) trend and only 0.008 Mach for a standard deviation. This is within the tolerances requested by the program executor of 0.01 Mach. This is an important statement because the data is able to be analyzed in the parameter estimates with a greater degree of certainty. The other information that can be taken from Table 4.11 is that the average starting Mach number was 1.082 and this analysis reviewed 135 of the original 386 test points.

Now it is important to look at the parameter estimates. Because of the removal of the test point altitude data, the test point Mach data can be removed from the estimates information as well. This can also be determined based on the information that was collected in the previous sections. The test point terms (indicating the test point altitude and Mach number) will always be significant to the results. That said, their contribution to the estimates table is irrelevant since the test point altitude and Mach will always be the most significant variables. Table 4.12 shows the sorted parameter estimates for the high altitude test data at the starting Mach response point.

Table 4.12: Sorted Parameter Estimates for Starting Mach Response

Term	Estimate		Standard Error		t-Ratio	Prob > |t|
Temperature	-0.0023		9.34	E-05	-24.50	<0.0001
Drag Index	-0.0003		3.24	E-05	-9.75	<0.0001
(Temperature)*(Drag Index)	-4.18	E-05	4.58	E-06	-9.13	<0.0001
(Weight)*(Temperature)	-4.44	E-08	5.72	E-08	-0.78	0.4387
Weight	-2.22	E-07	4.05	E-07	-0.55	0.5838
(Weight)*(Drag Index)	-1.00	E-08	1.98	E-08	-0.50	0.6147

Using the table above as a guide as was done previously, it can be shown that the terms

of significance are similarly temperature and drag index and their interaction. A

comparison of the data from Table 4.3 and Table 4.12 will be conducted in a later

section. From this information, the weight and its interactions with other parameters

carries almost no sensitivity to the Dive Planning model. This data will be reiterated in

the figure below, Figure 4.12. In this figure it will be possible to determine that the

temperature is the most significant term. This significance indicates a great sensitivity to

the model during the calculation of the starting Mach responses. See Figure 4.12.
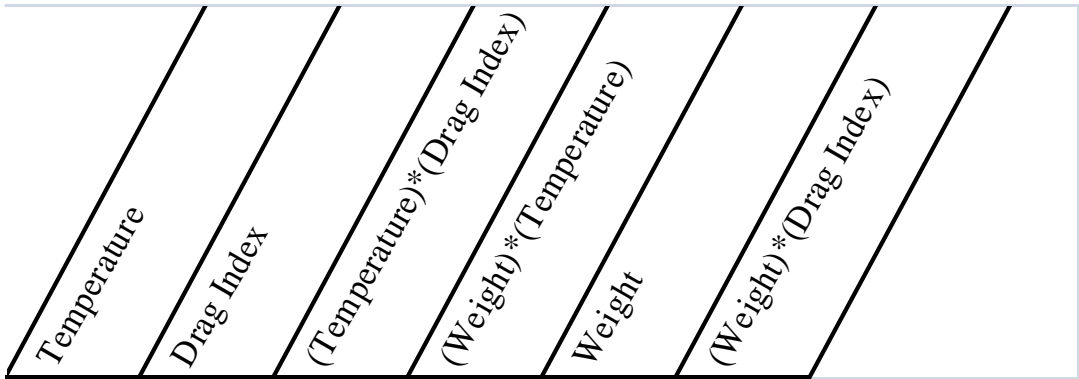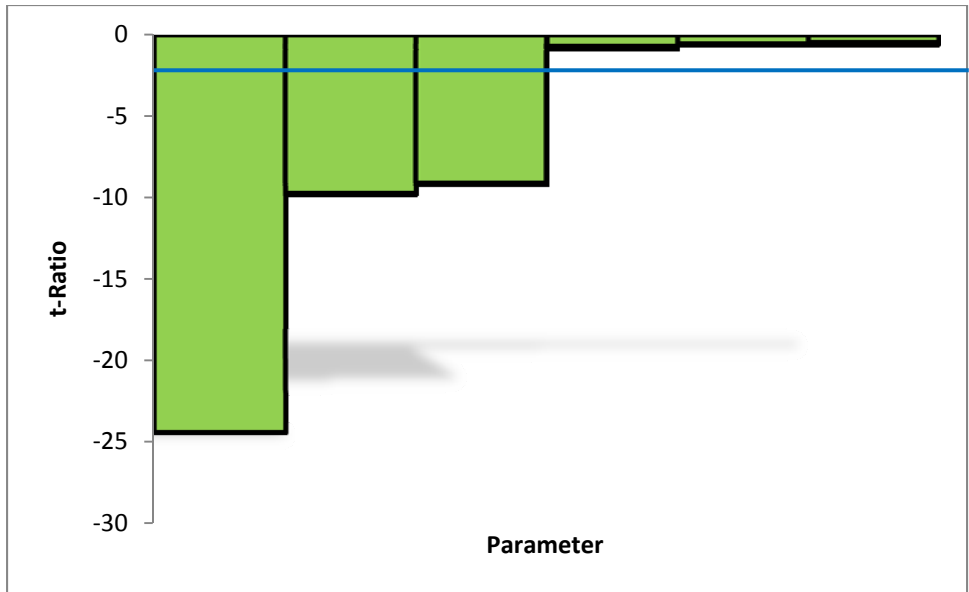
Figure 4.12: Starting Mach Sensitivity Probability Plot

From this view of the sensitivity probability plot, the sensitivity envelope contained within the two blue lines indicates that, as stated earlier, the weight and its interaction with the other parameters has little effect on the starting Mach predictions and calculations. In order to verify that this information is an accurate representation, the interaction profile must be considered. The interaction profile for the starting Mach response is shown in Figure 4.13.
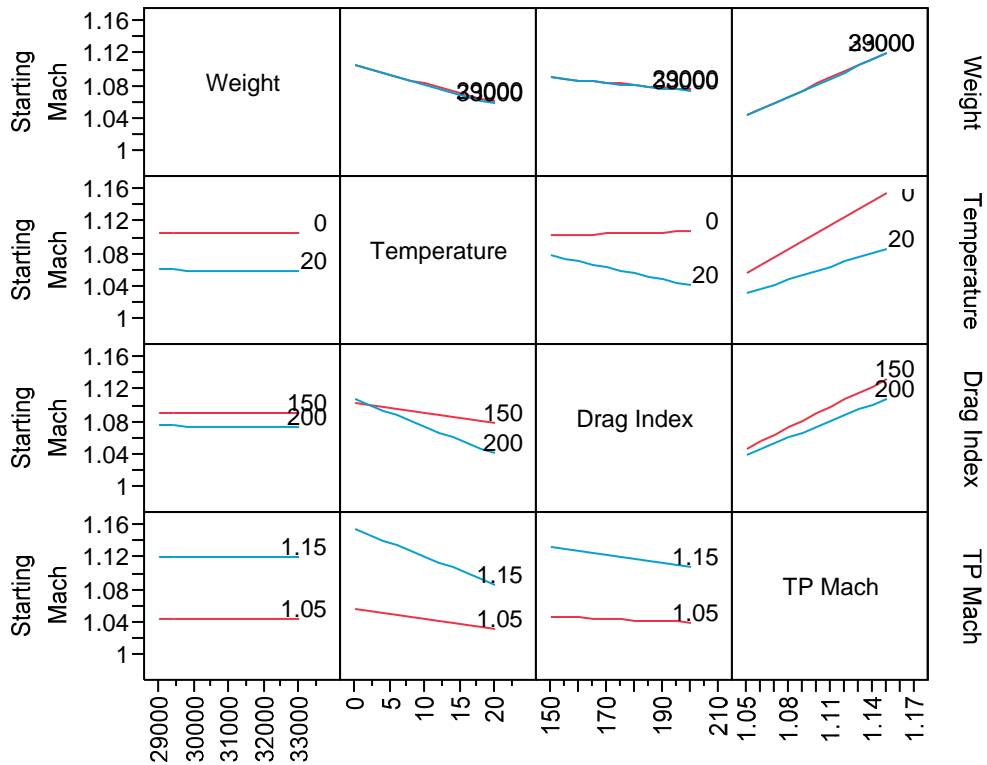
Figure 4.13: Interaction Profile for Starting Mach Response

The majority of the information presented here indicates that the data in the parameter estimates table and chart are accurate. There is one consideration in the temperature versus drag index block where the lines have an intersection point. From this information it can be inferred that the drag index information may be concealed by the temperature parameter. However, since the drag index remained a significant variable, there is no need to reevaluate the solution. It is possible that the drag index can have a greater effect than the temperature, but that information will be reviewed in a later section.

In summary, at the high altitude condition, the Starting Mach response is still driven primarily by the temperature and drag index variables. The weight parameter carries very little significance and the dive model has a much lower sensitivity on the

123

output than from the complete set of data. From this assessment, it can be implied that changes or miscalculations in weight have little to no effect on the Starting Mach response. The next portion of the starting condition is the Starting Altitude response.

4.3.2 Analysis of High Altitude Starting Altitude Response

The starting altitude response can provide slightly different insight in regards to the deviation of the information. Looking at the figure below, the Leverage plot shown in Figure 4.14, the data is no longer clustered in bands, but rather a much more realistic spread of the data. There is a large grouping at the 20,000 foot actual band, but that is understandable since a majority of the points used for this analysis were attainable using steady-level flight and positive excess power conditions.
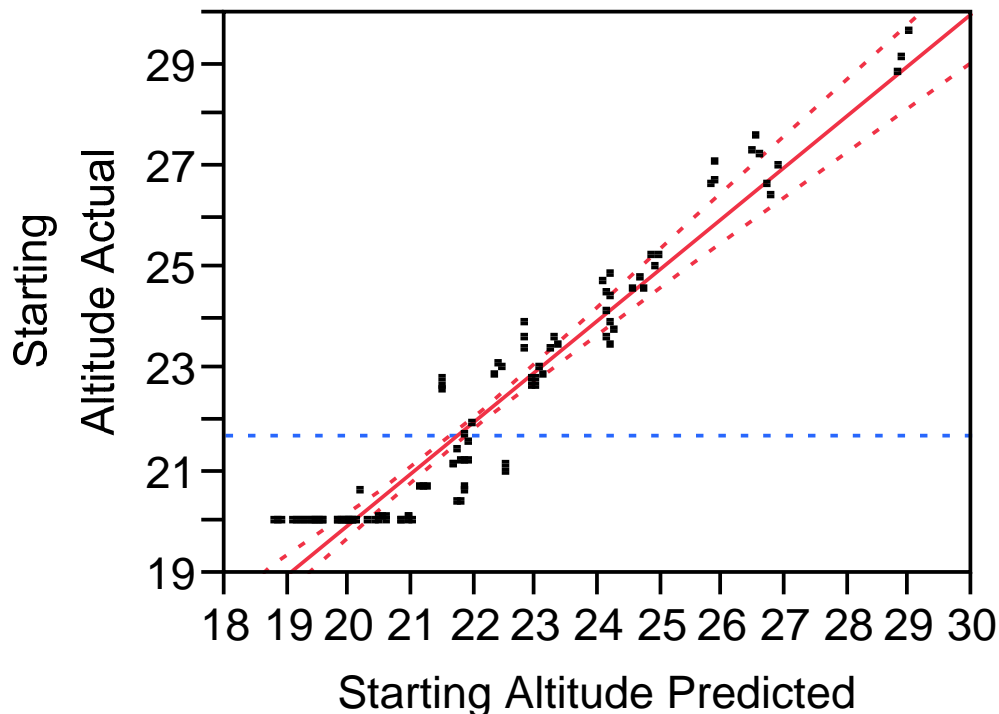
Figure 4.14: Leverage Plot for Starting Altitude Response

Another important observation on this Leverage plot that could not be made on the previous one involves the banding of the data between the dashed lines. This indicates that for the majority of the non-positive P_S data points, the data fell within the mean. The data band of positive excess power points disrupts the fit of the data. This is illustrated by the R^2 values within Table 4.13.

Table 4.13: Summary of Fit Table for Starting Mach Response

R^2	0.922
R^2 Adjusted	0.915
Root Mean Square Error	0.701
Mean of Response	21.743
Observations	135

The critical observation here involves the comparison of the adjusted R^2 value. Note that it is several percent lower in value than the previous adjusted R^2 value. These values can be compared because they are adjusted to incorporate the degrees of freedom for the particular response. The other considerable note that can be taken from this table is that the root mean square error is over 700 feet. This value, unlike the previous error, is outside the altitude band preset for the experiment. This variation indicates that there may possibly be some data overshadowing or that one of the parameters has a significantly heavier probability for sensitivity than the other terms. That analysis can be verified by considering Table 4.14.

Table 4.14: Sorted Parameter Estimates for Starting Altitude Response

Term	Estimate		Standard Error		t-Ratio	Prob > |t|
Temperature	0.2371		0.0085		27.80	<0.0001
Drag Index	0.0304		0.0030		10.29	<0.0001
(Temperature)*(Drag Index)	0.0039		0.0004		9.25	<0.0001
Weight	1.11	E-05	0.00004		0.30	0.7640
(Weight)*(Temperature)	1.33	E-06	5.22	E-06	0.26	0.7989
(Weight)*(Drag Index)	-3.33	E-08	1.81	E-06	-0.02	0.9853

This table, nearly identical to the previous sorted parameter estimates table, shows very consistent information. The weight and its interactions are once again very insignificant. The probability for sensitivity is remarkably low in comparison to the temperature, drag index, and their interaction. That can be reiterated by observing the t-Ratios. The difference between weight and temperature is nearly 100 fold. By looking at the response sensitivity probability plot, all of the information just discussed can be verified. See Figure 4.15 showing this information.
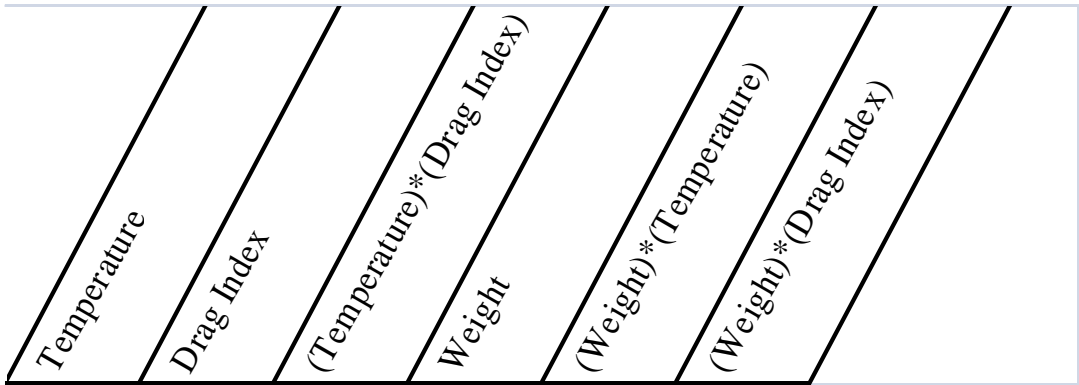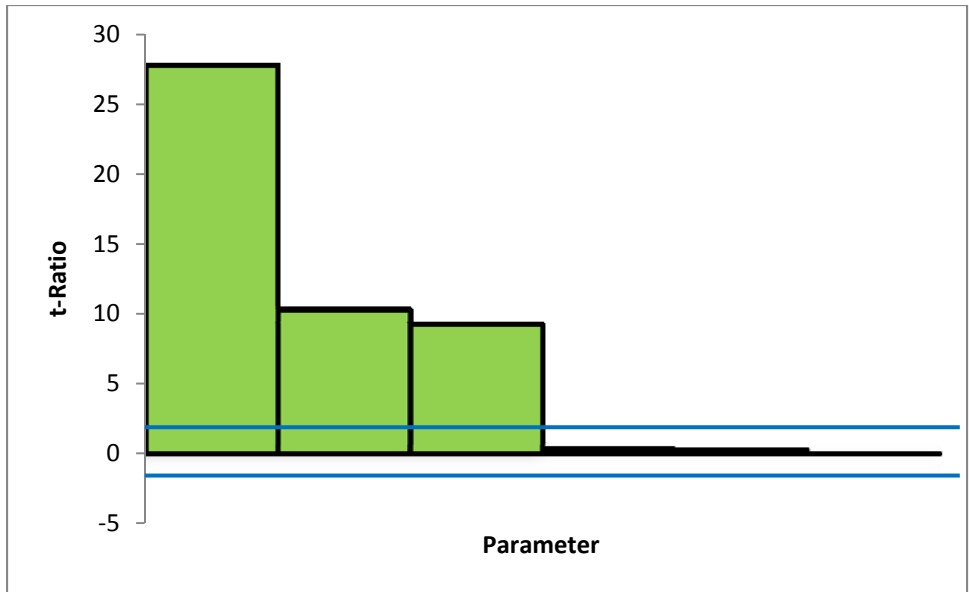
Figure 4.15: Starting Altitude Response Sensitivity Probability Plot

This plot shows that the model will be highly sensitive to the temperature and the drag index. The weight and its interactions will provide little adjustment to the response data should a variation occur during the flight test. However, this data can be skewed by the adverse effect of one parameter masking the effects of another. The interaction plot, shown in Figure 4.16 indicates that temperature will have an overshadowing effect on drag index and test point Mach number. This masking by the temperature is the same effect from the previous response. It can also therefore be neglected as an important

overshadowing because the drag index still remained quite significant, particularly in comparison to the effect on the weight. The weight, despite being insignificant, was not masked by any other term. This can be seen through the illustration of parallel lines throughout all of the weight interactions seen in Figure 4.16.
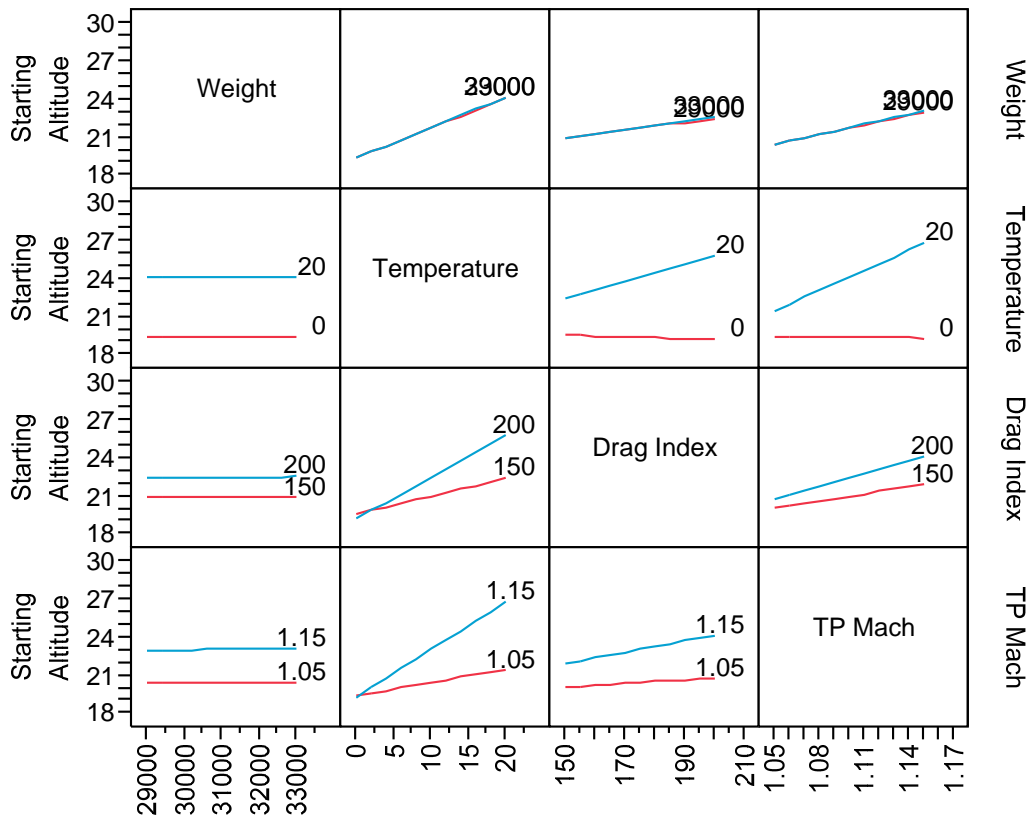
Figure 4.16: Interaction Profile for Starting Altitude Response

As with the previous results from the section 4.2 as well as the Starting Mach response for the high altitude case, the starting conditions are driven by the temperature, drag index, and the interaction of the two. Variations in weight, particularly at the high altitude condition, are insignificant to the starting condition responses of the dive planning model. This insensitivity to the weight parameter allows the test engineers to

plan more flight tests at the high altitude condition knowing that the variation in weight will have little to no effect on the predicted starting condition responses. In the optimal solution, the Dive Angle response and recovery responses would have similar outcomes for the high altitude condition. By looking at these responses next, the efficiency of the dive model can be fully evaluated.

4.3.3 Analysis of High Altitude Dive Angle Response

As with the previous analyses, the first area of consideration for analysis for the dive angle response is the actual by predicted plot, or the Leverage plot. The Leverage plot for the dive angle response is shown below in Figure 4.17.
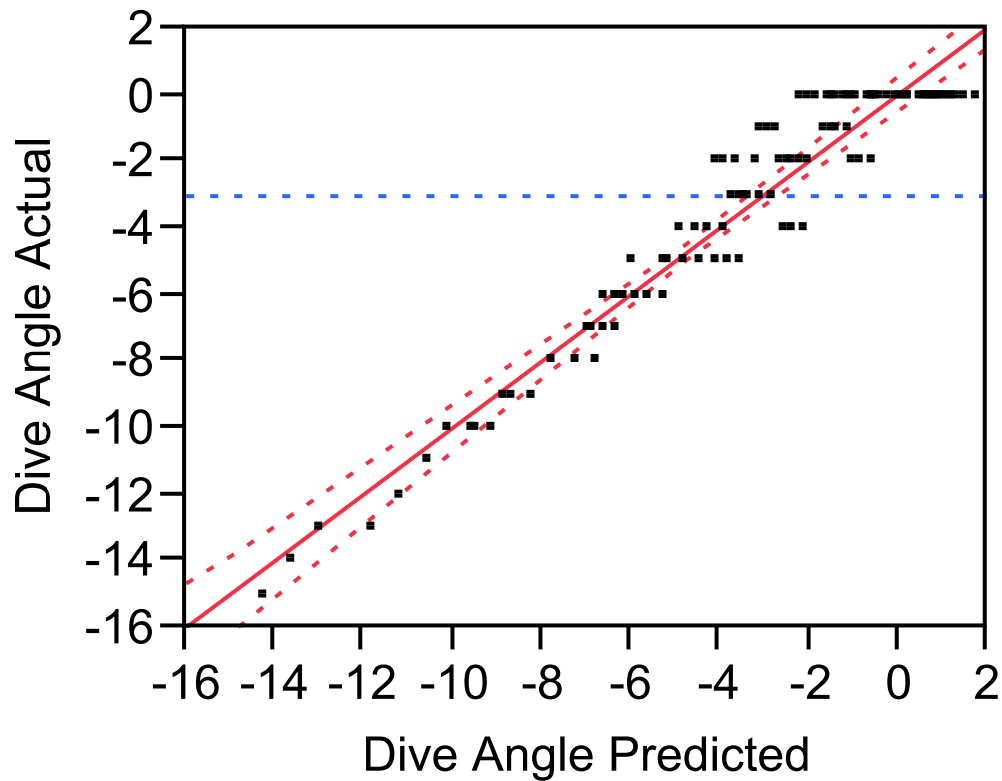
Figure 4.17: Leverage Plot for Dive Angle Response

By observing the data that the JMP software was able to predict plotted against the actual results, it can be see that with the exception of the data points requiring no dive planning, the data fits fairly well within the bounds of certainty. The summary of fit table, shown below in Table 4.15, illustrates how accurately the program was able to predict the next result based on the previous calculations. This is the essence of this figure above. It gives the user information on how consistent the data is from point to point. Table 4.15 is shown below.

Table 4.15: Summary of Fit Table for Dive Angle Response

R^2	0.943
R^2 Adjusted	0.938
Root Mean Square Error	0.942
Mean of Response	-2.985°
Observations	135

Comparing the R^2 Adjusted value to some of the previous values for the starting altitude and starting Mach responses, the data for the dive angle can be more accurately predicted by the computer models. The dive angle response follows a general trend based on the changes in the starting conditions; the dive angle differences are predictable for all test points.

The next set of relevant information provides the information about the sensitivity of the data itself. The sorted parameter estimates table for the dive angle response, seen below, can provide insight into the significance of each initializing parameter to the dive angle response. Table 4.16 contains this information.

130

Table 4.16: Sorted Parameter Estimates for Dive Angle Response

Term	Estimate		Standard Error		t-Ratio	Prob > |t|
Temperature	-0.3830		0.0115		-33.40	<0.0001
Drag Index	-0.0369		0.0040		-9.29	<0.0001
(Temperature)*(Drag Index)	-0.0040		0.0006		-7.20	<0.0001
Weight	9.44	E-05	4.97	E-05	1.90	0.0595
(Weight)*(Temperature)	1.22	E-05	7.02	E-06	1.74	0.0843
(Weight)*(Drag Index)	3.33	E-07	2.43	E-06	0.14	0.8912

The information that Table 4.16 provides is that it indicates that weight has a much greater significance on dive angle than on the starting conditions for the dive planning. Although still not significant enough to be a primary factor, as has been consistent for all the high altitude conditions, the weight parameter is starting to become more sensitive toward the dive angle response. Observing this same information visually through Figure 4.18 may provide a clearer understanding.

This plot illustrates the t-Ratio and Prob >|t| values more clearly. Once conclusion that can also be taken from this is that the t-Ratios are negative for all of the significant parameters and positive for all the insignificant terms. Although the sign of the t-Ratio is not necessarily important for these discussions, it does coincide with the desire to maximize the dive angle final response (indicating a number that is the least negative). Another important conclusion that can be drawn from this figure is that the results indicate a very high dependence on the temperature as a condition of dive angle response. This indicates that at high altitude test points, there could possibly be a large variation in required dive angle as compared to the predicted dive model when the temperature varies just slightly as each day progresses.
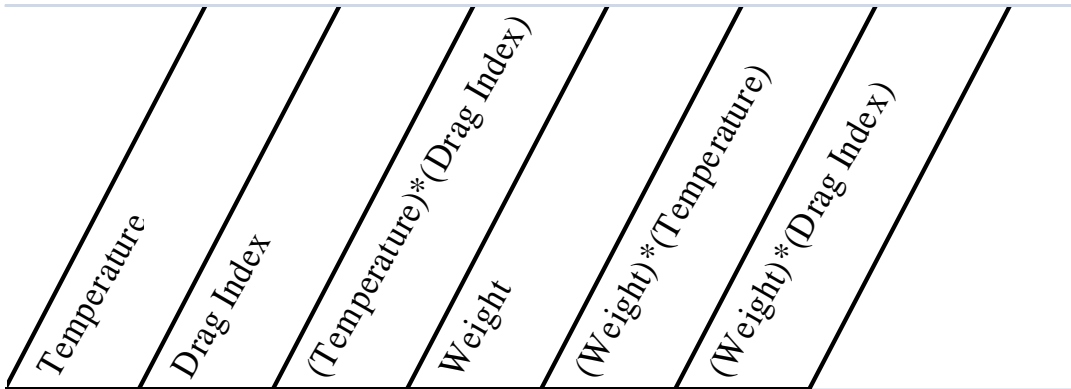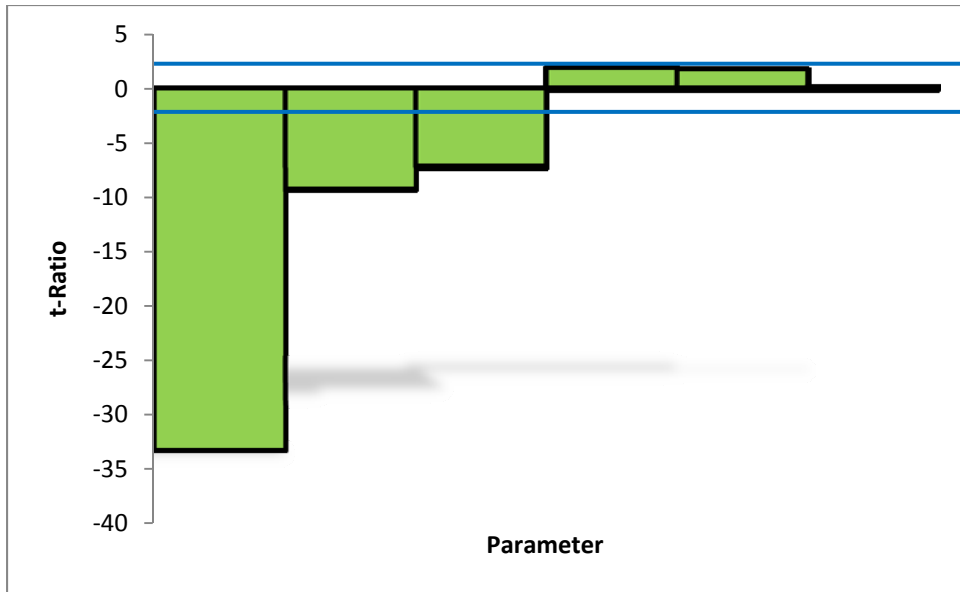
Figure 4.18: Dive Angle Response Sensitivity Probability Plot

The last figure that needs to be considered is the interaction profiles between the parameters. The interaction plot for the dive angle response is shown in Figure 4.19.
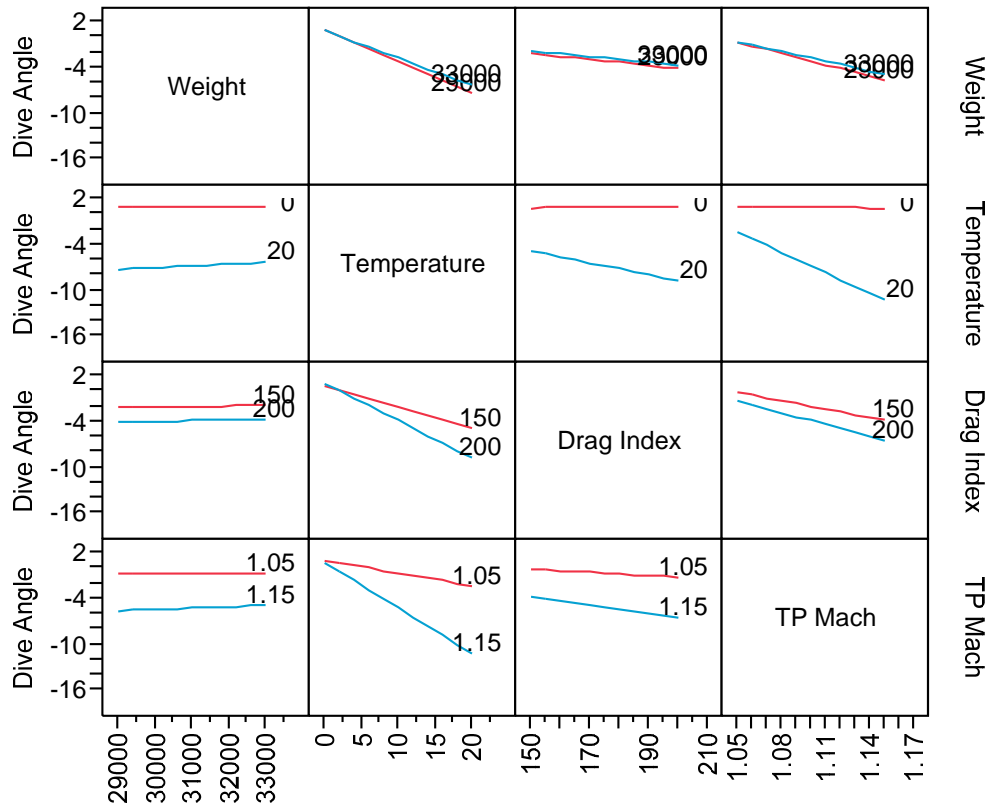
Figure 4.19: Interaction Profiles for the Dive Angle Response

From this figure, the interactions between temperature, weight, and drag index appear to be parallel in general indicating no masking of variables by another. The one consideration that should be made from this analysis is that the TP Mach number and temperature have a fairly significant reaction. This reaction may be skewing the values for the temperature sensitivity slightly and increasing their represented importance more than the variable actually is. The variation also appears to be more reactive as the Mach number increases as well, meaning that as the aircraft velocity increases (and velocity can be used here since the altitude is a constant control for this analysis) there is a greater probability that the test point location is driving the significance of the temperature in regards to the dive angle response.

In conclusion, the Dive Angle response is still only controlled by the temperature, drag index, and the interaction of the two variables. The weight, while more vital to this response than to the starting condition responses, still does not drive the results of the Dive Planning model. This is different from the full data set results which included weight as a significant input variable. This difference becomes important in increasing the number of test runs that can be conducted at a high altitude condition. In order to ensure that the model is insensitive to changes in weight at high altitudes, the final two responses are analyzed next, the Start Recovery response and the End Recovery response.

4.3.4 Analysis of High Altitude Start Recovery Altitude

The next response that is discussed for the high altitude case is the starting recovery condition. This response had variations in the Leverage plot that appear to be more consistent with the first two responses than with the dive angle response. The reason being that the program was not able to as accurately predict the result for the starting recovery altitude as it was able to for the dive angle. Figure 4.20 is the Leverage plot for this response. The bands of data that are visible for each actual starting condition are an important observation. These horizontal groups of data provide information that the JMP Modeling software was not able to preemptively predict each result from the initial conditions.
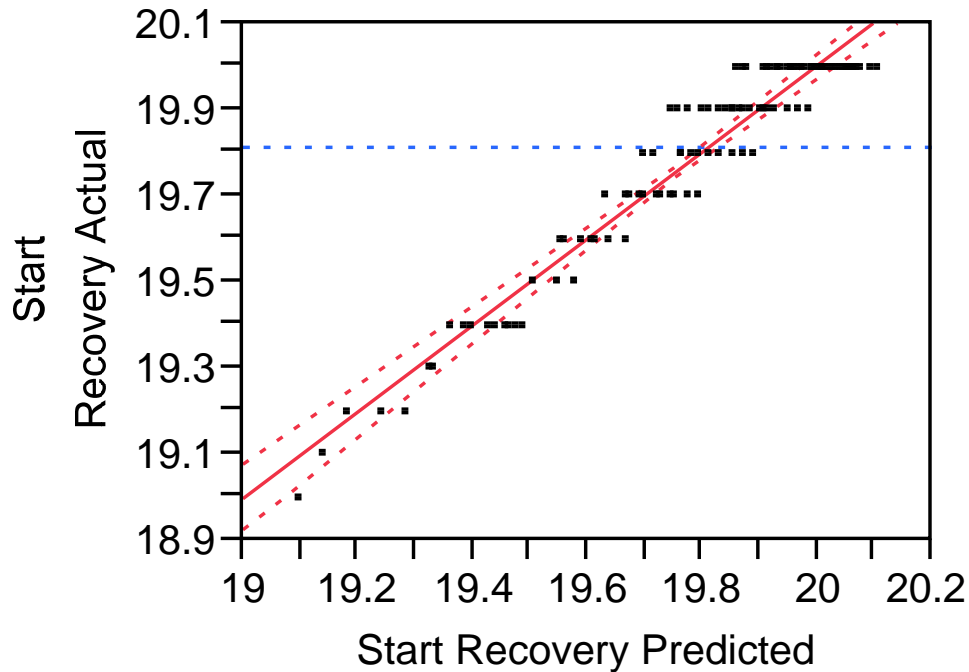
Figure 4.20: Leverage Plot for Start Recovery Altitude Response

The Summary of Fit Table confirms this result, particularly when observing the R^2 Adjusted parameter. See Table 4.17.

Table 4.17: Summary of Fit Table for Start Recovery Altitude Response

R^2	0.942
R^2 Adjusted	0.938
Root Mean Square Error	0.060
Mean of Response	19.813
Observations	135

The information that can also be obtained from this chart is that the typical recovery altitude begins at approximately 19,800 feet. This is somewhat consistent with the information that has already been discussed because the recoveries are beginning below the test point condition. This is a good verification that the model is running accurately.

The sorted parameter estimates table can provide additional insight into the reasoning behind the program's inability to accurately predict results. Table 4.18 contains the data for the estimates.

Table 4.18: Sorted Parameter Estimates for Start Recovery Altitude Response

Term	Estimate		Standard Error		t-Ratio	Prob > |t|
Temperature	-0.0238		0.0007		-32.48	<0.0001
Drag Index	-0.0022		0.0003		-8.59	<0.0001
(Temperature)*(Drag Index)	-0.0003		3.59	E-05	-7.31	<0.0001
Weight	6.67	E-06	3.17	E-06	2.10	0.0375
(Weight)*(Temperature)	8.33	E-07	4.48	E-07	1.86	0.0654
(Weight)*(Drag Index)	3.33	E-08	1.55	E-07	0.21	0.8304

This table provides a very important statistical result. The start recovery altitude response is the first response for the high altitude condition where weight is considered statistically significant. Although miniscule in comparison to the temperature, drag index, and their interaction, it still carries a minor significance to the response and outputs from the Dive Planning model will be sensitive to variations in weight. The figure below, the sensitivity probability plot for this response, illustrates that result.
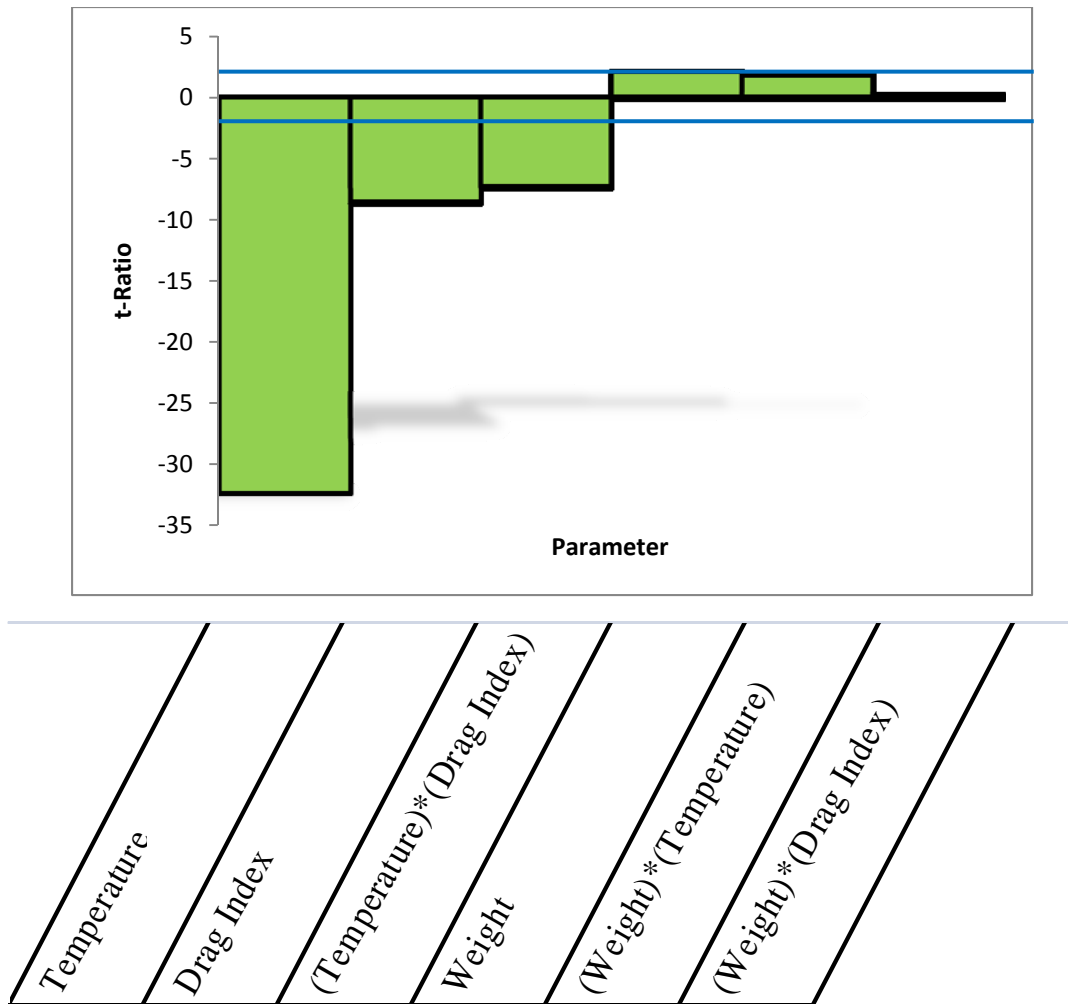
Figure 4.21: Start Recovery Altitude Sensitivity Probability Plot

Here, the dark blue lines indicate the bounds for the parameters that are sensitive. It can

be seen that weight does have some significance, although it is not on the order of

magnitude that the temperature and drag index carry.

The last figure to be evaluated for this response is the interaction profiles. This

confirms that no two variables are cancelling out the results of one another or skewing

the data on one result versus another. Figure 4.22 has the interaction profile plot for this

response.
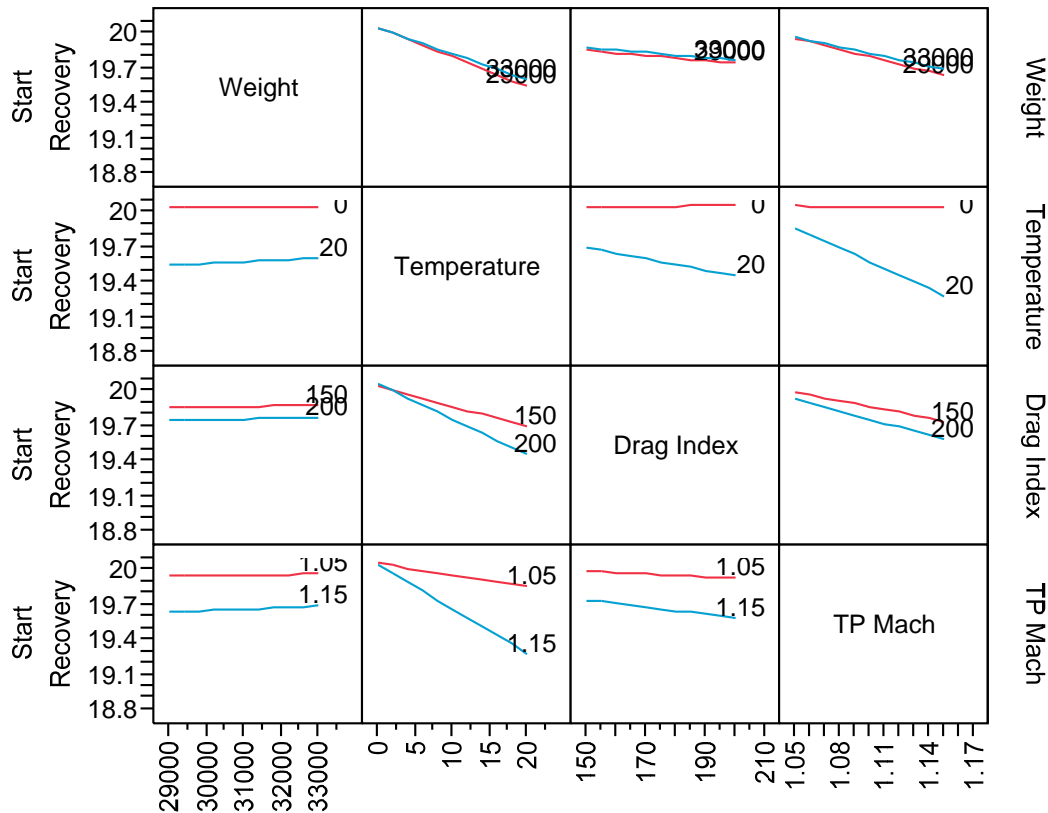
Figure 4.22: Interaction Profiles for Start Recovery Altitude Response

As was present in the previous response interaction profile, there is a possibility of the temperature t-Ratio and significance value being inflated by the TP Mach parameter. However, there is still little indication of an error in the ratios between the three primary parameters. So from this information, the temperature value may be slightly masked or inflated, but the ratios between each of the other parameters are accurate.

From the analysis of the Start Recovery response, the model does show sensitivity to changes in the weight of the aircraft. This is important because, up to this point, the weight was insignificant to the responses of the model. By incorporating the weight as a primary variable of concern (even if it is the lowest in terms of significance), the model now requires predictions of the weight with some accuracy to properly model the

recovery conditions. The last response that needs to be analyzed for the high altitude

condition is the End Recovery response. This response is discussed in the next section.

4.3.5 Analysis of High Altitude End Recovery Response

The last parameter to be evaluated is the end recovery altitude response. As

before, the first analysis for these high altitude conditions involves the Leverage plot.

The Leverage plot below, Figure 4.23, provides information about the accuracy of the

predicted data. Once again, the majority of the response values are fairly accurately

predicted by the model until the data approaches the positive excess power test points.

Those points provide some distortion of the data.
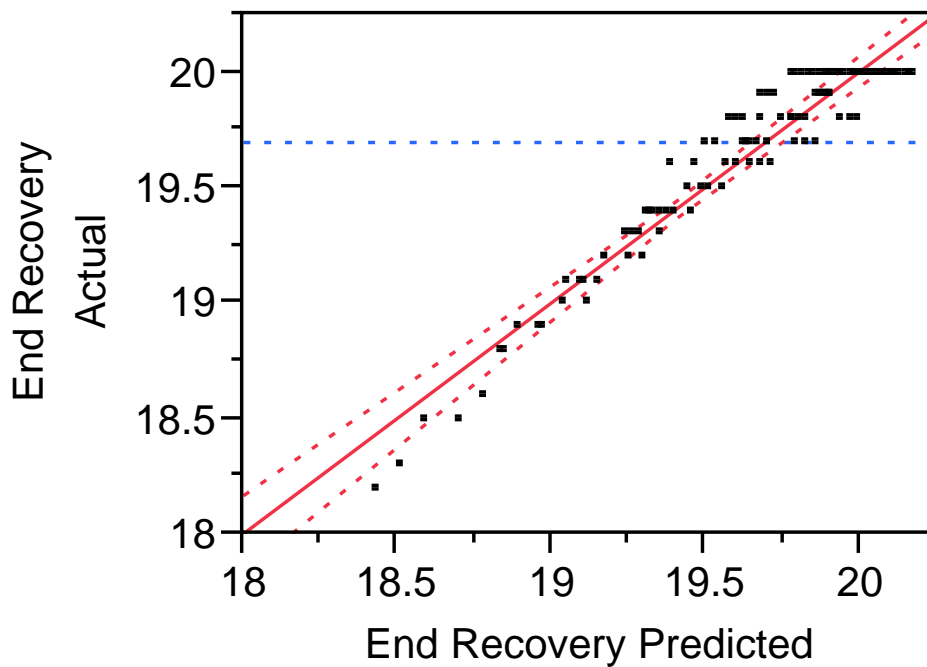
Figure 4.23: Leverage Plot for End Recovery Altitude Response

The interesting information that this plot also illustrates is that the end recovery altitude

was particularly difficult for the model to predict. Even the points that are located farther

away from the mean of the response, points that have typically been fairly accurately predicted, now are shown outside the range of acceptable tolerances for the data. This result is most like attributed to the fact that the end recovery altitude response is the most varied from the Dive Planning model. The end recovery altitude is dependent on all the other responses as well as the given inputs. This added level of uncertainty most likely was the driving force behind the increased error in prediction.

Table 4.19, shown below, provides the summary of fit information and indicates the increased error values that were just discussed.

Table 4.19: Summary of Fit Table for End Recovery Altitude Response

R^2	0.938
R^2 Adjusted	0.934
Root Mean Square Error	0.107
Mean of Response	19.695
Observations	135

Once the discovery of the increased error is discussed, it provides even greater uncertainty to the mean of the response value of 19,695 feet. This value now cannot be guaranteed because of the associated error that the model is attributing to its ability to predict results. This is a particularly important concern since the end recovery altitude parameter is the most vital in regards to safety. If this value contains the most error, then improvements must be made to eliminate this error and present more accurate values for end recovery altitudes.

The estimates of the parameters table indicate the parameters that are most responsible for the error and the parameters that are subject to the greatest sensitivity and require more precision in their estimates. Table 4.20 is shown below.

Table 4.20: Sorted Parameter Estimates for End Recovery Altitude Response

Term	Estimate		Standard Error		t-Ratio	Prob > |t|
Temperature	-0.0397		0.0013		-30.61	<0.0001
Drag Index	-0.0039		0.0004		-8.61	<0.0001
(Temperature)*(Drag Index)	-0.0004		6.35	E-05	-6.79	<0.0001
Weight	1.11	E-05	5.62	E-06	1.98	0.0501
(Weight)*(Temperature)	2.00	E-06	7.94	E-07	1.89	0.0613
(Weight)*(Drag Index)	1.00	E-07	2.75	E-07	0.36	0.7169

The table above verifies the trend that temperature and drag index terms are the most

significant followed by their interaction. The weight, for this response, remains

insignificant and has a low sensitivity to the Dive Planning model. The information

above can be illustrated graphically as well through Figure 4.24.
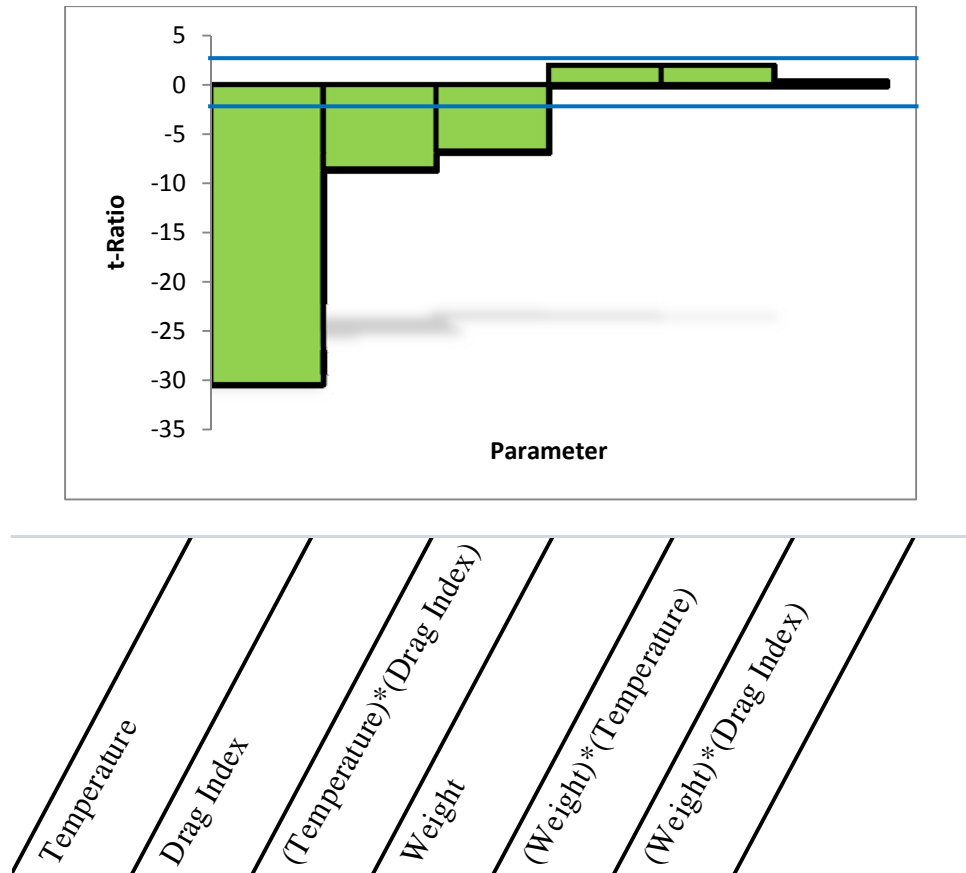
Figure 4.24: End Recovery Altitude Sensitivity Probability Plot

The bars indicating the parameters that are sensitive just enclose the weight term and its interactions. The temperature and drag index are more significant by several orders of magnitude and are the driving variables in the dive planning model for the high altitude conditions.

The interaction profiles, shown below, indicate consistent information from the earlier analysis for the high altitude condition. The test point Mach and temperature values have some interaction overlap but the rest of the parameters are shown to be accurate. The parallel lines for each of the terms prove that these significances are correct and no values are distorted by the interaction of two or more parameters. This interaction profile is shown in Figure 4.25.
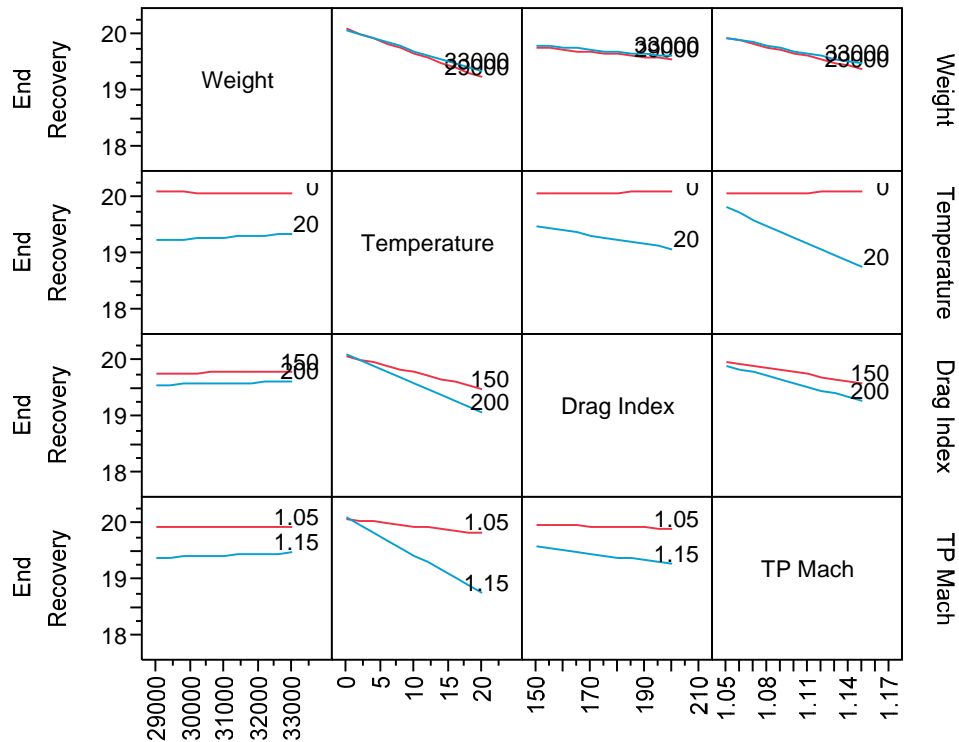
Figure 4.25: Interaction Profile for the End Recovery Altitude Response

From this analysis, the primary conclusion is that the model is insensitive to the weight when it is determining the End Recovery Altitude response. This is an important conclusion because even though the start recovery altitude is sensitive to changes in weight, the primary response associated with test safety is the end recovery altitude. Knowing that the weight is insignificant provides the operator the ability to ignore changes in weight (within some margin of reason) and can schedule several test runs at high altitude test points without requiring a refueling or a readjustment to the aircraft weight. Eliminating the need to refuel after each test run increases the efficiency by allowing the test pilot to maintain speed and climb to a new starting altitude without having to traverse the transonic region of the flight envelope twice for a refueling a reset.

Knowing that the weight is insignificant at the high altitude condition also improves flight test safety. Safety is improved because the variation in aircraft weight from the high rate of fuel burn during a test dive is insignificant to the final recovery response produced by the model. This insignificance informs the engineer and pilot that the model results, at least for the high altitude condition, have an increased fidelity. The next section discusses a summary of the both sets of results and how they are applicable to the model.

4.4 Discussion of Significance, Sensitivity, and Applications to the Model

The ultimate purpose of this study is to determine which variables carry the most significance in the Dive Planning program and which variables are the most sensitive to even minor variations. From looking at all the data together, there are several assumptions that can be made and some from the original hypothesis can be verified or

corrected. The first assumption that can be verified is that temperature carries the greatest significance when analyzing both the complete set of data and the high altitude data independently. This is very important because the temperature variation from standard day can be rather significant, especially within the tropopause. The data collection required to keep up with this variation can cause significant problems.

The next variable of importance was drag index. Although not originally a variable that was expected to present any real variation in the results, the test data proves otherwise. The drag index term was the second most significant and therefore the second most sensitive parameter in both data sets. It carried nearly an identical sensitivity probability to temperature when analyzing the complete set of data, but in the high altitude case became approximately a third significant in comparison to the temperature term.

The next variable of importance was not the weight as was originally hypothesized, but rather the interaction between the temperature and the drag index. So from this statement, it can be assumed that not only will there be a significant change in the model's outputs when the temperature and drag index are varied independently, but their variation with respect to one another will drive the solution of the model as well. This interaction was also much more sensitive at the high altitude case, a difference from the first two variables discussed: temperature and drag index independently.

The next discovery that was obtained from reviewing the final results of the experiment was that weight, while having some significance, was not a critical variable. The results that the Dive Planning model produces are not particularly sensitive to variations in the weight. This lack of sensitivity was present in both the high altitude

case as well as the complete data set for all of the test points in question. However, in the complete data set, weight carried a minimal significance, but the significance was present for the data. Contradictory to the original hypothesis, weight actually carried no significance at all in the high altitude conditions. The potential energy generated from the additional height above the Earth was minimal in comparison to the kinetic energy gained through the dive acceleration.

The two interactions involving weight (weight interacting with temperature and weight interacting with drag index) are the least significant variables present in the system. The Dive Planning model is not sensitive to minor changes in these values and in the high altitude case study, the weight and drag index interaction is almost completely irrelevant all together. The value for the high altitude case has a sensitivity probability of 0.8077. Since values under 0.05 are considered sensitive or significant in the model's predictions, this interaction provides no impact to the model's outputs.

There may be questions in regards to variable weighting. Although some variables were evaluated over a more extreme range of results, the JMP program compensates for this. The compensation is through the R^2 Adjusted values. These were important because the greater the variation between the R^2 nominal and the adjusted values, the greater the weight of one variable over another in the model. Because the R^2 and R^2 Adjusted terms were relatively equal throughout all of the test points, the range of each variable chosen most likely played a minimal role in providing uncertainty to the results.

Table 4.21, shown below, contains a summary of the results from both the high altitude and the complete set of data. It was from this data table that the conclusions

about the final results were made. Note that the values presented are averages of the absolute values of the t-Ratios and averages of the sensitivity probabilities as well.

Table 4.21: Summary of Results from Both Sets of Data

Term	Complete Data Set t-Ratio Average	Complete Data Set Prob > |t| Average	High Altitude Data Set t-Ratio Average	High Altitude Data Set Prob > |t| Average
Temperature	30.304	< 0.0001	29.758	< 0.0001
Drag Index	24.560	< 0.0001	9.306	< 0.0001
(Temperature)*(Drag Index)	2.754	0.0069	7.936	< 0.0001
Weight	6.574	0.0275	1.366	0.2990
(Weight)*(Temperature)	1.020	0.3191	1.306	0.2895
(Weight)*(Drag Index)	1.056	0.3408	0.246	0.8077

The results for the table above were critical in providing an overall understanding of the results presented by the JMP program. By looking at these results, it can once again be stated that temperature and drag index are the most important variables. The indication that weight is not as important as originally predicted alleviates a primary concern for accurately modeling the aircraft weight through a high-speed dive. This is important because as the aircraft enters the dive at full afterburner after already expending a significant amount of fuel reaching a condition of negative P_S, the fuel consumption changes the weight of the aircraft drastically. Knowing that this rapidly changing variable carries minimal significance allows the test engineers to more crudely predict the weight at the test point and not worry about the possibility of a significant change in the predicted dive angle and the predicted recovery altitudes.

The other conclusion that can be drawn from these results is that the temperature and drag index are significant. Developing accurate and precise models for the drag index of certain stores now becomes critical in the dive planning process. The benefit of this information being one of the variables most sensitive to variation is that once the drag index is calculated, there is a very poor chance that the value will change in the midst of a dive profile. With the exception of releasing an external store or one breaking away from the aircraft, the drag index will remain constant throughout the entire flight test. This does place some priority on determining the drag index for each munition for each aircraft, but once the values are determined, the back end calculations for the dive planning can be considered extremely accurate.

The last area of concern from the conclusions is about the importance of temperature in the flight test profile. It was originally assumed that this value would be critical to the Dive Planning model predictions, as it was. A note of benefit though is that based on the t-Ratio averages, it provides little difference if the temperature variations are at high altitude or low altitude. It becomes only important that the variation is minimized to decrease the possibility of variations in the model results. The dive model will be highly sensitive to a variation in temperature of even one or two degrees, but it is possible to model this information more accurately. For this experiment, a standard lapse rate was used for temperature variation throughout the atmosphere. However, during most flight test programs, weather balloon sounding data is used that provides a table of temperatures and altitudes for all possible flight conditions. Using this data will produce a lower error in the overall temperature variation and the weather balloon can be operated several times throughout the day to ensure that the temperature calculations are remaining fairly

constant. This will alleviate some of the possible sensitivity in the model's outputs for the dive angles and recovery altitudes.

V. Conclusions and Recommendations

This chapter will summarize the results of this study. It will also indicate areas for improvement and the possible recommendations for future research to help improve the Dive Planning model and the overall safety of the flight test program.

5.1 Summary

As can be derived from the title and the information presented throughout this thesis, the purpose of this study is to provide information that can improve the safety and efficiency of a flight test program that conducts negative P_S tests. By presenting a sensitivity analysis and determining the variables of the Dive Planning model that are critical in order to develop a dive angle, starting conditions, and recovery conditions, flight test programs can reduce the number of attempts at each test point as well as prevent possible accidents and crashes from data that is misrepresented.

The analysis took a Dive Planning model developed by Capt. Benjamin George (U.S. Air Force) and operated that program using 405 trial runs. The results from the dive model were then inputted into a full factorial matrix using a sensitivity analysis software program called JMP 8.0. That software was then used to analyze the responses to the trials and determine which variables carried the most significance in determining the results and which variables or combinations were insignificant and which are the most critical in determining accurate and precise results.

Taking the dive planning model and developing the test runs and the sensitivity analysis can provide valuable information to test pilots and engineers. The research contained in this thesis indicates which variables have the most significance and those

results are summarized below. By determining the sensitivity each variable has to the results of the model, the test engineers and test pilots can improve test efficiency and safety. By knowing which parameters will generate large errors when uncertainty is introduced, test points that may occur around hazardous conditions (such as low altitude test points) can be reevaluated. Test points that are insensitive to parameters such as weight can be run repeatedly without the cost of refueling and time spent returning to the zero excess power condition.

The results of the experiment can be summarized into these four main points:

1. Temperature and drag index variations will provide the greatest variation to the results presented by the Dive Planning model. Having accurate predictions and measurements for these values will alleviate the possibility of a miscalculated dive angle, starting condition, or recovery altitudes. Knowing, for both high altitude and low altitude conditions, that these two parameters have the greatest sensitivity to the model allows for the test engineers to predict the measurements more precisely. Small errors in the input variables can escalate into a large error in the responses of the Dive Planning model. These errors can increase the risk factor for a pilot, particularly when the test points are at low altitude conditions.

2. Weight, despite original assumptions, is not as critical a variable as originally perceived. Particularly at high altitude test points, the weight provides no significance to the model's solutions. The reasoning behind this is associated with the energy height curves.

Because the energy height curves are more horizontal than vertical at lower altitudes, the substitution of potential energy for kinetic energy has a lower effect at higher altitudes. This also explains why the weight increases its significance as the altitude decreases because of the energy curve profiles. In other words, at higher altitudes, the kinetic energy the dominant term and at lower altitudes the potential energy becomes more dominant in regards to the sensitivity of the input variables. The closer the test points become to sea level, the more critical the weight becomes to inducing errors in the flight model. This can improve the efficiency of the flight test program by alleviating the need to refuel and reset the aircraft weight after every test run. Since weight is insignificant to the results, particularly at high altitude, the aircraft can run several test runs before needing to refuel and traverse the transonic flight region.

3. The interaction of temperature and drag index is significant to the model and the results of the model are highly sensitive to variations in these parameters as a relationship. This significance also increases with altitude but is still a critical concern at lower altitudes as well. The information about drag index and temperature must be as accurate and precise as possible prior to being utilized by the Dive Planning software.

4. The interactions of weight and the other variables are virtually irrelevant to the determination of results by the model. Particularly the

interaction between weight and drag index at high altitudes. This result can be foreseen based on the irrelevance of weight independently at high altitudes and the insignificance of the combination of the two at lower altitudes. Although the first point stated that the drag index and temperature were critical, that was an analysis based on the variables independently. Independently, they have a strong influence on the model responses. Their relationship to one another is not dependent on any response and the model is insensitive to changes in the relationship between the parameters of weight and temperature (Weight*Temperature) and weight and drag index (Weight*Drag Index).

5.2 Conclusions

The Dive Planning model and the ability to predict dive angles and starting conditions greatly improves the efficiency of flight testing. By knowing which parameters are more sensitive at lower altitude test points and which variables are more sensitive at higher altitude test points only increases the ability for the engineer to provide test pilots with accurate predictions for dive angle and starting conditions. This will ultimately drive down the cost of flutter envelope expansion flight testing by decreasing the number of missed test points (due to inaccurate predictions) and decreasing the overall cost for fuel, manpower, and testing equipment. Being able to conduct fewer trials and obtain the same information will eventually lower the cost for this portion of the developmental flight test program.

As was previously stated, knowing the insignificance of weight at high altitude allows for the test engineers and pilots to plan several test runs on one tank of fuel. Although the aircraft weight is changing significantly, the results from the dive planning model should remain fairly consistent despite changes in the weight input. The other indication from this result is that lower altitude test points are slightly more sensitive to variations in weight. While they need not be monitored as closely as variations in temperature or drag index, variations in weight can still cause minor deviations in the model results at lower altitudes. These improvements in efficiency can help lower the costs of flutter envelope expansion tests and increase the number of tests that can be executed for the same cost (time costs and financial costs).

The other purpose behind this study was to improve safety. While the outputs from the model of dive angle and starting conditions improve efficiency by reducing the number of required tests, the recovery altitudes must be accurate to improve flight test program safety. Having inaccurate results for recovery altitudes, particularly at low altitude test points (the test points where, as shown in Chapter 2, flutter testing is the most prevalent), can result in the loss of life and the loss of valuable resources. By knowing that variations in temperature, drag index, and weight (at low altitudes) are sensitive to variations in regards to the model predictions, test engineers can ensure that they are measuring the variables more carefully at higher risk test points. Also, by understanding that certain test points and responses may be subject to greater variation based on imprecise measurements of the input variables, test engineers and pilots can eliminate dangerous test points until further calculations can be accomplished. Knowing the importance of these variations and their sensitivity to developing errors on the Dive

153

Planning model will allow the test engineers and test pilots to prepare more adequately for hazardous test points and also cancel test points that could cause the possibility of a crash.

Having an understanding of the input variables that drive the Dive Planning model and of their sensitivity is critical to improving safety and efficiency. With improvements in the test program such as these, there is a possibility for a high reduction in cost and loss of resources, including not only aircraft and fuel, but in some unfortunate fatal scenarios, personnel as well. Understanding sensitivity of variables and how they drive models in any form of testing only improves the conditions for the test.

5.3 Recommendations for Future Work

In any study there can always be made recommendations for improvements and recommendations for future studies. One particular area that will be beneficial is conducting a sensitivity analysis on a much more detailed scope. This analysis was focused on generating a sensitivity analysis for the model in its entirety. However, having an understanding of the sensitivity of each variable for each test point and how the variables interact to create the results from the model could provide additional insight into future flight test program improvements. Such as was done for the high altitude case of this analysis, conducting a sensitivity analysis for each altitude and Mach number independently could provide valuable insight for each test point. This extension of the research could provide insight into which variables are critical at several specific conditions, as opposed to the overall understanding of which variables have the greatest sensitivity.

Another recommendation for future studies would be to look at the model itself. From an examination of the model and through running the program several times, there might be benefit in developing the model for individual aircraft. At this point, the model uses excess power data for particular aircraft, but does not truly optimize the solution for an individual aircraft and its individual aerodynamic properties. With the improvements in optimization software that have been developed over the last several years, incorporating actual aircraft data (such as the F-16 model from Stevens and Lewis [21]) and optimizing the final dive planning results about from a step by step analysis might prove beneficial in advancing the fidelity of the model as a whole.

Appendix A. Data Tables for Use by JMP Software

A.1 Description of Appendix A

A few notes must be discussed in relation to the data presented in this Appendix. The first data table, Table A.2.1 through Table A.2.15 show the complete 405 data points required by the JMP software for a full factorial design analysis. The nineteen (19) points that were omitted from the data are included in this table but are highlighted in yellow. The data points that are highlighted in red indicate test points that were achievable at steady-level flight. This means that these points were in the positive P_S region of the flight envelope and did not require dive planning in order to be reached.

The data presented here is sorted by the pattern of the factorial design. The five (5) digit code represents each of the design factors in the factorial design. The pattern number indicates the design factors in the following order:

1st Digit:	Weight
2nd Digit:	Temperature
3rd Digit:	Drag Index
4th Digit:	TP (Test Point) Altitude
5th Digit:	TP Mach Number

The results for each of these data points are then shown to the right. Below is a table that indicates the Pattern values for the tables in this Appendix. This is a sample of how the Pattern values coordinate with each design factors.

Table A.1.1: Pattern Determination Table

Pattern	Weight	Temperature	Drag Index	TP Altitude	TP Mach Number
11111	33000	0	150	5000	1.05
22222	31000	5	175	10000	1.10
33333	29000	10	200	20000	1.15
34311	29000	15	200	5000	1.05
35322	29000	20	200	10000	1.10

A.2 Tables for the Complete Data Set

Table A.2.1: Complete Data Set (Set 11111-11333)

Pattern	Weight (lbs.)	Temperature (°C)	Drag Index	TP Altitude (ft)	TP Mach	Starting Mach	Starting Altitude (ft)	Dive Angle (°)	Start Recovery Altitude (ft)	End Recovery Altitude (ft)
11111	33000	0	150	5000	1.05	1.03	7600	-8	4500	4200
11112	33000	0	150	5000	1.1	1.06	9500	-13	4200	3500
11113	33000	0	150	5000	1.15	1.1	11600	-18	3800	2700
11121	33000	0	150	10000	1.05	1.04	10400	-2	9900	9800
11122	33000	0	150	10000	1.1	1.08	12200	-6	9600	9400
11123	33000	0	150	10000	1.15	1.12	13700	-11	9300	8800
11131	33000	0	150	20000	1.05	1.05	20000	0	20000	20000
11132	33000	0	150	20000	1.1	1.1	20000	0	20000	20000
11133	33000	0	150	20000	1.15	1.15	20000	0	20000	20000
11211	33000	0	175	5000	1.05	1.02	8700	-11	4300	3900
11212	33000	0	175	5000	1.1	1.05	10800	-16	4000	3100
11213	33000	0	175	5000	1.15	1.05	14900	-23	3500	1800
11221	33000	0	175	10000	1.05	1.03	11600	-4	9800	9700
11222	33000	0	175	10000	1.1	1.08	12800	-9	9400	9100
11223	33000	0	175	10000	1.15					
11231	33000	0	175	20000	1.05	1.05	20000	0	20000	20000
11232	33000	0	175	20000	1.1	1.1	20000	0	20000	20000
11233	33000	0	175	20000	1.15	1.15	20000	0	20000	20000
11311	33000	0	200	5000	1.05	1.02	9500	-12	4300	3800
11312	33000	0	200	5000	1.1					
11313	33000	0	200	5000	1.15	1.03	15600	-26	3300	1200
11321	33000	0	200	10000	1.05	1.04	11400	-6	9600	9500
11322	33000	0	200	10000	1.1	1.07	13000	-11	9300	8800
11323	33000	0	200	10000	1.15	1.08	16300	-17	8900	7900
11331	33000	0	200	20000	1.05	1.05	20000	0	20000	20000
11332	33000	0	200	20000	1.1	1.1	20000	0	20000	20000
11333	33000	0	200	20000	1.15	1.15	20000	0	20000	20000

Indicates test points attainable with Positive P_S at steady-level flight
Indicates test points that caused unknown failure in model execution

Table A.2.2: Complete Data Set (Set 12111-12333)

Pattern	Weight (lbs.)	Temperature (°C)	Drag Index	TP Altitude (ft)	TP Mach	Starting Mach	Starting Altitude (ft)	Dive Angle (°)	Start Recovery Altitude (ft)	End Recovery Altitude (ft)
12111	33000	5	150	5000	1.05	1.03	8000	-8	4500	4200
12112	33000	5	150	5000	1.1	1.06	10400	-13	4200	3500
12113	33000	5	150	5000	1.15	1.09	12600	-19	3800	2500
12121	33000	5	150	10000	1.05	1.04	11100	-3	9800	9800
12122	33000	5	150	10000	1.1	1.08	12700	-8	9500	9200
12123	33000	5	150	10000	1.15	1.11	14600	-13	9200	8500
12131	33000	5	150	20000	1.05	1.05	20000	0	20000	20000
12132	33000	5	150	20000	1.1	1.1	20000	0	20000	20000
12133	33000	5	150	20000	1.15	1.15	20100	-1	19900	19900
12211	33000	5	175	5000	1.05	1.02	9000	-11	4300	3900
12212	33000	5	175	5000	1.1	1.05	11300	-17	3900	2900
12213	33000	5	175	5000	1.15					
12221	33000	5	175	10000	1.05	1.03	12100	-5	9700	9600
12222	33000	5	175	10000	1.1	1.08	13600	-10	9400	9000
12223	33000	5	175	10000	1.15	1.1	15500	-16	9000	8000
12231	33000	5	175	20000	1.05	1.05	20000	0	20000	20000
12232	33000	5	175	20000	1.1	1.1	20000	0	20000	20000
12233	33000	5	175	20000	1.15	1.14	20700	-2	19900	19800
12311	33000	5	200	5000	1.05	1.02	9900	-12	4300	3700
12312	33000	5	200	5000	1.1					
12313	33000	5	200	5000	1.15	1.03	16600	-27	3300	900
12321	33000	5	200	10000	1.05	1.03	11900	-7	9600	9400
12322	33000	5	200	10000	1.1	1.07	13900	-12	9300	8700
12323	33000	5	200	10000	1.15					
12331	33000	5	200	20000	1.05	1.05	20000	0	20000	20000
12332	33000	5	200	20000	1.1	1.1	20000	0	20000	20000
12333	33000	5	200	20000	1.15	1.14	21200	-3	19800	19700

■ Indicates test points attainable with Positive P_S at steady-level flight
■ Indicates test points that caused unknown failure in model execution

Table A.2.2: Complete Data Set (Set 13111-13333)

Pattern	Weight (lbs.)	Temperature (°C)	Drag Index	TP Altitude (ft)	TP Mach	Starting Mach	Starting Altitude (ft)	Dive Angle (°)	Start Recovery Altitude (ft)	End Recovery Altitude (ft)
13111	33000	10	150	5000	1.05	1.03	8700	-8	4500	4200
13112	33000	10	150	5000	1.1	1.05	11300	-14	4100	3400
13113	33000	10	150	5000	1.15	1.08	13800	-20	3700	2300
13121	33000	10	150	10000	1.05	1.03	11900	-4	9800	9700
13122	33000	10	150	10000	1.1	1.07	14000	-9	9400	9100
13123	33000	10	150	10000	1.15	1.1	16200	-14	9100	8300
13131	33000	10	150	20000	1.05	1.05	20000	0	20000	20000
13132	33000	10	150	20000	1.1	1.1	20000	0	20000	20000
13133	33000	10	150	20000	1.15	1.13	21900	-3	19800	19700
13211	33000	10	175	5000	1.05	1.02	9400	-11	4300	3900
13212	33000	10	175	5000	1.1	1.04	12100	-17	3900	2900
13213	33000	10	175	5000	1.15	1.07	14700	-24	3400	1500
13221	33000	10	175	10000	1.05	1.03	12700	-6	9600	9500
13222	33000	10	175	10000	1.1	1.07	14400	-12	9200	8700
13223	33000	10	175	10000	1.15	1.09	16800	-18	8800	7700
13231	33000	10	175	20000	1.05	1.05	20000	0	20000	20000
13232	33000	10	175	20000	1.1	1.09	20400	-1	19900	19900
13233	33000	10	175	20000	1.15	1.12	22900	-5	19700	19500
13311	33000	10	200	5000	1.05	1.01	10100	-13	4200	3600
13312	33000	10	200	5000	1.1	1.04	12600	-20	3700	2400
13313	33000	10	200	5000	1.15	1.02	17600	-28	3200	700
13321	33000	10	200	10000	1.05	1.03	12900	-8	9500	9200
13322	33000	10	200	10000	1.1	1.06	15000	-14	9100	8400
13323	33000	10	200	10000	1.15	1.09	17400	-20	8700	7300
13331	33000	10	200	20000	1.05	1.05	20000	0	20000	20000
13332	33000	10	200	20000	1.1	1.09	21000	-2	19900	19800
13333	33000	10	200	20000	1.15	1.12	23800	-6	19600	19400

■ Indicates test points attainable with Positive P_S at steady-level flight
■ Indicates test points that caused unknown failure in model execution

159

Table A.2.4: Complete Data Set (Set 14111-14333)

Pattern	Weight (lbs.)	Temperature (°C)	Drag Index	TP Altitude (ft)	TP Mach	Starting Mach	Starting Altitude (ft)	Dive Angle (°)	Start Recovery Altitude (ft)	End Recovery Altitude (ft)
14111	33000	15	150	5000	1.05	1.02	9800	-8	4500	4200
14112	33000	15	150	5000	1.1	1.04	12900	-14	4100	3400
14113	33000	15	150	5000	1.15	1.06	15400	-21	3600	2000
14121	33000	15	150	10000	1.05	1.02	13300	-5	9700	9600
14122	33000	15	150	10000	1.1	1.06	15600	-10	9400	8900
14123	33000	15	150	10000	1.15	1.09	17900	-16	8900	8000
14131	33000	15	150	20000	1.05	1.05	20000	0	20000	20000
14132	33000	15	150	20000	1.1	1.09	21400	-2	19900	19800
14133	33000	15	150	20000	1.15	1.12	23500	-6	19600	19400
14211	33000	15	175	5000	1.05	1.01	10000	-11	4300	3800
14212	33000	15	175	5000	1.1	1.03	13500	-17	3900	2900
14213	33000	15	175	5000	1.15	1.05	16200	-25	3400	1200
14221	33000	15	175	10000	1.05	1.02	13800	-7	9600	9300
14222	33000	15	175	10000	1.1	1.05	16200	-13	9200	8500
14223	33000	15	175	10000	1.15	1.08	18900	-19	8800	7500
14231	33000	15	175	20000	1.05	1.05	20100	-1	19900	19900
14232	33000	15	175	20000	1.1	1.07	22800	-4	19800	19700
14233	33000	15	175	20000	1.15	1.1	25200	-8	19500	19200
14311	33000	15	200	5000	1.05	1.01	10700	-13	4200	3600
14312	33000	15	200	5000	1.1	1.03	13900	-20	3700	2400
14313	33000	15	200	5000	1.15	1	19200	-29	3100	400
14321	33000	15	200	10000	1.05	1.02	13800	-9	9500	9100
14322	33000	15	200	10000	1.1	1.05	16600	-15	9100	8200
14323	33000	15	200	10000	1.15	1.07	19400	-22	8600	6900
14331	33000	15	200	20000	1.05	1.04	20600	-2	19900	19800
14332	33000	15	200	20000	1.1	1.06	24400	-5	19700	19600
14333	33000	15	200	20000	1.15	1.07	27200	-10	19400	18900

    Indicates test points attainable with Positive P$_S$ at steady-level flight
    Indicates test points that caused unknown failure in model execution

Table A.2.5: Complete Data Set (Set 15111-15333)

Pattern	Weight (lbs.)	Temperature (°C)	Drag Index	TP Altitude (ft)	TP Mach	Starting Mach	Starting Altitude (ft)	Dive Angle (°)	Start Recovery Altitude (ft)	End Recovery Altitude (ft)
15111	33000	20	150	5000	1.05	1.01	10600	-9	4400	4100
15112	33000	20	150	5000	1.1	1.03	14200	-15	4000	3200
15113	33000	20	150	5000	1.15	1.05	17200	-22	3500	1800
15121	33000	20	150	10000	1.05	1.01	14300	-7	9600	9300
15122	33000	20	150	10000	1.1	1.05	17100	-12	9200	8700
15123	33000	20	150	10000	1.15	1.07	19600	-18	8800	7600
15131	33000	20	150	20000	1.05	1.04	20600	-2	19900	19800
15132	33000	20	150	20000	1.1	1.07	23000	-5	19700	19500
15133	33000	20	150	20000	1.15	1.11	24600	-9	19400	19000
15211	33000	20	175	5000	1.05	1	11000	-11	4300	3800
15212	33000	20	175	5000	1.1	1.02	15000	-18	3800	2700
15213	33000	20	175	5000	1.15	1.04	18600	-25	3300	1200
15221	33000	20	175	10000	1.05	1	15900	-8	9500	9200
15222	33000	20	175	10000	1.1	1.04	18400	-14	9100	8400
15223	33000	20	175	10000	1.15	1.05	21100	-21	8600	7100
15231	33000	20	175	20000	1.05	1.02	22600	-4	19800	19700
15232	33000	20	175	20000	1.1	1.06	24900	-7	19600	19300
15233	33000	20	175	20000	1.15	1.09	27000	-11	19300	18800
15311	33000	20	200	5000	1.05	1	11900	-13	4200	3600
15312	33000	20	200	5000	1.1	1.01	15300	-21	3700	2200
15313	33000	20	200	5000	1.15	1.03	19100	-29	3100	400
15321	33000	20	200	10000	1.05	1.01	15500	-10	9400	9000
15322	33000	20	200	10000	1.1	1.03	18700	-17	8900	7900
15323	33000	20	200	10000	1.15	1.04	22000	-24	8400	6500
15331	33000	20	200	20000	1.05	1.01	23400	-5	19700	19600
15332	33000	20	200	20000	1.1	1.03	26700	-9	19400	19100
15333	33000	20	200	20000	1.15	1.05	29600	-13	19200	18500

   🟥 Indicates test points attainable with Positive P_S at steady-level flight
   🟨 Indicates test points that caused unknown failure in model execution

Table A.2.6: Complete Data Set (Set 21111-21333)

Pattern	Weight (lbs.)	Temperature (°C)	Drag Index	TP Altitude (ft)	TP Mach	Starting Mach	Starting Altitude (ft)	Dive Angle (°)	Start Recovery Altitude (ft)	End Recovery Altitude (ft)
21111	31000	0	150	5000	1.05	1.03	7700	-8	4500	4200
21112	31000	0	150	5000	1.1	1.06	9700	-13	4200	3500
21113	31000	0	150	5000	1.15					
21121	31000	0	150	10000	1.05	1.04	10400	-2	9900	9800
21122	31000	0	150	10000	1.1	1.08	12200	-6	9600	9400
21123	31000	0	150	10000	1.15	1.12	13600	-12	9200	8600
21131	31000	0	150	20000	1.05	1.05	20000	0	20000	20000
21132	31000	0	150	20000	1.1	1.1	20000	0	20000	20000
21133	31000	0	150	20000	1.15	1.15	20000	0	20000	20000
21211	31000	0	175	5000	1.05	1.02	8900	-11	4300	3900
21212	31000	0	175	5000	1.1					
21213	31000	0	175	5000	1.15	1.05	14700	-25	3400	1400
21221	31000	0	175	10000	1.05	1.04	11400	-5	9700	9600
21222	31000	0	175	10000	1.1	1.08	12600	-10	9400	9000
21223	31000	0	175	10000	1.15	1.12	14100	-16	9000	8000
21231	31000	0	175	20000	1.05	1.05	20000	0	20000	20000
21232	31000	0	175	20000	1.1	1.1	20000	0	20000	20000
21233	31000	0	175	20000	1.15	1.15	20000	0	20000	20000
21311	31000	0	200	5000	1.05	1.01	9300	-13	4200	3600
21312	31000	0	200	5000	1.1					
21313	31000	0	200	5000	1.15	1.04	15200	-28	3200	800
21321	31000	0	200	10000	1.05	1.04	11500	-6	9600	9500
21322	31000	0	200	10000	1.1	1.07	12800	-12	9300	8700
21323	31000	0	200	10000	1.15	1.08	16300	-18	8800	7700
21331	31000	0	200	20000	1.05	1.05	20000	0	20000	20000
21332	31000	0	200	20000	1.1	1.1	20000	0	20000	20000
21333	31000	0	200	20000	1.15	1.15	20000	0	20000	20000

■ Indicates test points attainable with Positive P_S at steady-level flight
■ Indicates test points that caused unknown failure in model execution

Table A.2.7: Complete Data Set (Set 22111-22333)

Pattern	Weight (lbs.)	Temperature (°C)	Drag Index	TP Altitude (ft)	TP Mach	Starting Mach	Starting Altitude (ft)	Dive Angle (°)	Start Recovery Altitude (ft)	End Recovery Altitude (ft)
22111	31000	5	150	5000	1.05	1.03	8300	-8	4500	4200
22112	31000	5	150	5000	1.1	1.06	10500	-14	4100	3400
22113	31000	5	150	5000	1.15					
22121	31000	5	150	10000	1.05	1.04	11100	-3	9800	9800
22122	31000	5	150	10000	1.1	1.08	12700	-8	9500	9200
22123	31000	5	150	10000	1.15	1.11	14800	-13	9200	8500
22131	31000	5	150	20000	1.05	1.05	20000	0	20000	20000
22132	31000	5	150	20000	1.1	1.1	20000	0	20000	20000
22133	31000	5	150	20000	1.15	1.15	20100	-1	19900	19900
22211	31000	5	175	5000	1.05	1.02	9300	-11	4300	3900
22212	31000	5	175	5000	1.1					
22213	31000	5	175	5000	1.15	1.04	15800	-25	3400	1300
22221	31000	5	175	10000	1.05	1.03	11800	-6	9600	9500
22222	31000	5	175	10000	1.1	1.07	13600	-11	9300	8800
22223	31000	5	175	10000	1.15	1.11	15400	-17	8900	7900
22231	31000	5	175	20000	1.05	1.05	20000	0	20000	20000
22232	31000	5	175	20000	1.1	1.1	20000	0	20000	20000
22233	31000	5	175	20000	1.15	1.14	20700	-2	19900	19800
22311	31000	5	200	5000	1.05	1.01	9800	-13	4200	3600
22312	31000	5	200	5000	1.1					
22313	31000	5	200	5000	1.15	1.02	16700	-29	3100	500
22321	31000	5	200	10000	1.05	1.04	11900	-7	9600	9400
22322	31000	5	200	10000	1.1	1.07	13800	-13	9200	8600
22323	31000	5	200	10000	1.15	1.06	17900	-20	8700	7400
22331	31000	5	200	20000	1.05	1.05	20000	0	20000	20000
22332	31000	5	200	20000	1.1	1.1	20000	0	20000	20000
22333	31000	5	200	20000	1.15	1.14	21200	-3	19800	19700

■ Indicates test points attainable with Positive P_S at steady-level flight
■ Indicates test points that caused unknown failure in model execution

163

Table A.2.8: Complete Data Set (Set 23111-23333)

Pattern	Weight (lbs.)	Temperature (°C)	Drag Index	TP Altitude (ft)	TP Mach	Starting Mach	Starting Altitude (ft)	Dive Angle (°)	Start Recovery Altitude (ft)	End Recovery Altitude (ft)
23111	31000	10	150	5000	1.05	1.02	8600	-9	4400	4100
23112	31000	10	150	5000	1.1	1.05	11300	-15	4000	3200
23113	31000	10	150	5000	1.15	1.07	13800	-22	3600	1900
23121	31000	10	150	10000	1.05	1.03	12100	-4	9800	9700
23122	31000	10	150	10000	1.1	1.07	13700	-10	9400	8900
23123	31000	10	150	10000	1.15	1.1	16100	-15	9000	8200
23131	31000	10	150	20000	1.05	1.05	20000	0	20000	20000
23132	31000	10	150	20000	1.1	1.1	20000	0	20000	20000
23133	31000	10	150	20000	1.15	1.13	21600	-4	19700	19600
23211	31000	10	175	5000	1.05	1.02	9700	-11	4300	3900
23212	31000	10	175	5000	1.1	1.04	12500	-18	3900	2700
23213	31000	10	175	5000	1.15	1.02	17300	-26	3300	1100
23221	31000	10	175	10000	1.05	1.03	12400	-7	9600	9400
23222	31000	10	175	10000	1.1	1.06	14800	-12	9200	8700
23223	31000	10	175	10000	1.15	1.09	16800	-19	8800	7500
23231	31000	10	175	20000	1.05	1.05	20000	0	20000	20000
23232	31000	10	175	20000	1.1	1.09	20400	-1	19900	19900
23233	31000	10	175	20000	1.15	1.12	23000	-5	19700	19500
23311	31000	10	200	5000	1.05	1.01	10500	-13	4200	3600
23312	31000	10	200	5000	1.1					
23313	31000	10	200	5000	1.15	1.02	17800	-30	3100	300
23321	31000	10	200	10000	1.05	1.03	12500	-8	9500	9200
23322	31000	10	200	10000	1.1	1.05	15000	-15	9100	8300
23323	31000	10	200	10000	1.15	1.09	17200	-22	8600	7000
23331	31000	10	200	20000	1.05	1.05	20000	0	20000	20000
23332	31000	10	200	20000	1.1	1.09	21000	-2	19900	19800
23333	31000	10	200	20000	1.15	1.12	23500	-7	19600	19300

Indicates test points attainable with Positive P_S at steady-level flight

Indicates test points that caused unknown failure in model execution

Table A.2.9: Complete Data Set (Set 24111-24333)

Pattern	Weight (lbs.)	Temperature (°C)	Drag Index	TP Altitude (ft)	TP Mach	Starting Mach	Starting Altitude (ft)	Dive Angle (°)	Start Recovery Altitude (ft)	End Recovery Altitude (ft)
24111	31000	15	150	5000	1.05	1.02	9600	-9	4400	4100
24112	31000	15	150	5000	1.1	1.04	12800	-15	4000	3200
24113	31000	15	150	5000	1.15	1.06	15500	-22	3500	1800
24121	31000	15	150	10000	1.05	1.02	12800	-6	9600	9500
24122	31000	15	150	10000	1.1	1.06	15300	-11	9300	8800
24123	31000	15	150	10000	1.15	1.08	17900	-17	8900	7800
24131	31000	15	150	20000	1.05	1.05	20000	0	20000	20000
24132	31000	15	150	20000	1.1	1.09	21100	-3	19800	19700
24133	31000	15	150	20000	1.15	1.12	23600	-6	19600	19400
24211	31000	15	175	5000	1.05	1.01	10400	-11	4300	3800
24212	31000	15	175	5000	1.1	1.03	13600	-18	3800	2700
24213	31000	15	175	5000	1.15					
24221	31000	15	175	10000	1.05	1.02	13300	-8	9500	9200
24222	31000	15	175	10000	1.1	1.05	16000	-14	9100	8400
24223	31000	15	175	10000	1.15	1.07	19100	-20	8700	7300
24231	31000	15	175	20000	1.05	1.05	20100	-1	19900	19900
24232	31000	15	175	20000	1.1	1.07	22800	-4	19800	19700
24233	31000	15	175	20000	1.15	1.1	25000	-9	19400	19100
24311	31000	15	200	5000	1.05	1	10700	-14	4100	3400
24312	31000	15	200	5000	1.1	1.03	13600	-22	3600	2000
24313	31000	15	200	5000	1.15	1	19600	-30	3100	200
24321	31000	15	200	10000	1.05	1.02	14000	-9	9500	9100
24322	31000	15	200	10000	1.1	1.04	16600	-16	9000	8100
24323	31000	15	200	10000	1.15	1.07	19200	-24	8400	6500
24331	31000	15	200	20000	1.05	1.04	20600	-2	19900	19800
24332	31000	15	200	20000	1.1	1.06	23900	-6	19600	19400
24333	31000	15	200	20000	1.15	1.07	27600	-10	19400	18900

Indicates test points attainable with Positive P_S at steady-level flight
Indicates test points that caused unknown failure in model execution

Table A.2.10: Complete Data Set (Set 25111-25333)

Pattern	Weight (lbs.)	Temperature (°C)	Drag Index	TP Altitude (ft)	TP Mach	Starting Mach	Starting Altitude (ft)	Dive Angle (°)	Start Recovery Altitude (ft)	End Recovery Altitude (ft)
25111	31000	20	150	5000	1.05	1.01	11100	-9	4400	4100
25112	31000	20	150	5000	1.1	1.03	14100	-16	4000	3000
25113	31000	20	150	5000	1.15	1.05	17400	-23	3500	1600
25121	31000	20	150	10000	1.05	1.01	14500	-7	9600	9300
25122	31000	20	150	10000	1.1	1.04	17000	-13	9200	8500
25123	31000	20	150	10000	1.15	1.07	19500	-19	8700	7400
25131	31000	20	150	20000	1.05	1.04	20600	-2	19900	19800
25132	31000	20	150	20000	1.1	1.07	23100	-5	19700	19500
25133	31000	20	150	20000	1.15	1.11	24800	-9	19400	19000
25211	31000	20	175	5000	1.05	1.01	11400	-11	4300	3800
25212	31000	20	175	5000	1.1	1.02	15100	-19	3800	2500
25213	31000	20	175	5000	1.15	1.03	18500	-27	3200	800
25221	31000	20	175	10000	1.05	1.01	15300	-9	9400	9100
25222	31000	20	175	10000	1.1	1.03	18600	-15	9000	8200
25223	31000	20	175	10000	1.15	1.05	21300	-22	8600	6900
25231	31000	20	175	20000	1.05	1.02	22700	-4	19800	19700
25232	31000	20	175	20000	1.1	1.06	24500	-8	19500	19200
25233	31000	20	175	20000	1.15	1.1	26400	-12	19200	18600
25311	31000	20	200	5000	1.05	1	11800	-14	4100	3400
25312	31000	20	200	5000	1.1	1.01	15400	-22	3600	2000
25313	31000	20	200	5000	1.15	1.03	19600	-30	3000	100
25321	31000	20	200	10000	1.05	1.01	15200	-11	9300	8900
25322	31000	20	200	10000	1.1	1.02	18700	-18	8900	7700
25323	31000	20	200	10000	1.15	1.04	21900	-26	8300	6100
25331	31000	20	200	20000	1.05	1.01	23600	-5	19700	19600
25332	31000	20	200	20000	1.1	1.03	27100	-9	19400	19100
25333	31000	20	200	20000	1.15	1.06	29100	-14	19100	18300

■ Indicates test points attainable with Positive P_S at steady-level flight
■ Indicates test points that caused unknown failure in model execution

Table A.2.11: Complete Data Set (Set 31111-31333)

Pattern	Weight (lbs.)	Temperature (°C)	Drag Index	TP Altitude (ft)	TP Mach	Starting Mach	Starting Altitude (ft)	Dive Angle (°)	Start Recovery Altitude (ft)	End Recovery Altitude (ft)
31111	29000	0	150	5000	1.05	1.03	7900	-9	4500	4100
31112	29000	0	150	5000	1.1	1.06	9900	-14	4100	3400
31113	29000	0	150	5000	1.15	1.06	13700	-21	3600	2100
31121	29000	0	150	10000	1.05	1.04	10400	-2	9900	9800
31122	29000	0	150	10000	1.1	1.08	12000	-7	9600	9300
31123	29000	0	150	10000	1.15	1.12	13700	-12	9200	8600
31131	29000	0	150	20000	1.05	1.05	20000	0	20000	20000
31132	29000	0	150	20000	1.1	1.1	20000	0	20000	20000
31133	29000	0	150	20000	1.15	1.15	20000	0	20000	20000
31211	29000	0	175	5000	1.05	1.02	9000	-12	4300	3800
31212	29000	0	175	5000	1.1					
31213	29000	0	175	5000	1.15	1.05	15100	-26	3300	1200
31221	29000	0	175	10000	1.05	1.04	11400	-5	9700	9600
31222	29000	0	175	10000	1.1	1.08	12800	-10	9400	9000
31223	29000	0	175	10000	1.15	1.09	16000	-17	8900	7900
31231	29000	0	175	20000	1.05	1.05	20000	0	20000	20000
31232	29000	0	175	20000	1.1	1.1	20000	0	20000	20000
31233	29000	0	175	20000	1.15	1.15	20000	0	20000	20000
31311	29000	0	200	5000	1.05	1.01	9300	-14	4200	3500
31312	29000	0	200	5000	1.1	1.01	13300	-22	3600	2100
31313	29000	0	200	5000	1.15	1.04	15300	-30	3100	400
31321	29000	0	200	10000	1.05	1.04	11500	-6	9600	9500
31322	29000	0	200	10000	1.1					
31323	29000	0	200	10000	1.15	1.08	16300	-19	8800	7600
31331	29000	0	200	20000	1.05	1.05	20000	0	20000	20000
31332	29000	0	200	20000	1.1	1.1	20000	0	20000	20000
31333	29000	0	200	20000	1.15	1.15	20000	0	20000	20000

Indicates test points attainable with Positive P_S at steady-level flight
Indicates test points that caused unknown failure in model execution

Table A.2.12: Complete Data Set (Set 32111-32333)

Pattern	Weight (lbs.)	Temperature (°C)	Drag Index	TP Altitude (ft)	TP Mach	Starting Mach	Starting Altitude (ft)	Dive Angle (°)	Start Recovery Altitude (ft)	End Recovery Altitude (ft)
32111	29000	5	150	5000	1.05	1.02	8300	-9	4500	4100
32112	29000	5	150	5000	1.1	1.06	10400	-15	4100	3200
32113	29000	5	150	5000	1.15	1.04	15100	-22	3600	1900
32121	29000	5	150	10000	1.05	1.04	11200	-3	9800	9800
32122	29000	5	150	10000	1.1	1.08	12600	-9	9400	9100
32123	29000	5	150	10000	1.15	1.11	14900	-14	9100	8300
32131	29000	5	150	20000	1.05	1.05	20000	0	20000	20000
32132	29000	5	150	20000	1.1	1.1	20000	0	20000	20000
32133	29000	5	150	20000	1.15	1.15	20100	-1	19900	19900
32211	29000	5	175	5000	1.05	1.02	9100	-12	4300	3700
32212	29000	5	175	5000	1.1	1.05	11500	-19	3800	2600
32213	29000	5	175	5000	1.15	1.04	16000	-27	3300	900
32221	29000	5	175	10000	1.05	1.03	11900	-6	9600	9500
32222	29000	5	175	10000	1.1	1.07	13500	-12	9300	8700
32223	29000	5	175	10000	1.15	1.07	17500	-19	8800	7500
32231	29000	5	175	20000	1.05	1.05	20000	0	20000	20000
32232	29000	5	175	20000	1.1	1.1	20000	0	20000	20000
32233	29000	5	175	20000	1.15	1.14	20700	-2	19900	19800
32311	29000	5	200	5000	1.05	1.01	9700	-14	4200	3500
32312	29000	5	200	5000	1.1	1	14200	-22	3600	2100
32313	29000	5	200	5000	1.15	1.03	16500	-30	3100	300
32321	29000	5	200	10000	1.05	1.04	11800	-8	9500	9200
32322	29000	5	200	10000	1.1	1.07	13900	-14	9100	8400
32323	29000	5	200	10000	1.15	1.07	17800	-21	8700	7200
32331	29000	5	200	20000	1.05	1.05	20000	0	20000	20000
32332	29000	5	200	20000	1.1	1.1	20000	0	20000	20000
32333	29000	5	200	20000	1.15	1.14	21200	-3	19800	19700

■ Indicates test points attainable with Positive P_S at steady-level flight
□ Indicates test points that caused unknown failure in model execution

Table A.2.13: Complete Data Set (Set 33111-33333)

Pattern	Weight (lbs.)	Temperature (°C)	Drag Index	TP Altitude (ft)	TP Mach	Starting Mach	Starting Altitude (ft)	Dive Angle (°)	Start Recovery Altitude (ft)	End Recovery Altitude (ft)
33111	29000	10	150	5000	1.05	1.02	9000	-9	4400	4100
33112	29000	10	150	5000	1.1	1.05	11200	-16	4000	3100
33113	29000	10	150	5000	1.15	1.08	13900	-23	3500	1700
33121	29000	10	150	10000	1.05	1.03	11900	-5	9700	9600
33122	29000	10	150	10000	1.1	1.07	13900	-10	9400	8900
33123	29000	10	150	10000	1.15	1.1	16300	-16	9000	8000
33131	29000	10	150	20000	1.05	1.05	20000	0	20000	20000
33132	29000	10	150	20000	1.1	1.1	20000	0	20000	20000
33133	29000	10	150	20000	1.15	1.13	21700	-4	19700	19600
33211	29000	10	175	5000	1.05	1.02	9600	-12	4300	3700
33212	29000	10	175	5000	1.1	1.04	12500	-19	3800	2600
33213	29000	10	175	5000	1.15	1.02	17600	-28	3200	700
33221	29000	10	175	10000	1.05	1.03	12500	-7	9600	9400
33222	29000	10	175	10000	1.1	1.06	14700	-13	9200	8500
33223	29000	10	175	10000	1.15					
33231	29000	10	175	20000	1.05	1.05	20000	0	20000	20000
33232	29000	10	175	20000	1.1	1.09	20400	-1	19900	19900
33233	29000	10	175	20000	1.15	1.12	22700	-6	19600	19400
33311	29000	10	200	5000	1.05	1.01	10300	-14	4100	3500
33312	29000	10	200	5000	1.1	1	14700	-23	3600	1900
33313	29000	10	200	5000	1.15	1.01	18400	-30	3100	300
33321	29000	10	200	10000	1.05	1.03	12700	-9	9500	9100
33322	29000	10	200	10000	1.1	1.06	14900	-16	9000	8100
33323	29000	10	200	10000	1.15					
33331	29000	10	200	20000	1.05	1.05	20000	0	20000	20000
33332	29000	10	200	20000	1.1	1.09	21100	-2	19900	19800
33333	29000	10	200	20000	1.15	1.12	23600	-7	19600	19300

    Indicates test points attainable with Positive P_S at steady-level flight
    Indicates test points that caused unknown failure in model execution

Table A.2.14: Complete Data Set (Set 34111-34333)

Pattern	Weight (lbs.)	Temperature (°C)	Drag Index	TP Altitude (ft)	TP Mach	Starting Mach	Starting Altitude (ft)	Dive Angle (°)	Start Recovery Altitude (ft)	End Recovery Altitude (ft)
34111	29000	15	150	5000	1.05	1.02	9300	-10	4400	4000
34112	29000	15	150	5000	1.1	1.04	12800	-16	4000	3000
34113	29000	15	150	5000	1.15	1.06	15400	-24	3400	1500
34121	29000	15	150	10000	1.05	1.02	13000	-6	9600	9500
34122	29000	15	150	10000	1.1	1.06	15200	-12	9200	8700
34123	29000	15	150	10000	1.15	1.09	17800	-18	8800	7600
34131	29000	15	150	20000	1.05	1.05	20000	0	20000	20000
34132	29000	15	150	20000	1.1	1.09	21100	-3	19800	19700
34133	29000	15	150	20000	1.15	1.12	23400	-7	19600	19300
34211	29000	15	175	5000	1.05	1.01	10300	-12	4300	3700
34212	29000	15	175	5000	1.1	1.03	13300	-20	3700	2400
34213	29000	15	175	5000	1.15					
34221	29000	15	175	10000	1.05	1.02	13800	-8	9500	9200
34222	29000	15	175	10000	1.1	1.05	16100	-15	9100	8200
34223	29000	15	175	10000	1.15	1.07	18900	-22	8600	6900
34231	29000	15	175	20000	1.05	1.05	20100	-1	19900	19900
34232	29000	15	175	20000	1.1	1.07	22700	-5	19700	19600
34233	29000	15	175	20000	1.15	1.1	25200	-9	19400	19100
34311	29000	15	200	5000	1.05	1	10600	-15	4100	3300
34312	29000	15	200	5000	1.1					
34313	29000	15	200	5000	1.15	1.01	20300	-30	3100	200
34321	29000	15	200	10000	1.05	1.02	13800	-10	9400	9000
34322	29000	15	200	10000	1.1	1.04	16600	-17	8900	7900
34323	29000	15	200	10000	1.15	1.07	19400	-25	8400	6300
34331	29000	15	200	20000	1.05	1.04	20700	-2	19900	19800
34332	29000	15	200	20000	1.1	1.06	24100	-6	19600	19400
34333	29000	15	200	20000	1.15	1.07	27300	-11	19300	18800

    Indicates test points attainable with Positive P_S at steady-level flight
    Indicates test points that caused unknown failure in model execution

Table A.2.15: Complete Data Set (Set 35111-35333)

Pattern	Weight (lbs.)	Temperature (°C)	Drag Index	TP Altitude (ft)	TP Mach	Starting Mach	Starting Altitude (ft)	Dive Angle (°)	Start Recovery Altitude (ft)	End Recovery Altitude (ft)
35111	29000	20	150	5000	1.05	1.01	10600	-10	4400	4000
35112	29000	20	150	5000	1.1	1.03	14200	-17	3900	2900
35113	29000	20	150	5000	1.15	1.05	17200	-25	3300	1200
35121	29000	20	150	10000	1.05	1.01	15000	-7	9600	9300
35122	29000	20	150	10000	1.1	1.05	17500	-13	9200	8500
35123	29000	20	150	10000	1.15	1.07	19900	-20	8700	7300
35131	29000	20	150	20000	1.05	1.04	20600	-2	19900	19800
35132	29000	20	150	20000	1.1	1.07	22900	-6	19600	19400
35133	29000	20	150	20000	1.15	1.11	24600	-10	19400	18900
35211	29000	20	175	5000	1.05	1	11400	-12	4300	3700
35212	29000	20	175	5000	1.1	1.01	15300	-20	3700	2400
35213	29000	20	175	5000	1.15	1.03	18700	-29	3100	400
35221	29000	20	175	10000	1.05	1.01	15800	-9	9400	9100
35222	29000	20	175	10000	1.1	1.03	18800	-16	9000	8100
35223	29000	20	175	10000	1.15	1.05	21500	-23	8500	6700
35231	29000	20	175	20000	1.05	1.02	22800	-4	19800	19700
35232	29000	20	175	20000	1.1	1.06	24700	-8	19500	19200
35233	29000	20	175	20000	1.15	1.1	26600	-13	19200	18500
35311	29000	20	200	5000	1.05	1	11700	-15	4100	3300
35312	29000	20	200	5000	1.1	1.01	15600	-24	3500	1600
35313	29000	20	200	5000	1.15	0.94	14400	-30	3000	100
35321	29000	20	200	10000	1.05	1.01	15600	-11	9300	8900
35322	29000	20	200	10000	1.1	1.03	18800	-19	8800	7600
35323	29000	20	200	10000	1.15	1.04	22300	-27	8200	5900
35331	29000	20	200	20000	1.05	1.01	23900	-5	19700	19600
35332	29000	20	200	20000	1.1	1.04	26600	-10	19400	19000
35333	29000	20	200	20000	1.15	1.07	28800	-15	19000	18200

██████ Indicates test points attainable with Positive P_S at steady-level flight
██████ Indicates test points that caused unknown failure in model execution

A.3 Tables for the High Altitude Data Set

The second table in this Appendix shows the data that was used by the JMP program for the analysis of the uncertainty at high altitude. Table A.3 only includes the test points at 20,000 feet altitude. The TP Altitude design factor has also been removed from the data since it is a constant. It should be noted that there are no points omitted (highlighted in yellow) from this data set, however, there are several points that were attainable at positive excess power conditions (highlighted in red).

Table A.3.1: Data Set for Uncertainty at High Altitude Analysis (Set 11131-13333)

Pattern	Weight (lbs.)	Temperature (°C)	Drag Index	TP Mach	Starting Mach	Starting Altitude (ft)	Dive Angle (°)	Recovery Altitude 1 (ft)	Recovery Altitude 2 (ft)
11131	33000	0	150	1.05	1.05	20000	0	20000	20000
11132	33000	0	150	1.1	1.1	20000	0	20000	20000
11133	33000	0	150	1.15	1.15	20000	0	20000	20000
11231	33000	0	175	1.05	1.05	20000	0	20000	20000
11232	33000	0	175	1.1	1.1	20000	0	20000	20000
11233	33000	0	175	1.15	1.15	20000	0	20000	20000
11331	33000	0	200	1.05	1.05	20000	0	20000	20000
11332	33000	0	200	1.1	1.1	20000	0	20000	20000
11333	33000	0	200	1.15	1.15	20000	0	20000	20000
12131	33000	5	150	1.05	1.05	20000	0	20000	20000
12132	33000	5	150	1.1	1.1	20000	0	20000	20000
12133	33000	5	150	1.15	1.15	20100	-1	19900	19900
12231	33000	5	175	1.05	1.05	20000	0	20000	20000
12232	33000	5	175	1.1	1.1	20000	0	20000	20000
12233	33000	5	175	1.15	1.14	20700	-2	19900	19800
12331	33000	5	200	1.05	1.05	20000	0	20000	20000
12332	33000	5	200	1.1	1.1	20000	0	20000	20000
12333	33000	5	200	1.15	1.14	21200	-3	19800	19700
13131	33000	10	150	1.05	1.05	20000	0	20000	20000
13132	33000	10	150	1.1	1.1	20000	0	20000	20000
13133	33000	10	150	1.15	1.13	21900	-3	19800	19700
13231	33000	10	175	1.05	1.05	20000	0	20000	20000
13232	33000	10	175	1.1	1.09	20400	-1	19900	19900
13233	33000	10	175	1.15	1.12	22900	-5	19700	19500
13331	33000	10	200	1.05	1.05	20000	0	20000	20000
13332	33000	10	200	1.1	1.09	21000	-2	19900	19800
13333	33000	10	200	1.15	1.12	23800	-6	19600	19400

Indicates test points attainable with Positive P_S at steady-level flight

Table A.3.1: Data Set for Uncertainty at High Altitude Analysis (Set 14131-21333)

Pattern	Weight (lbs.)	Temperature (°C)	Drag Index	TP Mach	Starting Mach	Starting Altitude (ft)	Dive Angle (°)	Recovery Altitude 1 (ft)	Recovery Altitude 2 (ft)
14131	33000	15	150	1.05	1.05	20000	0	20000	20000
14132	33000	15	150	1.1	1.09	21400	-2	19900	19800
14133	33000	15	150	1.15	1.12	23500	-6	19600	19400
14231	33000	15	175	1.05	1.05	20100	-1	19900	19900
14232	33000	15	175	1.1	1.07	22800	-4	19800	19700
14233	33000	15	175	1.15	1.1	25200	-8	19500	19200
14331	33000	15	200	1.05	1.04	20600	-2	19900	19800
14332	33000	15	200	1.1	1.06	24400	-5	19700	19600
14333	33000	15	200	1.15	1.07	27200	-10	19400	18900
15131	33000	20	150	1.05	1.04	20600	-2	19900	19800
15132	33000	20	150	1.1	1.07	23000	-5	19700	19500
15133	33000	20	150	1.15	1.11	24600	-9	19400	19000
15231	33000	20	175	1.05	1.02	22600	-4	19800	19700
15232	33000	20	175	1.1	1.06	24900	-7	19600	19300
15233	33000	20	175	1.15	1.09	27000	-11	19300	18800
15331	33000	20	200	1.05	1.01	23400	-5	19700	19600
15332	33000	20	200	1.1	1.03	26700	-9	19400	19100
15333	33000	20	200	1.15	1.05	29600	-13	19200	18500
21131	31000	0	150	1.05	1.05	20000	0	20000	20000
21132	31000	0	150	1.1	1.1	20000	0	20000	20000
21133	31000	0	150	1.15	1.15	20000	0	20000	20000
21231	31000	0	175	1.05	1.05	20000	0	20000	20000
21232	31000	0	175	1.1	1.1	20000	0	20000	20000
21233	31000	0	175	1.15	1.15	20000	0	20000	20000
21331	31000	0	200	1.05	1.05	20000	0	20000	20000
21332	31000	0	200	1.1	1.1	20000	0	20000	20000
21333	31000	0	200	1.15	1.15	20000	0	20000	20000

Indicates test points attainable with Positive P_S at steady-level flight

Table A.3.3: Data Set for Uncertainty at High Altitude Analysis (Set 22131-24333)

Pattern	Weight (lbs.)	Temperature (°C)	Drag Index	TP Mach	Starting Mach	Starting Altitude (ft)	Dive Angle (°)	Recovery Altitude 1 (ft)	Recovery Altitude 2 (ft)
22131	31000	5	150	1.05	1.05	20000	0	20000	20000
22132	31000	5	150	1.1	1.1	20000	0	20000	20000
22133	31000	5	150	1.15	1.15	20100	-1	19900	19900
22231	31000	5	175	1.05	1.05	20000	0	20000	20000
22232	31000	5	175	1.1	1.1	20000	0	20000	20000
22233	31000	5	175	1.15	1.14	20700	-2	19900	19800
22331	31000	5	200	1.05	1.05	20000	0	20000	20000
22332	31000	5	200	1.1	1.1	20000	0	20000	20000
22333	31000	5	200	1.15	1.14	21200	-3	19800	19700
23131	31000	10	150	1.05	1.05	20000	0	20000	20000
23132	31000	10	150	1.1	1.1	20000	0	20000	20000
23133	31000	10	150	1.15	1.13	21600	-4	19700	19600
23231	31000	10	175	1.05	1.05	20000	0	20000	20000
23232	31000	10	175	1.1	1.09	20400	-1	19900	19900
23233	31000	10	175	1.15	1.12	23000	-5	19700	19500
23331	31000	10	200	1.05	1.05	20000	0	20000	20000
23332	31000	10	200	1.1	1.09	21000	-2	19900	19800
23333	31000	10	200	1.15	1.12	23500	-7	19600	19300
24131	31000	15	150	1.05	1.05	20000	0	20000	20000
24132	31000	15	150	1.1	1.09	21100	-3	19800	19700
24133	31000	15	150	1.15	1.12	23600	-6	19600	19400
24231	31000	15	175	1.05	1.05	20100	-1	19900	19900
24232	31000	15	175	1.1	1.07	22800	-4	19800	19700
24233	31000	15	175	1.15	1.1	25000	-9	19400	19100
24331	31000	15	200	1.05	1.04	20600	-2	19900	19800
24332	31000	15	200	1.1	1.06	23900	-6	19600	19400
24333	31000	15	200	1.15	1.07	27600	-10	19400	18900

 Indicates test points attainable with Positive P_S at steady-level flight

Table A.3.4: Data Set for Uncertainty at High Altitude Analysis (Set 25131-32333)

Pattern	Weight (lbs.)	Temperature (°C)	Drag Index	TP Mach	Starting Mach	Starting Altitude (ft)	Dive Angle (°)	Recovery Altitude 1 (ft)	Recovery Altitude 2 (ft)
25131	31000	20	150	1.05	1.04	20600	-2	19900	19800
25132	31000	20	150	1.1	1.07	23100	-5	19700	19500
25133	31000	20	150	1.15	1.11	24800	-9	19400	19000
25231	31000	20	175	1.05	1.02	22700	-4	19800	19700
25232	31000	20	175	1.1	1.06	24500	-8	19500	19200
25233	31000	20	175	1.15	1.1	26400	-12	19200	18600
25331	31000	20	200	1.05	1.01	23600	-5	19700	19600
25332	31000	20	200	1.1	1.03	27100	-9	19400	19100
25333	31000	20	200	1.15	1.06	29100	-14	19100	18300
31131	29000	0	150	1.05	1.05	20000	0	20000	20000
31132	29000	0	150	1.1	1.1	20000	0	20000	20000
31133	29000	0	150	1.15	1.15	20000	0	20000	20000
31231	29000	0	175	1.05	1.05	20000	0	20000	20000
31232	29000	0	175	1.1	1.1	20000	0	20000	20000
31233	29000	0	175	1.15	1.15	20000	0	20000	20000
31331	29000	0	200	1.05	1.05	20000	0	20000	20000
31332	29000	0	200	1.1	1.1	20000	0	20000	20000
31333	29000	0	200	1.15	1.15	20000	0	20000	20000
32131	29000	5	150	1.05	1.05	20000	0	20000	20000
32132	29000	5	150	1.1	1.1	20000	0	20000	20000
32133	29000	5	150	1.15	1.15	20100	-1	19900	19900
32231	29000	5	175	1.05	1.05	20000	0	20000	20000
32232	29000	5	175	1.1	1.1	20000	0	20000	20000
32233	29000	5	175	1.15	1.14	20700	-2	19900	19800
32331	29000	5	200	1.05	1.05	20000	0	20000	20000
32332	29000	5	200	1.1	1.1	20000	0	20000	20000
32333	29000	5	200	1.15	1.14	21200	-3	19800	19700

Indicates test points attainable with Positive P_S at steady-level flight

Table A.3.5: Data Set for Uncertainty at High Altitude Analysis (Set 33131-35333)

Pattern	Weight (lbs.)	Temperature (°C)	Drag Index	TP Mach	Starting Mach	Starting Altitude (ft)	Dive Angle (°)	Recovery Altitude 1 (ft)	Recovery Altitude 2 (ft)
33131	29000	10	150	1.05	1.05	20000	0	20000	20000
33132	29000	10	150	1.1	1.1	20000	0	20000	20000
33133	29000	10	150	1.15	1.13	21700	-4	19700	19600
33231	29000	10	175	1.05	1.05	20000	0	20000	20000
33232	29000	10	175	1.1	1.09	20400	-1	19900	19900
33233	29000	10	175	1.15	1.12	22700	-6	19600	19400
33331	29000	10	200	1.05	1.05	20000	0	20000	20000
33332	29000	10	200	1.1	1.09	21100	-2	19900	19800
33333	29000	10	200	1.15	1.12	23600	-7	19600	19300
34131	29000	15	150	1.05	1.05	20000	0	20000	20000
34132	29000	15	150	1.1	1.09	21100	-3	19800	19700
34133	29000	15	150	1.15	1.12	23400	-7	19600	19300
34231	29000	15	175	1.05	1.05	20100	-1	19900	19900
34232	29000	15	175	1.1	1.07	22700	-5	19700	19600
34233	29000	15	175	1.15	1.1	25200	-9	19400	19100
34331	29000	15	200	1.05	1.04	20700	-2	19900	19800
34332	29000	15	200	1.1	1.06	24100	-6	19600	19400
34333	29000	15	200	1.15	1.07	27300	-11	19300	18800
35131	29000	20	150	1.05	1.04	20600	-2	19900	19800
35132	29000	20	150	1.1	1.07	22900	-6	19600	19400
35133	29000	20	150	1.15	1.11	24600	-10	19400	18900
35231	29000	20	175	1.05	1.02	22800	-4	19800	19700
35232	29000	20	175	1.1	1.06	24700	-8	19500	19200
35233	29000	20	175	1.15	1.1	26600	-13	19200	18500
35331	29000	20	200	1.05	1.01	23900	-5	19700	19600
35332	29000	20	200	1.1	1.04	26600	-10	19400	19000
35333	29000	20	200	1.15	1.07	28800	-15	19000	18200

Indicates test points attainable with Positive P_S at steady-level flight

Appendix B. Analysis of Variance Tables from JMP Program

This Appendix contains the information on the Analysis of Variance tables from the JMP 8.0 software program. The data contained in these tables was used to initially determine if any variables were significant to the solution. In many problems, no variables may play an effect on the solution. However, in the case of this experiment, the results were directly affected by at least one variable in each test run. The information that determines if any variable is significant is the Prob > F category. This is known as the observed significance probability. As long as the value is less than 0.05, then there is at least one significant variable.

The F-Ratio is the model mean square divided by the error mean square. Because there is an underlying assumption that all the regression parameters from the model are zero, the higher F-Ratio indicates the greater significance the terms have on the given response. The mean squares are calculated using the sum of the squares terms. The mean square is the sum of the squares divided by the number of degrees of freedom. The model mean square for a linear fit estimates the variance in the model under the hypothesis that the parameters are zero. The error mean square estimates the variance in the error term. The sum of the squares is the sum of the squared differences from the sample mean of the data. For each source, the model, the error, and the combined total, this value will be associated with the mean of the particular response evaluated. The degrees of freedom indicate the number of values used to estimate the given number of regression parameters. The model uses fifteen values for the full set of data and ten values for the partial set. The error is the difference between the number of test points and the C. Total, or combined total number of test runs.

B.1 Tables for the Complete Data Set

Table B.1.1: Analysis of Variance for Starting Mach Response

Source	Degrees of Freedom	Sum of Squares	Mean Square	F Ratio	Prob > F
Model	15	0.499381	0.033292	272.744	<.0001
Error	370	0.045163	0.000122		
C. Total	385	0.544544			

Table B.1.2: Analysis of Variance for Starting Altitude Response

Source	Degrees of Freedom	Sum of Squares	Mean Square	F Ratio	Prob > F
Model	15	8372.479	558.165	697.738	<.0001
Error	370	295.9866	0.8		
C. Total	385	8668.465			

Table B.1.3: Analysis of Variance for Dive Angle Response

Source	Degrees of Freedom	Sum of Squares	Mean Square	F Ratio	Prob > F
Model	15	26040.7	1736.05	1654.92	0.0000
Error	370	388.139	1.05		
C. Total	385	26428.84			

Table B.1.4: Analysis of Variance for Start Recovery Altitude Response

Source	Degrees of Freedom	Sum of Squares	Mean Square	F Ratio	Prob > F
Model	15	17094.82	1139.65	227881.3	0.0000
Error	370	1.85	0.0050		
C. Total	385	17096.68			

Table B.1.5: Analysis of Variance for End Recovery Altitude Response

Source	Degrees of Freedom	Sum of Squares	Mean Square	F Ratio	Prob > F
Model	15	19718.18	1314.55	38628.3	0.0000
Error	370	12.591	0.0340		
C. Total	385	19730.77			

B.2 Tables for the High Altitude Data Set

Table B.2.1: Analysis of Variance for Starting Mach Response

Source	Degrees of Freedom	Sum of Squares	Mean Square	F Ratio	Prob > F
Model	10	0.1841	0.18407	312.45	<0.0001
Error	124	0.0073	0.00006		
C. Total	134	0.1913			

Table B.2.2: Analysis of Variance for Starting Altitude Response

Source	Degrees of Freedom	Sum of Squares	Mean Square	F Ratio	Prob > F
Model	10	716.8416	71.6842	145.98	<0.0001
Error	124	60.8893	0.4910		
C. Total	134	777.7308			

Table B.2.3: Analysis of Variance for Dive Angle Response

Source	Degrees of Freedom	Sum of Squares	Mean Square	F Ratio	Prob > F
Model	10	1809.904	180.99	203.902	<0.0001
Error	124	110.0667	0.888		
C. Total	134	1919.97			

Table B.2.4: Analysis of Variance for Start Recovery Altitude Response

Source	Degrees of Freedom	Sum of Squares	Mean Square	F Ratio	Prob > F
Model	10	7.28	0.728	201.233	<0.0001
Error	124	0.4485	0.004		
C. Total	134	7.7286			

Table B.2.5: Analysis of Variance for End Recovery Altitude Response

Source	Degrees of Freedom	Sum of Squares	Mean Square	F Ratio	Prob > F
Model	10	21.4784	2.148	189.164	<0.0001
Error	124	1.4079	0.011		
C. Total	134	22.8864			

Bibliography

[1] Anderson, Jr., John D., *Aircraft Performance and Design*, McGraw-Hill, Boston MA, 1999, pp. 33

[2] Bryson, Jr., Arthur E. and Desai, Mukund N., "Energy-State Approximation in Performance Optimization of Supersonic Aircraft," *AIAA Guidance, Control, and Flight Dynamics Conference*, Paper 68-127, Vol. 6, AIAA, Pasadena CA, Dec. 1969, pp. 481-488

[3] George, Benjamin, *Dive Planning.m*, MATLAB Program, Ver. 2.2, Nov. 2008

[4] Jacques, David, "Terminal Effects and Delivery of Conventional Weapons," *Terminal Effects and Delivery of Conventional Weapons Lecture Notes*, Air Force Institute of Technology, Wright-Patterson Air Force Base OH, 2008, Chap. 1, pp. 17

[5] Kutyna, Maj Donald J. (USAF), "The Aerospace Research Pilot School", *Air University Review*, Vol. XXI, No. 1, Nov-Dec 1968, Aerospace Studies Institute, Maxwell Air Force Base AL, pp. 81-91

[6] Liebst, Bradley S., "Equations of Motion for Rigid Aircraft," *Aircraft Handling Qualities and Performance Lecture Notes*, Air Force Institute of Technology, Wright-Patterson Air Force Base OH, 2009, pp. 387-399

[7] Liefer, Randall K., Valasek, John, Eggold, David P., and Downing, David R., "Fighter Agility Metrics, Research and Test," *AIAA Atmospheric Flight Mechanics Conference*, Paper 90-2087, Vol. 29, No. 3, AIAA, Portland OR, May 1991, pp. 452

[8] Lind, Rick, "Flight-Test Evaluation of Flutter Prediction Models," *Journal of Aircraft*, Vol. 40, No. 5, AIAA, Gainesville FL, Oct. 2003, pp. 964-970

[9] Mathworks, Inc., The, "Product Description", *MATLAB 7.9* [online source], URL: http://www.mathworks.com/products/matlab/description1.html [cited 2 Feb. 2010]

[10] Nelson, Robert C., *Flight Stability and Automatic Control*, 2nd ed., McGraw-Hill Higher Education, Boston MA, 1998, pp. 36, 37

[11] Norton, Maj Bill (USAF), "Fast-Paced Flight Testing and the C-17 Experience," *SETP Symposium Proceedings*, 2000 Report, Lancaster CA, 44th Symposium Proceedings, Sept. 2000, pp. 286

[12]   Pamadi, Bandu, N., *Performance, Stability, Dynamics, and Control of Airplanes*, 2nd ed., AIAA Education Series, AIAA, Reston VA, 2004, pp. 56

[13]   Pohlman, Mitch and Kam, Clinton, "Energy Based Aerodynamic Modeling: Increasing Fidelity of Fixed-Wing Constructive Entities," *Warfighter Readiness Research Division, U.S. Air Force*, SpringSim '07, Vol. 2, 2007, pp. 329

[14]   Powell, John, "Airplane Performance", *U.S. Naval Test Pilot School Fixed Wing Flight Mechanics Lecture Notes*, U.S. Naval Test Pilot School, Patuxent River Naval Air Station MD, May 1992, Chap. 10

[15]   Raymer, Daniel, P., *Aircraft Design: A Conceptual Approach*, 4th ed., AIAA Education Series, AIAA, Reston VA, 2006, pp. 184

[16]   Rutowski, Edward S., "Energy Approach to the General Aircraft Performance Problem," *Aerodynamics Session, Annual Summer Meeting*, Institute of the Aeronautical Sciences (IAS, predecessor of AIAA), Los Angeles CA, Sept. 1953, pp. 187-191

[17]   Saarlas, Maido, *Aircraft Performance*, 1st ed., John Wiley & Sons, Hoboken NJ, 2007, pp. 1, 3-4

[18]   SAS Institute, Inc., "Why JMP® 8?," *JMP 8* [online source], Cary NC, 2010, URL: http://www.jmp.com/software/jmp8/whyjmp8.shtml [cited 2 Feb. 2010]

[19]   SAS Institute, Inc., *JMP 8.0 Help File*, Cary, North Carolina, 2010 [accessed from Wright State University, Dayton OH]

[20]   Slotine, Jean-Jacques E. and Li, Weiping, *Applied Nonlinear Control*, Prentice Hall International, Upper Saddle River NJ, 1991, pp. 8-9

[21]   Stevens, Brian L. and Lewis, Frank L., *Aircraft Control and Simulation*, 2nd ed., John Wiley & Sons, Hoboken NJ, 2003, pp. 59, 633

[22]   Ward, Donald T. and Strganac, Thomas W., "Advanced Flight Tests Lecture Notes," *The University of Kansas Continuing Education*, University of Kansas, Lawrence KS, Sept. 2009, Chap. 1-3, 9.1

[23]   Ward, Donald T., Strganac, Thomas W., and Niewoehner, Rob, *Introduction to Flight Test Engineering*, 3rd ed., Kendall/Hunt Publishing, Dubuque IA, 2006, Vol. I, pp. 1-2

[24]   Ward, Donald T., Strganac, Thomas W., and Niewoehner, Rob, *Introduction to Flight Test Engineering*, 1st ed., Kendall/Hunt Publishing, Dubuque IA, 2006, Vol. II, pp. 97-100

[25]   Wickert, Maj Douglas P. (USAF), *Flight Path Angle and Energy Height Planning for Negative-P_S Test Points*, Society of Experimental Test Pilots 2006 Symposium, 40th Flight Test Squadron, Eglin Air Force Base FL, 2005

Vita

Lieutenant Matthew Schneider graduated from Archbishop Spalding High School in Severn, Maryland in May 2003. He entered undergraduate studies at Embry-Riddle Aeronautical University in Daytona Beach, Florida where he graduated with honors with a Bachelors of Science degree in Aerospace Engineering. His focus was in Aeronautics and he also completed a minor in Psychology. At Embry-Riddle, he was a member of Sigma Gamma Tau, Omicron Delta Kappa, Psi Chi, the National Society of Collegiate Scholars, and was the National Commander of Arnold Air Society. Upon graduation, he commissioned into the United States Air Force as a 2nd Lieutenant.

His first assignment was at Wright-Patterson Air Force Base, Ohio at the Air Force Institute of Technology. In August 2008, he entered the Graduate School of Engineering & Management to earn a Masters of Science degree in Aeronautical Engineering with a specialty in Stability and Control and Control Theory. Here he served as the Vice President of Sigma Gamma Tau, the National Honor Society for Aerospace Engineering. He is also currently nearing the completion of a second Masters of Science degree in Biomedical Engineering with a focus in Ergonomics from Wright State University in Dayton, Ohio. Upon graduation from AFIT, he will be assigned to the Air Force Research Laboratory's Air Vehicles Directorate at Wright-Patterson Air Force Base, Ohio.

.

1. REPORT DATE (DD-MM-YYYY) 25-03-2010	2. REPORT TYPE Master's Thesis	3. DATES COVERED (From – To) Aug 2008 – Mar 2010

4. TITLE AND SUBTITLE	5a. CONTRACT NUMBER
Dive Angle Sensitivity Analysis for Flight Test Safety and Efficiency	5b. GRANT NUMBER
	5c. PROGRAM ELEMENT NUMBER

6. AUTHOR(S)	5d. PROJECT NUMBER
Schneider, Matthew T., 2nd Lieutenant, USAF	5e. TASK NUMBER
	5f. WORK UNIT NUMBER

7. PERFORMING ORGANIZATION NAMES(S) AND ADDRESS(S) Air Force Institute of Technology Graduate School of Engineering and Management (AFIT/EN) 2950 Hobson Way WPAFB OH 45433-7765	8. PERFORMING ORGANIZATION REPORT NUMBER AFIT/GAE/ENY/10-M20

9. SPONSORING/MONITORING AGENCY NAME(S) AND ADDRESS(ES) Dertien, Evan, Lt. Col., USAF (DSN: 872-9145) 40 FLTS/CC 505 West Choctawhatchee Ave., Building 54 Eglin Air Force Base, FL 32542	10. SPONSOR/MONITOR'S ACRONYM(S)
	11. SPONSOR/MONITOR'S REPORT NUMBER(S)

12. DISTRIBUTION/AVAILABILITY STATEMENT
APPROVED FOR PUBLIC RELEASE; DISTRIBUTION UNLIMITED.

13. SUPPLEMENTARY NOTES

14. ABSTRACT
Flutter envelope expansion is one of the most critical types of developmental flight tests, particularly for high-speed military aircraft. The regions that present the most dangerous flight profiles are those test points in the negative PS realm of the flight envelope. These points develop into high-speed dives and require an accurate predictive model to prevent possible testing accidents. As a flight test is conducted, several conditions such as aircraft weight and ambient air temperature can change, causing a drastic shift in the excess power profiles resulting in significant alteration in the test conditions. Using a dive planning model, a number of parameters were analyzed to determine the sensitivity to variations in data. This sensitivity analysis provided detailed information regarding the parameters that are most effected by minor variations in test conditions. The goal of this study was to improve the safety of flight test programs and increase test efficiency by improved test planning and execution.

15. SUBJECT TERMS
Negative Excess Power, Flutter Envelope Expansion, Dive Modeling, Sensitivity Analysis

16. SECURITY CLASSIFICATION OF:			17. LIMITATION OF ABSTRACT	18. NUMBER OF PAGES	19a. NAME OF RESPONSIBLE PERSON Huffman, Richard, AFIT/ENY
REPORT U	ABSTRACT U	c. THIS PAGE U	UU	201	19b. TELEPHONE NUMBER (Include area code) (937) 255-6565, ext 7490; e-mail: Richard.Huffman@afit.edu

Standard Form 298 (Rev: 8-98)
Prescribed by ANSI Std. Z39-18